Triblock Copolymers of Poly(2,3-dihydroxypropyl methacrylate) and Poly(propylene oxide): Synthesis, Behavior in Aqueous Solution and at the Air-Water Interface, and Interactions with Model Lipid Membranes

Dissertation

zur Erlagung des akademischen Grades
Doctor rerum naturalium (Dr. rer. nat.)

vorgelegt der
Naturwissenschaftlichen Fakultät II — Chemie und Physik
der Martin-Luther-Universität Halle-Wittenberg

von Herrn M. Sc. Elkin Mauricio Amado Zúñiga
geb. am 18. April 1974 in Bogotá, Kolumbien

Gutachter:

1. Prof. Dr. Andre Laschewsky (Potsdam - Golm)

2. Prof. Dr. Jörg Kreßler (Halle - Saale)

Halle (Saale), 14.01.2010

To my family.

"Amara radix, dulcis fructus"

(Martianus Capella, 5th century)

Contents

Abbreviations and Symbols

Abbreviations

AF4	Asymmetrical Flow Field-Flow Fractionation
AFM	Atomic Force Microscopy
ATRP	Atom Transfer Radical Polymerization
BAM	Brewster Angle Microscopy
BIB	2-bromoisobutyryl bromide
BLM	Bilayer (black) lipid membranes
bpy	2,2'-bipyridin
CMC	Critical Micellization Concentration
CMT	Critical Micellization Temperature
DLS	Dynamic Light Scattering
DMF	Dimethylformamide
DMM	(2,2-Dimethyl-1,3-dioxolan-4-yl)methyl methacrylate; solketal methacrylate
DMSO-d_6	Deuterated dimethyl sulfoxide
DMPC	1,2-Dimyristoyl-*sn*-glycero-3-phosphocholine
DMPC-d_{54}	1,2-Dimyristoyl-d54-*sn*-glycero-3-phosphocholine
DPhPC	1,2-Diphytanoyl-*sn*-glycero-3-phosphocholine
DPPC	1,2-Dipalmitoyl-*sn*-glycero-3-phosphocholine
DPPC-d_{62}	1,2-Dipalmitoyl-d62-*sn*-glycero-3-phosphocholine
DSC	Differential Scanning Calorimetry
FFF	Field-Flow Fractionation
FTIR	Fourier Transform Infrared Spectroscopy
GMA	2,3-dihydroxypropyl methacrylate; Glycerol monomethacrylate
GPC	Gel Permeation Chromatography
HEMA	2-hydroxyethyl methacrylate
HLB	Hydrophilic-lipophilic balance
IRRAS	Infrared Reflection Absorption Spectroscopy
ITC	Isothermal Titration Calorimetry
LC	Liquid condensed
LE	Liquid expanded
LCST	Lower critical solution temperature
MALS	Multiangle Light Scattering
MDR	Multidrug-resistant cancer
NMR	Nuclear Magnetic Resonance
PEO	Poly(ethylene oxide)
PGMA	Poly(2,3-dihydroxypropyl methacrylate); Poly(glycerol monomethacrylate)
P-gp	P-glycoprotein
PPO	Poly(propylene oxide)

TEA	Triethylamine
THF	Tetrahydrofuran
TMR	Tetramethylrhodamine-5-carbonyl azide

Symbols

A	Total surface area	[m^2]
A_m	Mean area available per molecule	[$Å^2 \cdot molecule^{-1}$]
b_j	Adsorption equilibrium constant for the j^{th} state	[M^{-1}]
C	Macromolecule concentration in the solution bulk	[M]
C_0	Total polymer concentration in trough	[M]
C_b	Actual polymer bulk concentration	[M]
D_{app}	Apparent diffusion coefficient	[$m^2 \cdot s^{-1}$]
E	Surface dilatational modulus; Gibbs elasticity	[$mN \cdot m^{-1}$]
E_0	Limiting Gibbs elasticity	[$mN \cdot m^{-1}$]
f_j	Fractional adsorption for the j^{th} state	
j	Conformational state of a macromolecules	
K	Surface compressional modulus	[$mN \cdot m^{-1}$]
k	Boltzmann constant = 1.38065×10^{-23}	[$J \cdot K^{-1}$]
L_w	Weight average contour length	[nm]
m	Degree of polymerization of PGMA block	
M_n	Number average molar mass	[$g \cdot mol^{-1}$]
M_w	Weight average molar mass	[$g \cdot mol^{-1}$]
n	Degree of polymerization of PPO block	
N_A	Avogadro constant = 6.02214×10^{23}	[mol^{-1}]
N_{agg}	Micellar aggregation number	
N_S	Number of moles adsorbed at the interface	[mol]
p-	Electromagnetic radiation polarized in-plane (*parallel*)	
q	Scattering vector	[nm^{-1}]
R	Ideal gas constant = 8.31447	[$J \cdot mol^{-1} \cdot K^{-1}$]
RA	Reflectance-absorbance	
R	Sample single-beam reflectance spectrum	
R_0	Reference single beam reflectance spectrum	
R_{core}	Radius of micellar core	[nm]
$R_{g,}$	Radius of gyration	[Å]
R_F	Two-dimensional Flory's radius	[Å]
R_h	Apparent hydrodynamic radii	[nm]
s-	Electromagnetic radiation polarized perpendicular to propagation plane	
V/S	Volumen-to-surface ratio	[mm]
y	Exponent in surface equation of state (Eq. 3.3)	

Greek symbols

α	Constant of intermolecular interaction	
γ	Surface tension	[mN·m^{-1}]
γ_0	Surface tension of a neat water surface	[mN·m^{-1}]
γ_{eq}	Surface tension at equilibrium	[mN·m^{-1}]
Γ	Polymer adsorption	[mol·m^{-2}]
Γ_j	Polymer adsorption for the j^{th} state	[mol·m^{-2}]
Γ	Decay rate	[ms^{-1}]
δ	Infrared deformation bending in-plane vibration mode	
δ	NMR signal chemical shift	[ppm]
$\Delta G_{mic.}$	Free energy of micellization	[kJ·mol^{-1}]
$\Delta H_{mic.}$	Micellization enthalpy	[kJ·mol^{-1}]
$\Delta S_{mic.}$	Micellization entropy	[kJ·mol^{-1}·K^{-1}]
$\Delta\Pi$	Surface pressure increase	[mN·m^{-1}]
η	Solvents viscosity	[mPa·s]
θ	Fraction of surface covered	
θ_0 / θ_{eq}	Initial/equilibrium tilt angle with the surface normal	[°]
κ	Monolayer compressibility	[m·mN^{-1}]
λ	Wavelength	[nm]
ν	Infrared stretching vibration mode	
ν_{as} / ν_s	Infrared antisymmetric/symmetric stretching vibration	
$\tilde{\nu}$	Wavenumber	[cm^{-1}]
Π	Surface pressure	[mN·m^{-1}]
Π_0 / Π_{eq}	Surface layer initial/equilibrium surface pressure	[mN·m^{-1}]
Π_{in}	Maximum penetration surface pressure	[mN·m^{-1}]
Π_M	Equivalent surface pressure for comparison with a biologically relevant bilayer membrane	[mN·m^{-1}]
Π_{max}	Maximum surface pressure	[mN·m^{-1}]
Π_{out}	Surface pressure at squeeze-out onset	[mN·m^{-1}]
Π_{LE-LC}	LE to LC transition surface pressure	[mN·m^{-1}]
Π^*	Surface pressure for adsorption at neat air-water interface	[mN·m^{-1}]
ω	Average molar area	[m²·mol^{-1}]
ϖ	Average surface area occupied per molecule	[Å^2·molecule^{-1}]
ω_0	Molar area increment	[m²·mol^{-1}]
ω_{max}	Maximal molar area	[m²·mol^{-1}]
ω_{min}	Minimal molar area	[m²·mol^{-1}]

Part I. **General Introduction**

1 Block Copolymers and Lipid Membranes

The sealing effect of damaged cell membranes by some members of the Poloxamer family of block copolymers has been known for almost three decades. There has been an intense and prolific research activity around this issue for around two decades (reflected by more than thousand articles published about this topic). However, until now the keystone of such biomedical effect, *i.e.* the exact mechanism of interaction between an amphiphilic block copolymer and a biological membrane, has remained elusive. This lack of understanding is partially due to limitations when using exclusively commercially available block copolymers for research. In the past there was little interest in the synthesis of tailor-made or in thoroughly characterized model amphiphilic block copolymers which might contribute to a better understanding of the interactions with lipids.

1.1 Biological Membranes

Biological membranes are essential components of cells and their organelles. They mainly consist of lipids and proteins. Membranes determine the boundary between the inside and outside of cellular compartments, and their respective ion and protein concentrations. They also control the transport of substances into the cell and are important players in the metabolism of cells. Furthermore, due to the presence of enzymatic proteins, the large overall surface of membranes gives rise to a plethora of catalytic properties.[1] Lipids forming biological membranes are amphiphilic in nature thus organizing themselves in water in various aggregation states.[2] In a cell membrane they arrange in a double layer of about 5 nm thickness into which proteins are embedded. Their hydrophilic moieties are exposed to water and their hydrophobic tails are hidden from water in the inner part of the membrane. A simplified model of such a bilayer together with the chemical structure of two common 1,2-diacylphosphocholines, a class of phospholipids naturally occurring in cell membranes, are shown in Figure 1.1.

1.2 Model Lipid Membranes

In order to study the interactions between amphiphilic polymers and biological membranes, simplified model membranes are commonly used. The most relevant aggregation forms of lipids used as models are shown in Figure 1.2a-d.

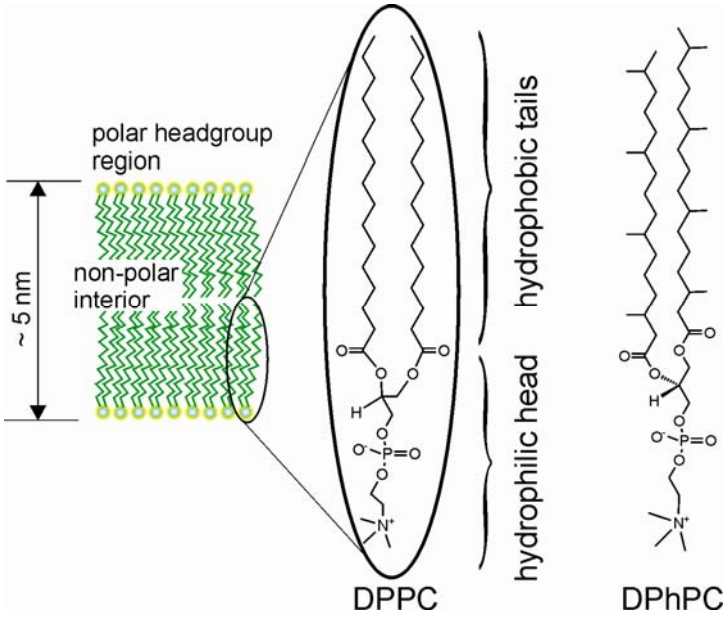

Figure 1.1: General organization and dimensions of a phospholipid bilayer and the chemical structure of two common 1,2-diacylphosphocholines.

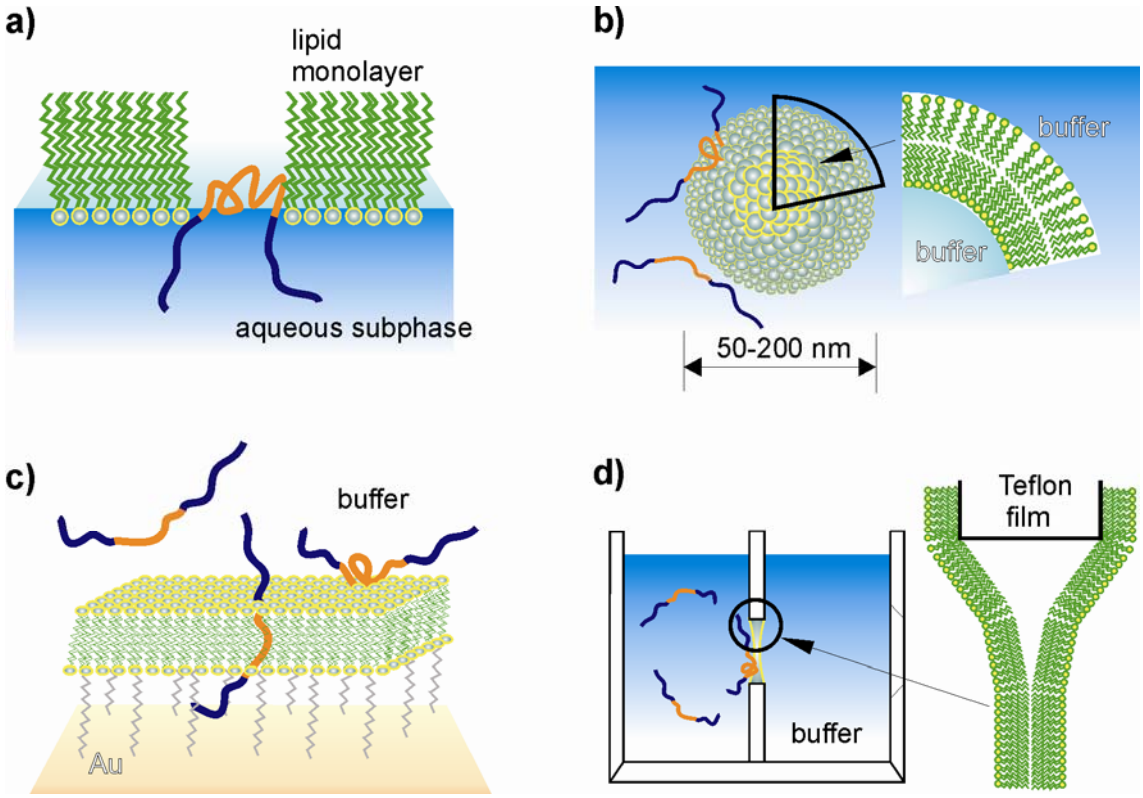

Figure 1.2: Model lipid membranes frequently used for the study of interactions with water soluble amphiphilic block copolymers. a) Langmuir monolayer and block copolymer adsorbed at the air-water interface. b) Lipid liposomes. c) Tethered bilayer lipid membrane on a gold solid support. d) Chamber for studying electrical properties and ion transport of bilayer (black) lipid membranes and the effect of adsorbed polymer.

Langmuir monolayers spread at the air-water interface of a Teflon trough and compressed to a given surface pressure through mobile barriers, are used as models of the outer leaflet of a cell membrane. They allow investigating interactions with monolayers in different physical states and packing order of the alkyl chains, from a disordered gaseous-like up to a tightly packed solid analogue state. The large surface area that can be covered homogeneously by a Langmuir monolayer enables to carry out X-ray or neutron reflection measurements and allows to follow the adsorption processes of block copolymers to lipid monolayers (Figure 1.2a) by time-resolved film thickness variation. Special spectroscopic techniques as IR or Raman can also be applied to Langmuir monolayers. Particularly helpful for obtaining information at the monolayer molecular level, such as conformation and orientation of the molecules, is Infrared Reflection Absorption Spectroscopy (IRRAS). An overview of the different techniques available for characterizing the interactions of block copolymers with lipid Langmuir films and the kind of information obtained can be found in Table 1.1.

As already mentioned, Langmuir monolayers represent only half of a cell membrane. Some model systems have also been developed that mimic both leaflets and allow studying interactions with a complete membrane. The most frequently employed model systems are spherical liposomes (Figure 1.2b) and planar bilayers tethered to solid supports (Figure 1.2c) or bilayer (black) lipid membranes (BLM) (Figure 1.2d). Liposomes are formed from dried lipid films by hydration and subsequent mechanical treatment. Unilamellar vesicles in the size range from 15-200 nm are easily obtained. They are employed to study adsorption phenomena in conjunction with thermal characterization techniques as ITC and DSC as well as dynamic light scattering. Also vesicles with micrometer size, so called giant unilamellar vesicles, can be obtained with special techniques. They are adequate for investigations with different light microscopy techniques such as confocal laser scanning or fluorescence microscopy. A summary of the characterization techniques commonly used for investigating the interaction of block copolymers and lipid bilayers can be found in Table 1.1 together with some key references.

1.3 Modes of Interaction of Amphiphilic Block Copolymers with a Lipid Membrane

A general requirement for a non-ionic block copolymer to associate with biological membranes is that the polymer has to be amphiphilic, whereby the hydrophobic effect induces the penetration of the polymer into the hydrophilic-hydrophobic interfacial layer of the membrane. Depending on the particular molecular architecture and the size of the hydrophobic block compared to the bilayer thickness of the membrane there are various possible modes of interaction between the polymer blocks and the lipid bilayer as illustrated in Figure 1.3.

Table 1.1: Overview of the most common techniques for the characterization of the interaction between block copolymers and lipid model membranes and the type of information obtained.

Characterization technique	Relevance	Ref.
Langmuir monolayer films		
Surface pressure (Π)- Mean molecular area (A) isotherms	Changes due to polymer adsorption: monolayer state, phase transitions, monolayer compressibility and stability.	3
Brewster Angle Microscopy (BAM)	External probe-free visualization of changes in monolayer morphology, formation of domains/aggregates, phase separation, reflectivity.	4
Fluorescence Microscopy	Visualization of domain formation with a fluorescence label.	5
Infrared Reflection Absorption Spectroscopy (IRRAS)	Changes in lipid/block copolymer molecular conformation and orientation. Monolayer composition.	3, 4
X-ray reflectivity	Changes in structure of the film in the surface normal direction from the electron density profile, layer thickness.	6
Neutron reflectivity	Changes in structure of the film in the surface normal direction, layer thickness. Enhanced contrast compared to X-rays with deuterated blocks and contrast matching in D_2O.	7
X-ray Grazing Incidence Diffraction (GISAXS, GIWAXS)	Changes in type of molecular packaging within the monolayer	6
Liposomes		
Isothermal Titration Calorimetry (ITC)	Thermodynamic parameters for the binding of polymer to the membrane. Partition coefficient, binding enthalpy.	8
Differential Scanning Calorimetry (DSC)	Changes in the thermotropic phase behavior of the lipid. Enthalpy, phase transitions.	9
Fluorescence spectroscopy	Influence of polymer in the flip-flop rate of membrane lipids, membrane permeability towards fluorescent molecules, pore formation.	10, 11
Cryo-Transmission Electron Microscopy (c-TEM)	Visualization of changes in liposome morphology and size.	12
Quartz Crystal Microbalance (QCM)	Polymer binding isotherm	13
Dynamic Light Scattering (DLS)	Changes in the hydrodynamic radius of liposomes, aggregation.	9
Giant Unillamelar Vesicles (GUV)		
Confocal Laser Scanning Microscopy (CLSM)	Visualization of domain formation on liposome surface with a fluorescence label.	14
Bilayer (black) Lipid Membranes (BLM)		
Electrical / Ion conductivity	Variation in ion permeability of the membrane. Transient or permanent pore formation. Membrane potentials.	10, 15

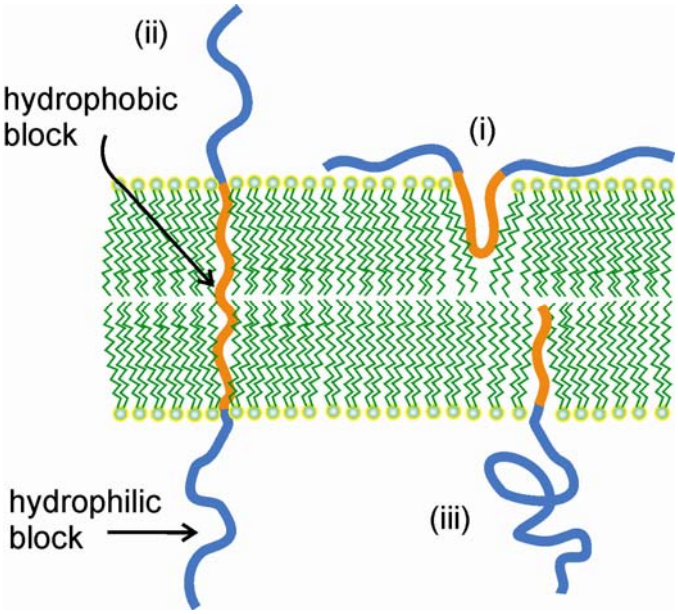

Figure 1.3: Different modes of interaction of amphiphilic di- and triblock copolymers with a lipid membrane: (i) partial insertion, (ii) trans-membrane spanning and (iii) anchoring by a short alkyl- or perfluorinated chain.

ABA triblock copolymers having a hydrophobic middle block match closely the polar/non-polar/polar structure of the bilayer. Since the middle block shows a strong affinity for the likewise hydrophobic inner part of the membrane, it tends to localize there, while the hydrophilic blocks extends into the water phase.[16] ABA polymers whose hydrophobic block length is less than the thickness of the bilayers insert only partially and weakly into the membrane, leaving their hydrophilic blocks delocalized at the membrane-water interface (Figure 1.3-(i)). ABA block copolymers whose hydrophobic block length is enough to span the bilayer integrate tightly in the membrane, projecting their hydrophilic blocks into the water phase on opposite sides of the bilayer[16] (Figure 1.3-(ii)). In this case, a further requirement is imposed on the chemical nature of the hydrophobic middle block since an alkyl-based block would be too hydrophobic and renders the whole molecule water insoluble.[17] In contrast, polyether-based blocks, such as poly(propylene oxide), exhibit a moderate hydrophobicity due to the presence of the polar ether groups and are suitable for trans-membrane spanning insertion. Another interaction type is found for amphiphilic copolymers bearing a short end hydrophobic block (semi-telechelics, Figure 1.3-(iii)), in that case the binding to the membrane through the hydrophobic anchor is facilitated. The anchor can be an alkyl chain as in poly(ethylene oxide)-lipid conjugates[18] or a perfluorinated moiety as commonly used to enhance membrane binding of drugs.[19]

1.4 Poly(propylene oxide)-based Triblock Copolymers

Amphiphilic triblock copolymers of the type PEO-*b*-PPO-*b*-PEO, *i.e.* having a ABA architecture comprising a hydrophobic poly(propylene oxide) (PPO) middle block and two poly(ethylene oxide) (PEO) hydrophilic outer blocks, are amphiphilic in nature and are known

under the generic name Poloxamers and the trademarks Pluronics® or Synperonics®. They find widespread application, partially because of their commercial availability, in investigations dealing with colloids and non-ionic surfactants,[20-22] drug delivery of poorly water-soluble drugs inside micelles[23,24] or hydrogels,[25] and cancer therapies.[26]

In particular, hydrophobic PEO-*b*-PPO-*b*-PEO copolymers, *i.e.* those having a large PPO hydrophobic block compared to the hydrophilic PEO blocks, have been shown to facilitate the permeation of relatively large molecules, including the anticancer drug doxorubicin, across lipid bilayers,[27] to exhibit ionophoric activity[28] and to act as chemosensitizing agents for the treatment of multidrug-resistant cancer (MDR) tumors by inhibiting the activity of drug efflux transporters such as P-glycoprotein (P-gp).[29] Some of them are even able to actually enter the cell.[30] Conversely, hydrophilic copolymers having larger PEO blocks are inactive in enhancing drug accumulation and are too hydrophilic to bind and translocate across a cell membrane.[30] However, they have been reported to inhibit thrombosis[31] and to help to seal electroporated cell membranes.[32,33] In the end, such biochemical effects are related with the copolymer ability to interact with biological membranes, a property that has been found to be determined ultimately by (i) the hydrophilic-lipophilic balance (HLB) of the copolymer, which depends on its ratio of hydrophilic to hydrophobic units, and (ii) the actual length of the PPO block.[30] Consistent with these conclusions derived from studies with lipid bilayers, it has been reported recently that the PPO block is responsible for regulating the capabilities of PEO-*b*-PPO-*b*-PEO to interact and insert into lipid monolayers.[34,35]

1.5 Motivation and Aim of this Work

Summarizing the last section, previous investigations have shown that a larger PPO block renders the copolymer bulkier, increasing the extent of the structural changes brought about by the copolymer in the lipid layer and promotes its retention, although simultaneously its ability to translocate across a bilayer or cell membrane is compromised and its initial insertion capability is reduced. Although it would be desirable to improve the retention ability of the copolymer up to surface pressures relevant for biological membranes (~35 mN/m for blood-brain barrier at 37°C or 31-35 mN/m for erythrocyte membrane at room temperature[36]) without reducing its insertion capability, a compromise must necessarily be made between both opposing properties within the PEO-*b*-PPO-*b*-PEO family.

The alternative strategy proposed in this work to surmount that limitation consists in replacing the PEO block by a more suitable hydrophilic block. The logic behind this proposal is the fact that the main role of the hydrophilic PEO block in the interaction with a lipid membrane is limited to balance the hydrophobicity of the PPO block making the copolymer hydrophilic enough for avoiding micellization and stay in solution, while remaining hydrophobic enough to bind and penetrate the lipid layer. The PEO block itself is of minor importance regarding the interaction with a lipid membrane.[27] However, this is not necessarily the case for amphiphiles not based on PEO having a bulkier hydrophilic block. It has been

pointed out in recent publications dealing with the interaction of non-ionic amphiphilic copolymers and detergents with lipid bilayers[36,37] and cells,[38] that not only the HLB or bulk hydrophobicity of a copolymer determines its membrane disturbing ability, but also the specific chemical structure of the molecule plays a role. It was found that a bulky hydrophilic block induces a disturbance in the liquid-crystalline packing of lipid bilayers in addition to the effect caused by the hydrophobic block alone. Particularly, copolymers having a branched polyglycerol as hydrophilic block showed a far more pronounced effect on membrane structure as compared to copolymers with linear PEO blocks. It was postulated that such additional perturbation effects arise from the hydrophilic block being dragged into the headgroup region of the outer bilayer leaflet as the hydrophobic block inserts into the fatty acid region of the membrane. Moreover, once incorporated, the hydroxyl groups of polyglycerol might form hydrogen bonds with the lipid headgroups, additionally anchoring the copolymer.[37]

Since PEO-*b*-PPO-*b*-PEO copolymers with a degree of polymerization of the PPO middle block (*n*) between 30-60 PO units are expected to have the ability to penetrate the cell membrane[30] and show a marked hypersensitization effect on MDR cancer cells,[39,40] a similar PPO block with a molar mass of 2000 g·mol^{-1} (*n*~34 units) was chosen for this study. Glycerol monomethacrylate (GMA; 2,3-dihydroxypropyl methacrylate), a highly hydrophilic monomer having two hydroxyl groups on every repeat unit, was chosen as the hydrophilic moiety because:

(i) The structure of its bulky side chain group resembles closely the monomeric unit of the branched polyglycerols mentioned above, which should increase its membrane disturbing ability as compared to a PEO block.

(ii) Each GMA monomeric unit possesses one ester and one diol moiety, both belonging to the class of binding elements known as type-I units, *i.e.* two groups having a pair of hydrogen bonding acceptor moieties located in a spatial configuration that would allow the binding to transmembrane sequences of P-gp, which are rich in hydrogen bond donor groups, and most likely to other related transporters such as the multi-drug resistance-associated protein MRP1 which show overlapping substrate specificities with P-gp.[36] If the affinity to P-gp were higher than the affinity of a drug coadministered with the copolymer, it could act as inhibitor of P-gp, enhancing in this way drug uptake by MDR cancer cells.

(iii) The hydroxyl moieties of GMA are readily subject to chemical modification for the covalent attachment of diverse probes such as fluorescence labels (see Appendix 8.1) or electron spin resonance (ESR) labels to the PGMA blocks and could be also conjugated with biologically active molecules such as peptides or drugs. This introduces a great flexibility when compared to PEO blocks whose EO repeating units possess no reactive moieties.

(iv) PGMA is biocompatible and possesses high water affinity. It has been used in biomedical and pharmaceutical applications such as hydrogels and soft contact lenses.[41,42] It also has been investigated as material for ultra filtration barriers mimicking the behavior of natural membranes in kidneys[43] and as biocompatible coating for implantable glucose sensors.[44]

Based on this background, the main objective of the present work is to synthesize a series of novel water soluble amphiphilic triblock copolymers of ABA architecture comprising a PPO middle block and two poly(2,3-dihydroxypropyl methacrylate), also named PGMA poly(glycerol monomethacrylate), outer blocks of varying length. In a second step of this investigation, their micellization in aqueous solutions as well as their adsorption behavior at the air-water interface are studied. Finally, their adsorption kinetics and concomitant interactions with phospholipid model membranes are investigated in order to gain a better insight into the PGMA-*b*-PPO-*b*-PGMA-membrane interactions on the molecular level.

1.6 References

[1] Heimburg, T. *Soft Matter* **2009**, *5*, 3145.

[2] Blume, A. *Lipids*, in: D.Walz, J. Tessié, G. Milazzo (Ed.s) *Bioelectrochemistry of membranes*, Birkhaeuser, Basel, **2004**, p 61.

[3] E. Amado, A. Kerth, A. Blume, J. Kressler, *Langmuir* **2008**, *24*,10041.

[4] E. Amado, A. Kerth, A. Blume, J. Kressler, *Soft Matter* **2009**, *5*, 669.

[5] Maskarinec, S. A.; Lee, K. Y. *Langmuir* **2003**, *19*,1809.

[6] Wu,G.; Majewski, J.; Ege, C.; Kjaer, K.; Weygand, M. J.; Lee, K. Y. C. *Biophys. J.* **2005**, 89 3159.

[7] Majewski, J.; Kuhl, T. L.; Wong, J. Y.; Smith, G. S. *Rev. Molec. Biotech.* **2000**, *74,* 207.

[8] Heerklotz,H.; Seelig, J. *Biochim. Biophys. Acta* **2000**, *69,* 1508.

[9] Castile, J. D.; Taylor, K. M. G.; Buckton, G. *Int. J. Pharm.* **2001**, *221,* 197.

[10] Eurokova,V. Y.; Krylova, O. O.; Antonenko,Y. N.; Melik-Nubarov, N. S. *Biochim. Biophys. Acta* **2000**, *73,* 1468.

[11] Demina, T.; Grozdova, I.; Krylova, O.; Zhirnov, A.; Istratov, V.; Frey, H.; Kautz, H.; Melik-Nubarov, N. *Biochemistry* **2005**, *44,* 4042.

[12] Johnsson, M.; Silvander, M.; Karlsson, G.; Edwards, K. *Langmuir* **1999**, *15,* 6314.

[13] Johnsson, M.; Bergstrand, N.; Edwards, K.; Stalgren, J. J. R. *Langmuir* **2001**, *17,* 3902.

[14] Kurz, A.; Bunge,A.; Windeck, A.-K.; Rost, M.; Flasche, W.; Arbuzova, A.; Strohbach, D.; Müller, S.; Liebscher, J.; Huster, D.; Herrmann, A. *Angew. Chem. Int. Ed.* **2006**, *45,* 4440.

[15] Krylova, O. O.; Pohl, P.; *Biochemistry* **2004**, *43,* 3696.

[16] Lee, B.; Firestone, M. A. *Biomacromolecules* **2008**, *9,* 1541.

[17] Demina, T.; Grozdova, I.; Krylova, O.; Zhirnov, A.; Istratov, V.; Frey, H.; Kautz, H.; Melik-Nubarov, N. *Biochemistry* **2005**, *44*, 4042.

[18] Momekova, D.; Rangelov, S.; Lambov, N.; Karlsson, G.; Almgren, M. *J. Dispersion Sci. Technol.* **2008**, *29*, 1106.

[19] Gerebtzoff, G.; Li-Blatter, X.; Fischer, H.; Frentzel, A.; Seelig, A. *ChemBioChem* **2004**, *5*, 676.

[20] Alexandridis, P.; Athanassiou, V. ; Fukuda, S. ; Hatton, T.A. *Langmuir* **1994**, *10*, 2604.

[21] Alexandridis, P.; Holzwarth, J.F.; Hatton, T.A. *Macromolecules* **1994**, *27*, 2414.

[22] Wanka, G.; Hoffmann, H.; Ulbricht, W. *Macromolecules* **1994**, *27*, 4145.

[23] Chiappetta, D.A.; Sosnik, A. *Eur. J. Pharm. Biopharm*. **2007**, *66*, 303.

[24] Munshi, N.; Rapoport, N.; Pitt, W.G. *Cancer Lett*. **1997**, *118*, 13-19.

[25] Escobar-Chávez, J.J.; López-Cervantes, M.; Naik, A.; Kalia, Y.N.; Quintanar-Guerrero, D.; Ganem-Quintanar, A. *J. Pharm. Pharmaceut. Sci*. **2006**, *3*, 339.

[26] Kabanov, A.V.; Batrakova, E.V.; Alakhov, V.Y. *Adv. Drug Delivery Rev*. **2002**, *54*, 759.

[27] Eurokova, V.Y.; Krylova, O.O.; Antonenko, Y.N.; Melik-Nubarov, N.S. *Biochim. Biophys. Acta* **2000**, *1468*, 73.

[28] Krylova, O.O.; Pohl, P. *Biochemistry* **2004**, *43*, 3696.

[29] Miller, D.W.; Batrakova, E.V.; Kabanov, A.V. *Pharm. Res*. **1999**, *16*, 396.

[30] Kabanov, A.V.; Batrakova, E.V.; Miller, D.W. *Adv. Drug Delivery Rev*. **2003**, *55*, 151.

[31] Armstrong, J.K.; Meiselman, H.J.; Fisher, T.C. *Thrombosis Res*. **1995**, *79*, 437.

[32] Sharma, V.; Stebe, K.; Murphy, J.C.; Tung, L. *Biophys. J*. **1996**, *71*, 3229.

[33] Maskarinec, S.A.; Haning, J.; Lee, R.C.; Lee,K.Y. *Biophys. J*. **2002**, *82*, 1453.

[34] Frey, S.L.; Zhang, D.; Carignano, M.A.; Szleifer, I.; Lee, K.Y. *J. Chem. Phys*. **2007**, *127*, 114904.

[35] Maskarinec, S.A.; Lee, K.Y. *Langmuir* **2003**, *19*, 1809.

[36] Seelig, A.; Gerebtzoff, G. *Expert Opin. Drug Metabol. Toxicol*. **2006**, *2*, 733.

[37] Demina, T.; Grozdova, I.; Krylova, O.; Zhirnov, A.; Istratov, V.; Frey, H.; Kautz, H.; Melik-Nubarov, N. *Biochemistry* **2005**, *44*, 4042.

[38] Pavlov, D.N.; Alexandrova, N.A.; Krylova, O.O.; Pohl, P.; Melik-Nubarov, N.S. *J. Drug Del. Sci. Tech*. **2006**, *16*, 259.

[39] Batrakova, E.; Lee, S.; Li, S.; Venne, A.; Alakhov, V.; Kabanov, A.; *Pharm. Res*. **1999**, *16*, 1373.

[40] Sommer, K.; Kaiser, S.; Krylova, O.O.; Kressler, J.; Pohl, P.; Busse, K. *J. Med. Chem.* DOI: 10.1021/jm800177c.

[41] Gates, G.; Harmon, J.P.; Ors, J.; Benz, P. *Polymer* **2003**, *44*, 207.

[42] Gates, G.; Harmon, J.P.; Ors, J.; Benz, P. *Polymer* **2003**, *44*, 215.

[43] Leung, B.K.; Robinson, G.B. *J. Appl. Polym. Sci*. **1993**, *47*, 1207.

[44] Wang, C.; Yu, B.; Knudsen, B.; Harmon, J.; Moussy, F.; Moussy, Y. *Biomacromolecules* **2008**, *9*, 561.

Part II. Triblock Copolymers of Poly(2,3-dihydroxypropyl methacrylate) and Poly(propylene oxide): Synthesis, Chemical Characterization, Micellization in Aqueous Solutions, and Adsorption Behavior at the Air-Water Interface

2 Synthesis of PGMA-*b*-PPO-*b*-PGMA by Atom Transfer Radical Polymerization and Micellization in Aqueous Solutions

2.1 Introduction

It is widely known that amphiphilic triblock copolymers with sufficiently long blocks and flexible backbones self-assemble spontaneously into micelles when dissolved in a solvent selective for one of the blocks.[1] If the polymer is water soluble, such micelles are able to solubilize nonpolar compounds providing a route for the incorporation of a variety of hydrophobic substances, including drugs, into water-based formulations.[2] Triblock copolymers of the ABA type PEO-*b*-PPO-*b*-PEO are well-known examples. They are commercially successful as emulsifiers for perfluororganics in blood replacement formulations. They have also been shown to facilitate the permeation of relatively large molecules across lipid bilayers[3] and to act as sensitizing agents for the treatment of multidrug-resistant cancer tumors.[4] In this stage of the present investigation a series of novel triblock copolymers with architecture PGMA-*b*-PPO-*b*-PGMA is synthesized by atom transfer radical polymerization technique. Afterwards, their micellization behavior in aqueous solutions is studied.

2.1.1 Monomer Requirements Regarding the Polymerization Technique

2,3-Dihydroxypropyl methacrylate, also known as glycerol monomethacrylate (GMA), is a highly hydrophilic monomer of commercial interest. Hydrogels based in GMA have already been studied for some years.[5] Due to its increased hydrophilicity GMA is a candidate for replacing the less hydrophilic 2-hydroxyethyl methacrylate (HEMA) in products such as soft contact lenses, hydrogels, drug delivery and other medical applications.[6,7] Furthermore, it has been investigated as material for ultra filtration barriers mimicking the behavior of natural membranes in kidneys.[8]

Anionic polymerization has been traditionally the chosen technique for the preparation of well defined block copolymers, especially because of the predictable molar masses, exact block compositions and very narrow molar mass distributions, and hence low polydispersities, which can be obtained. However, this technique possesses also the significant drawback of having stringent requirements regarding monomer purity, nearly complete moisture exclusion and demanding polymerization conditions, including very low temperatures. Moreover, the presence of functionalities in the monomers can cause undesirable side reactions and therefore, sometimes the monomer functional groups need to be protected during the

polymerization. In fact, HEMA cannot be polymerized by anionic polymerization due to the labile proton on the hydroxy group.[9] In contrast to anionic polymerization, atom transfer radical polymerization (ATRP) technique tolerates well water and other minor impurities and the reaction takes place at a convenient temperature range, typically from 0 to 100°C, while still yielding polymers with molar masses predetermined by the ratio of monomer to initiator and low polydispersities.[10,11] Also a wide variety of monomers such as styrenes, acrylates and methacrylates have already been successfully polymerized by ATRP.[12]

Poly(glycerol monomethacrylate) (PGMA) homopolymer and copolymers with styrenes, isoprene and some methacrylates have been synthesized before by anionic polymerization of the protected monomer (2,2-Dimethyl-1,3-dioxolan-4-yl)methyl methacrylate (DMM), otherwise known as solketal methacrylate (SMA), followed by the hydrolysis of the acetonide protective group.[13-16] On the other hand, GMA monomer has recently been directly homo- and copolymerized by ATRP.[17-20] However, there has been only one report of PDMM preparation by ATRP[21] to date, but not for the synthesis of triblock copolymers.

2.1.2 Investigation of Polymeric Micelles

For the application of polymeric micelles as nanocarriers, *i.e.*, for incorporating noncovalently hydrophobic substances into the hydrophobic core of the micelle, the problem of their stability upon dissolution is of fundamental importance. The key parameter characterizing the micelle stability during dissolution is the critical micellization concentration (CMC). At a given temperature, micelles are formed at polymer concentrations equal to or exceeding the CMC value. Therefore, several independent methods are employed for the determination of the CMC values for the PGMA-*b*-PPO-*b*-PGMA copolymers, namely: surface tension (Wilhelmy plate method), isothermal titration calorimetry (ITC) and a fluorescent probe technique with pyrene as probe molecule. Also the size range of micelles is an important parameter for anticipating the interaction with cells and tissues upon administration in organisms if the micelles were to be used as microcontainers for drug delivery. Therefore, micelle dimensions and the influence of temperature on micellar size are studied by dynamic light scattering.

2.2 Experimental - Synthetic Procedures

2.2.1 Materials

2,2-Dimethyl-4-hydroxymethyl-1,3-dioxolan (Solketal, 97%), 2,2'-bipyridin (99.5%) and Cu(I)Cl for analysis were purchased from Merck, methacryloyl chloride (97%), triethylamine (98%) and $Cu(II)Cl_2$ (97%) were purchased from Fluka. Poly(propylene oxide) dihydroxy-terminated (M_n~2000 g·mol^{-1}) and 2-bromoisobutyryl bromide (98%) were purchased from Aldrich.

2.2.2 Monomer Synthesis

(2,2-Dimethyl-1,3-dioxolan-4-yl)methyl methacrylate (DMM) was synthesized from 2,2-Dimethyl-4-hydroxymethyl-1,3-dioxolan and methacryloyl chloride according to a method reported elsewhere.[22] Briefly, freshly distilled triethylamine (59.7 g, 0.61 mol) was mixed in 200 mL benzene with isopropylidene glycerol (80.4 g, 0.61 mol) and cooled to ~0°C in a water-ice bath. Methacryloyl chloride (47.7 g, 0.46 mol) was vacuum distilled (Tb~44°C, 70 mbar), diluted in 100 mL benzene and added dropwise along 2 h, with stirring in a water-ice bath under argon atmosphere. The mixture was agitated for 20 h more at room temperature. The reaction mixture was filtered for removing the precipitated triethylamine hydrochloride, and the solution was washed twice with 250 mL distilled water and dried with anhydrous sodium sulphate. After filtration, 0.5 g methylene blue was added and benzene was evaporated under reduced pressure yielding a pale orange liquid. The product was purified by fractional distillation at 66-67°C (5 mbar) to give 65.8 g (0.33 mol, 72% yield) of (2,2-dimethyl-1,3-dioxolan-4-yl)methyl methacrylate as colorless liquid. 0.5 g methylene blue was added as inhibitor. See Figure 2.1.

2.2.3 Macro-initiator Synthesis

The ABA triblock copolymer was prepared using an alkylbromide derivative of poly(propylene oxide) as macro-initiator (PPO-Br) for the polymerization of (2,2-dimethyl-1,3-dioxolan-4-yl)methyl methacrylate by ATRP. The macroinitiator was synthesized by reacting the terminal hydroxy groups of poly(propylene oxide) dihydroxy-terminated (M_n~2000 g·mol^{-1}) with excess 2-bromoisobutyryl bromide (BIB) in the presence of triethylamine (TEA) in a molar ratio [PPO]:[BIB]:[TEA] 1:4:4, for two days at room temperature, according to literature.[23-25]

2.2.4 Triblock Copolymer Synthesis

The PDMM-*b*-PPO-*b*-PDMM triblock copolymers were synthesized following an ATRP method.[26] The PPO-Br macroinitiator was used to polymerize DMM in solution at 40°C using a Cu(I)Cl/Cu(II)Cl_2/2,2'-bipyridin (bpy), catalytic system at a molar ratio of 1/1/0.2/2.5 for [PPOBr]/[Cu(I)Cl]/[Cu(II)Cl_2]/[bpy],respectively. In a typical procedure Cu(I)Cl and Cu(II)Cl_2 were pestled and added together with bpy into a schlenk flask equipped with a stirring bar. This flask was then sealed with a rubber septum, evacuated, and filled with dry argon (three cycles). DMM was freshly vacuum distilled for removing the inhibitor and syringed into the reaction flask. The mixture was degassed via three freeze-thaw cycles. A solution of the PPO-Br macroinitiator dissolved in isobutyl acetate, which was freshly distilled from CaH_2, was separately degassed and transferred into the reaction flask under argon via a double-tipped needle. The added solvent was enough for getting a 20% v/v DMM solution in isobutyl acetate. After stirring, a dark brown reaction mixture was obtained. The temperature was increased to 40°C and the polymerization commenced. To monitor the extent

of polymerization of DMM, 1 mL aliquots were taken at regular intervals, quenched and immediately filtered through silica gel columns to remove the catalyst. A small amount of the filtrate was diluted with THF and evaluated by GPC. The reaction mixture was stirred for 20 h and then exposed to air while cooling. Termination occurred rapidly as indicated by the colour change from brown to green due to the aerial oxidation of Cu(I) to Cu(II). The reaction mixture was then passed through a silica gel column to remove the copper catalyst. After evaporating the solvent, the polymer was dissolved in THF and precipitated three times into cold hexane. After drying in a vacuum oven at room temperature a white, slightly yellow powder was obtained.

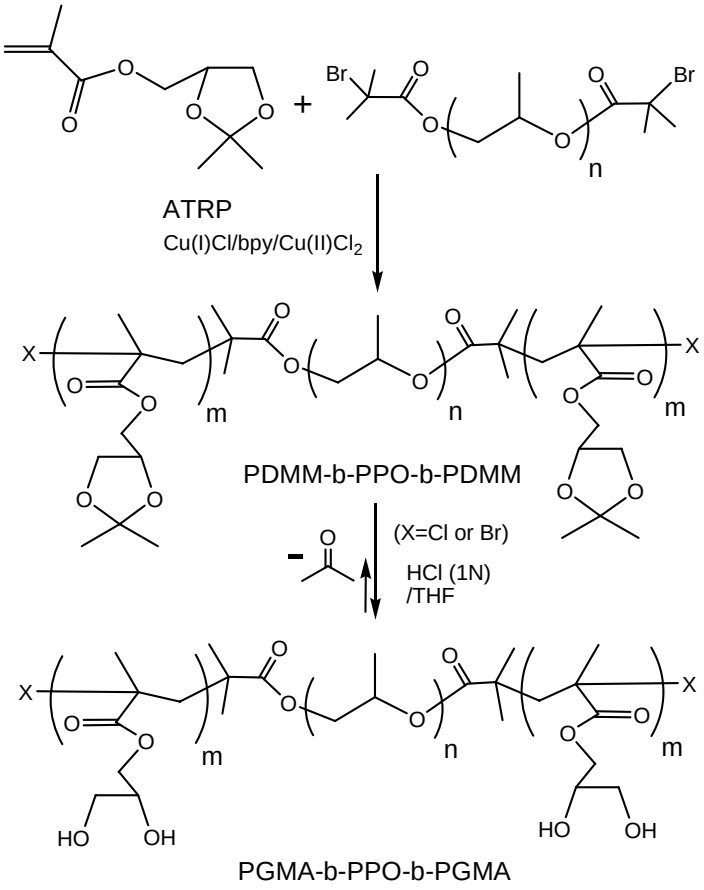

Figure 2.1: Reaction scheme for the ATRP synthesis of PDMM-*b*-PPO-*b*-PDMM using a PPO-based macroinitiator and further deprotection reaction for obtaining the PGMA-*b*-PPO-*b*-PGMA triblock copolymers.

2.2.5 Deprotection of PDMM-*b*-PPO-*b*-PDMM Triblock Copolymer

In a typical procedure,[14,15] the solution of PDMM-*b*-PPO-*b*-PDMM triblock copolymer (2.5 g) in THF (25 mL) was cooled in a water-ice bath and aqueous 1 N HCl (10 mL) was added dropwise. The solution became turbid on addition of aqueous HCl and was stirred at room temperature for 24 h. As the reaction proceeds the solution becomes gradually clear. The solution was poured into hexane-ethanol (10:1) to precipitate the polymer, which was

again reprecipitated from THF-methanol (1:4) to hexane-ethanol (4:l). Finally the deprotected polymer PGMA-*b*-PPO-*b*-PGMA was dried in a vacuum oven yielding a white powder.

2.3 Experimental - Characterization

2.3.1 Gel Permeation Chromatography (GPC)

Molar masses and molar mass distributions were assessed by GPC using THF as the mobile phase for the protected copolymers and water (GC Grade) for the deprotected ones. The GPC set-up comprised a Knauer apparatus coupled with a refractive index detector. Two Macherey-Nagel columns were used. The flow rate for the eluent was set at 1.0 $mL \cdot min^{-1}$. The columns working with THF were calibrated with a series of narrowly distributed poly(methyl methacrylate) standards, covering the M_w range from 500 to 400000 $g \cdot mol^{-1}$. The columns working with water were calibrated with PEO standards, covering the M_w range from 1500 to 23000 $g \cdot mol^{-1}$.

2.3.2 NMR, IR Spectroscopy

^{1}H NMR and ^{13}C NMR spectra were recorded on a Varian Inova 500 spectrometer in DMSO-d_6 (500 MHz for ^{1}H spectra, 100 MHz for ^{13}C spectra). Infrared (FTIR) analysis was performed on pressed KBr and spectra were recorded using a Bruker Vector 22 spectrometer.

2.3.3 Dynamic Light Scattering (DLS)

Measurements in the high temperature range, 15-45°C, were performed using a commercial equipment, ALV-NIBS/HPPS from ALV-Laser (Langen, Germany), which features a back scattering detection at a fixed scattering angle of 173°. The light source is a He-Ne laser (λ_0=632.8 nm) with a power output of 3 mW. For measurements in the low temperature range, 4-20°C, the equipment used was an ALV goniometer equipped with a Nd/YAG DPSS-200 laser (λ_0=532.8 nm) which enables measurements between 20 and 150°. The sample solutions were prepared in deionized water and filtered through 0.20 μm pore size filters into 1.5 mL volume cuvettes. The signal analyzer was an ALV-5000/E digital multiple–τ correlator. The correlation functions were analyzed by the CONTIN method, giving information on the distributions of decay rate (Γ). Apparent diffusion coefficients were obtained from $D_{app}=\Gamma/q^2$ [with $q=(4\pi n_o/\lambda)\sin(\theta/2)$ being the scattering vector, n_o=refractive index of the medium, λ=wavelength of the light, θ=scattering angle] and the corresponding apparent hydrodynamic radii, R_h (radius of the hydrodynamically equivalent sphere), were obtained via the Stokes-Einstein equation $R_h = kT/(6\pi\eta D_{app})$, where k is the

Boltzmann constant and η is the viscosity of the solvent, water in this case, corrected at the temperature T.

2.3.4 Multiangle Light Scattering (MALS)

Multiangle Light Scattering in water was employed for obtaining absolute molar masses and micellar aggregation numbers (N_{agg}) after separation of the sample in fractions by Asymmetrical Flow Field-Flow Fractionation (AF4). The details about these measurements are given in Appendix 8.2.

2.3.5 Isothermal Titration Calorimetry (ITC)

Heat of demicellization and dilution were measured using a VP-ITC titration microcalorimeter (MicroCal, Northampton, MA). The sample cell had a volume of 1.45 mL. It was filled with degassed water prior to each experiment. Polymer solutions with a concentration of around 30 times CMC were placed in a 250 μL continuously stirred (310 rpm) syringe. 50 aliquots (5 μL each) were injected into the sample cell at intervals of 480 s. Data analysis was carried out using Microcal ORIGIN software.

2.3.6 Fluorescence Measurements

Steady-state fluorescent spectra were measured using a Fluoromax 2 spectrometer (Jobin-Yvon) with a slit width of 0.5 mm (Band pass 2.125 nm) for both excitation and emission spectra. For the measurements, 1.5 mL of solution was placed in a 1.0×1.0 cm cell. All spectra were run on air-equilibrated solutions. For fluorescence emission spectra, $\lambda_{excitation}$ was 333 nm, and for excitation spectra, $\lambda_{emission}$ was 390 nm. Spectra were accumulated with an integration time of 0.1 s. Samples with a pyrene concentration of 5.4×0^{-7} M were prepared according to literature methods,[27] and were incubated at the measuring temperature for at least 24 h.

2.3.7 Surface Tension Measurements

The surface tension (γ) was measured by the Wilhelmy plate method, using a DCAT11 tensiometer (DataPhysics Instruments GmbH, Filderstadt, Germany) at 40°C. The temperature (±0.1 °C) was maintained by circulating thermostated water through the jacketed vessel containing the solution. The concentration of solution was varied by adding aliquots of stock solution of concentration of around 30×CMC through an automatic injection system. The plate was previously cleaned by heating it in a flame.

2.3.8 Adsorption at the Air-Water Interface

Adsorption experiments were performed using a circular home-built Teflon trough with a total area of 7.07 cm^2 and a volume of 11.3 mL. Polymer solutions were injected into the subphase with a Hamilton syringe through a Teflon jacket just above the bottom of the trough. The subphase was stirred with a tiny rolling sphere to ensure a homogeneous distribution of the sample without perturbing the surface. The increase of surface pressure due to the injected triblock copolymer was measured by the Wilhelmy plate method. The temperature of the subphase was maintained at 40°C by circulating thermostated water through the jacketed vessel containing the solution and inside the walls of a covering box designed to minimize water evaporation.

2.4 Results and Discussion

2.4.1 Triblock Copolymer Synthesis

Although GMA monomer has already been directly copolymerized by ATRP,[17-20] the high polarity of GMA and of the obtained PGMA makes it necessary to use very polar solvents, such as DMF, DMSO or methanol, to dissolve them, which can dramatically affect the structure and function of the catalytic species involved in ATRP.[9] Besides, due to the synthetic routes used to produce GMA, the commercial "monomer" contains in reality as much as 8% of 1,3-dihydroxypropyl methacrylate impurity, which leads after the polymerization to statistical copolymers rather than homogeneous PGMA homopolymers or blocks.[28] Consequently, in this study the protected monomer DMM was used instead, which allows to apply for the ATRP procedure similar conditions to the ones used for the thoroughly studied and well documented ATRP of methyl methacrylate (MMA).[29-31]

The choice of a 2-bromoisobutyrate for the alkyl bromide initiator was based on the finding that, since it is close in imitating the structure of the propagating methacrylate chain end it has been employed successfully in the ATRP synthesis of polar methacrylate monomers as shown by Beers *et al.*[9] It has also been shown that the use of a mixed halide initiator/catalyst system of the type R-Br/Cu(I)Cl, that is, alkyl bromide initiators in combination with copper chloride catalyst, exhibits faster initiation than the R-Cl/CuCl system and slower propagation than R-Br/CuBr. A fast rate of initiation relative to the rate of propagation is essential for a successful controlled radical polymerization. Moreover, due to the carbon-chlorine bond being stronger than the corresponding carbon-bromine bond there is a tendency of the polymer chain ends to be terminated by chlorine instead of bromine.[31] Additionally, side reactions observed in R-Br/Cu(I)Br-initiated ATRP of MMA causing the deviation of molar mass as a function of conversion[32] could be minimized with the mixed halide initiator/catalyst system, leading to better control over the molar mass at high conversions of monomer to polymer.

A ligand/Cu(I)Cl molar ratio of two has been used because although the rate of ATRP polymerization of MMA using Cu(I) halide/R-X systems reaches a maximum when the ligand/Cu(I)Cl molar ratio equals approximately 1, the reaction mixture requires too long to become homogeneous for an equimolar ratio, while Cu(I) halides dissolve much faster when an excess of ligand is used.[30] Finally, $Cu(II)Cl_2$ was added in a low molar ratio ($[Cu(II)Cl_2]_0/[Cu(I)Cl]_0$=0.2) to the reaction mixtures to increase the initial concentration of the deactivating species in solution, so as to reduce the concentration of propagating radicals and the amount of irreversible termination. The reaction scheme for the ATRP synthesis of the PGMA-*b*-PPO-*b*-PGMA triblock copolymer is outlined in Figure 2.1.

The GPC chromatograms in THF for the initial PPO_{34}-Br macroinitiator and the obtained PDMM-*b*-PPO-*b*-PDMM triblock copolymers are shown in Figure 2.2. All copolymers showed a symmetrical, monomodal molar mass distribution. The absence of more than one peak or tailing on the elution curve shows that neither homopolymers, nor diblock copolymers were produced during the polymerization. Thus, it can be claimed that only triblock copolymers were obtained. The polydispersities were quite acceptable ranging from 1.29 to around 1.40, see Table 2.1.

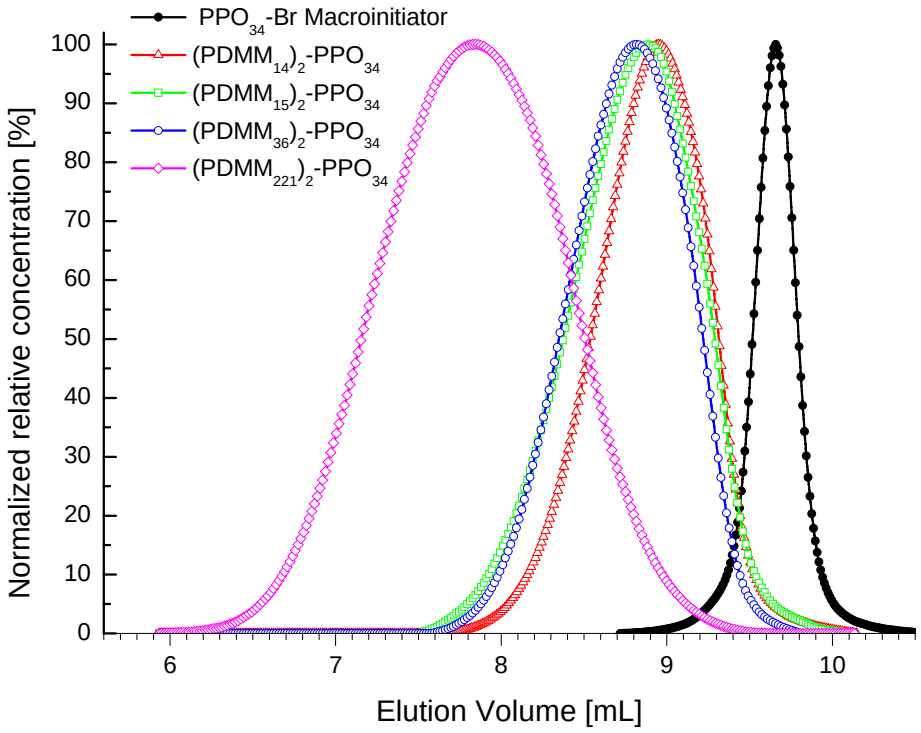

Figure 2.2: GPC chromatograms in THF for the PPO_{34}-Br macroinitiator and the synthesized PDMM-*b*-PPO-*b*-PDMM triblock copolymers.

Table 2.1: Polydispersities, Molar Masses and Degree of Polymerization for the PGMA-*b*-PPO-*b*-PGMA Triblock Copolymers. Micellar Apparent Hydrodynamic Radii (R_h) in the Temperature Range 15-40°C from DLS.

Sample	M_w/M_n [a]	*m* [b] (^{1}H NMR)	M_n (^{1}H NMR) [g/mol]	R_h [nm]
$(PGMA_{221})_2$-PPO_{34}	1.39	221	73000	~50
$(PGMA_{36})_2$-PPO_{34}	1.29	36	13600	11.4±1.8
$(PGMA_{15})_2$-PPO_{34}	1.40	15	6600	14.0±3.0
$(PGMA_{14})_2$-PPO_{34}	1.32	14	6400	10.2±1.4

[a] GPC of PDMM-*b*-PPO-*b*-PDMM in THF, PMMA standards
[b] Degree of Polymerization per PGMA block from ^{1}H NMR in DMSO-d_6

Figure 2.3 shows typical ^{1}H NMR spectra obtained for the PGMA-*b*-PPO-*b*-PGMA triblock copolymer before (a) and after (b) the deprotection reaction. The degree of polymerization for the PGMA blocks, *m*, is calculated from the ratio between the integral of the peak corresponding to the methyl group from the PPO block (peak 1, integral I_1 ,3H) and the integral of the peak corresponding to the methyl groups from both PGMA blocks (peak f, integral I_f ,6H) according to the equation: $m = (I_f \times n)/ (2 \times I_1)$, being the degree of polymerization for the PPO, $n = 34$.

On the other hand, it was found that, when the spectra are recorded in DMSO-d_6, clear peaks for each hydroxy group (-OH) of the PGMA block are obtained at 4.64 ppm (CH_2 O**H**, peak a, integral I_a ,1H) and at 4.88 ppm (CH_2 CH(O**H**)CH_2, peak a', integral $I_{a'}$,1H). These signals are well separated from the backbone peaks and do not shift or broaden as could be expected in other solvents. From the integrals for these peaks, similar values for *m* are obtained according to the equation: $m = [(I_a + I_{a'}) \times 1.5 \times n] / (2 \times I_1)$. Having *m*, the average molar masses of the original PDMM-*b*-PPO-*b*-PDMM triblock copolymers were calculated (see Table 2.1).

The differences between the M_n values obtained from ^{1}H NMR and those from GPC measurements were quite considerable: GPC values were as high as twice the ^{1}H NMR values for the two shortest copolymers. This is partially due to the fact that PMMA homopolymers were used as standards for GPC calibration. Due to the bulky acetonide ring the hydrodynamic volumes of both polymers at the same molar masses are presumably too different.

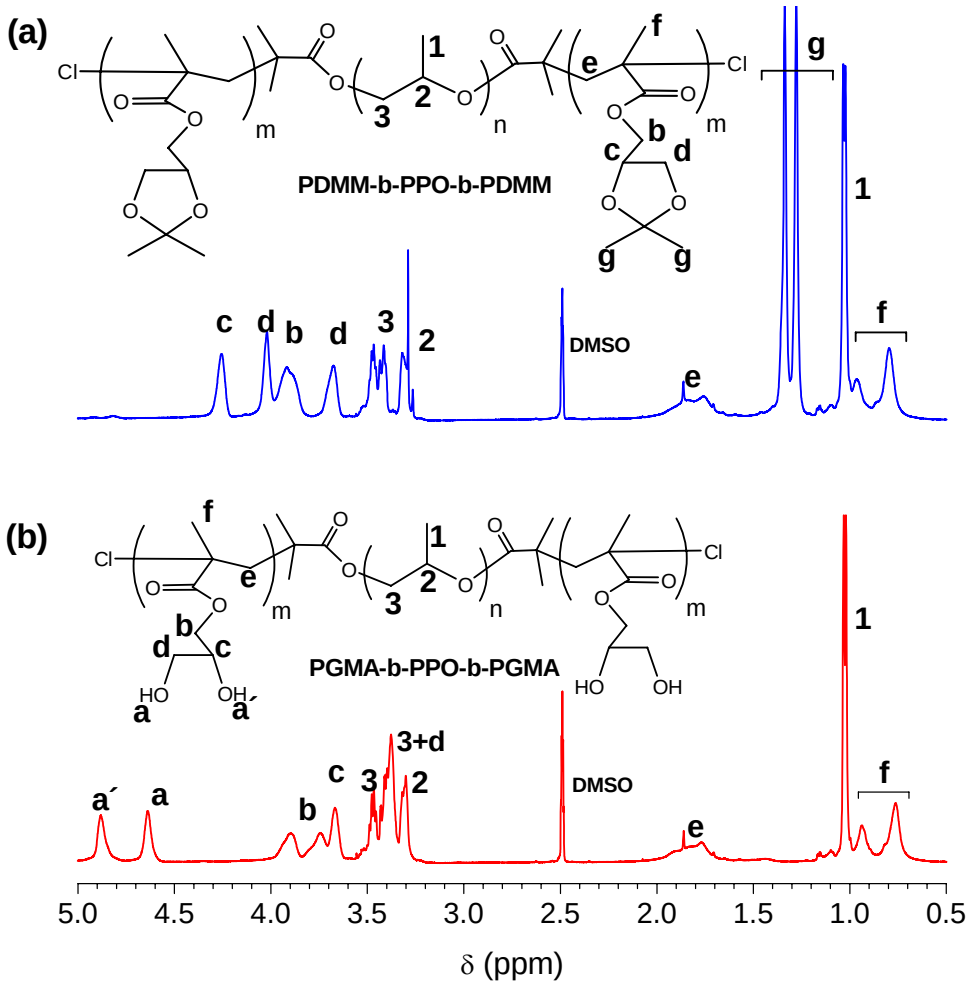

Figure 2.3: ^{1}H NMR spectra (500 MHz in DMSO-d_6). (a) $(PDMM_{14})_2$-PPO_{34} protected triblock copolymer (b) $(PGMA_{14})_2$-PPO_{34} after the deprotection reaction (HCl 1N, 24 h at room temperature).

Large disagreements between GPC and ^{1}H-NMR measurements in similar situations have been reported before.[9,16] Moreover, it is also possible that inside the GPC column additional effects, such as partitioning, were present besides the desired size exclusion separation mechanism.[33] Furthermore, it is not sure that THF is a completely nonselective solvent for both of the blocks (PDMM and PPO). Thus the elution behavior of the block copolymers may strongly depend on composition.

2.4.1.1 Removal of the Acetal Protecting Group

The 1,3-dioxolane ring in PDMM-*b*-PPO-*b*-PDMM was readily cleaved to regenerate the diol function by treating the copolymer with 1 N HCl in THF at room temperature for 24 h. In the ^{1}H NMR spectra of PGMA-*b*-PPO-*b*-PGMA (Figure 2.3), the methyl proton signals of the 1,3-dioxolane ring at 1.28 and 1.34 ppm ($C(C\underline{\mathbf{H}}_3)_2$) thoroughly disappeared after deprotection of PDMM-*b*-PPO-*b*-PDMM. Likewise, in the ^{13}C NMR spectra (Figure 2.4) the carbon signals of the dioxolane ring at 108.78 ppm ($O\underline{\mathbf{C}}O$) and at 25.15 and 26.46 ppm ($C(\underline{\mathbf{C}}H_3)_2$) also disappeared.

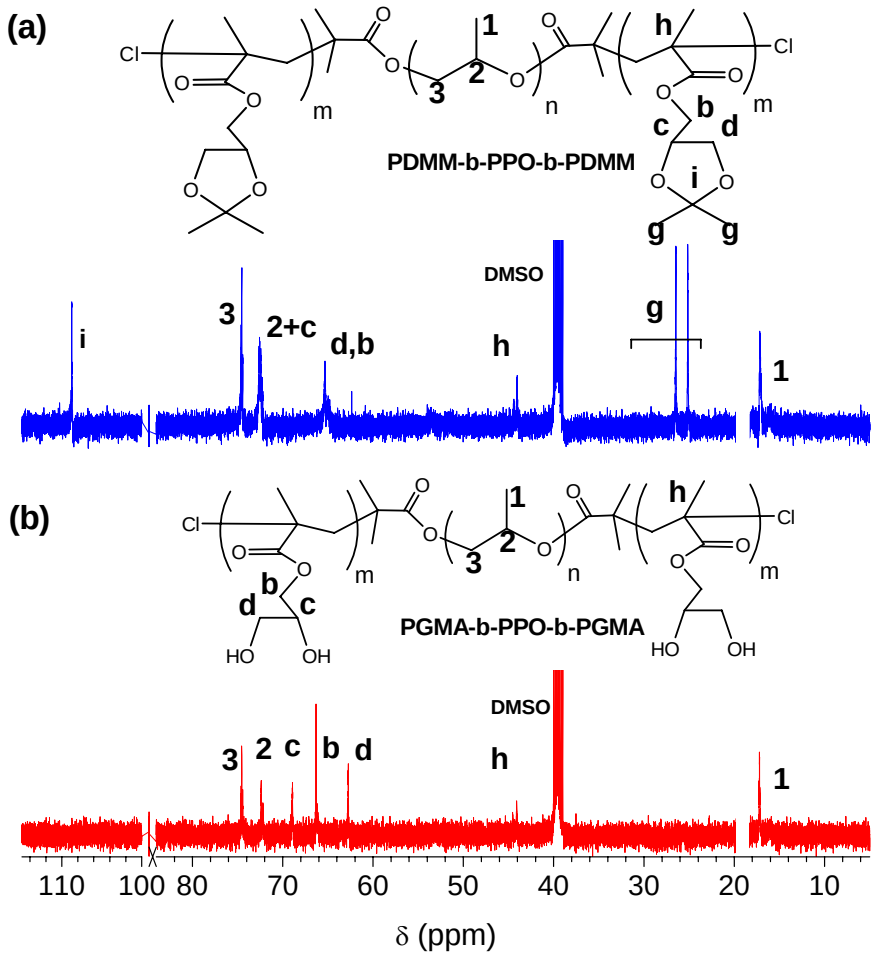

Figure 2.4: ^{13}C NMR spectra (100 MHz in DMSO-d_6). (a) $(PDMM_{15})_2$-PPO_{34} triblock copolymer (b) $(PGMA_{15})_2$-PPO_{34} after the deprotection reaction (HCl 1N, 24 h at room temperature).

Figure 2.5 shows the comparison between FTIR spectra in KBr of the PGMA-*b*-PPO-*b*-PGMA triblock copolymer before (a) and after (b) the deprotection reaction. A very strong OH stretching band due to the diol function appeared after deproctection at 3000-3750 cm^{-1}. Also a new band at 1119 cm^{-1} corresponding to the (**C-O**) stretching vibration from a secondary alcohol is observed. The deformation bands due to the geminal methyl group of the dioxolane ring (C(**CH_3**)**$_2$**) at 1372-1382 cm^{-1} (doublet) almost disappeared after deprotection. Accordingly, the methyl (-**CH_3**) asymmetrical stretching band at 2988 cm^{-1} decreased significantly. The characteristic carbonyl (**C=O**) stretching band shifted from 1733 cm^{-1} to lower frequencies 1728 cm^{-1}. This shift has been ascribed before to hydrogen bonding between the carbonyl and diol groups in the deprotected polymers.[34,14] Also the disappearance of the peaks at 513 and 842 cm^{-1} coming from the acetonide ring is in agreement with the removal of the protecting group. On the other hand, while the (**C-O-C**) stretching absorption at 1087 cm^{-1} coming from only the acetal group disappears, the (**C-O-C**) stretching absorption coming from both the ester and acetal groups at 1055 cm^{-1} is still present after the deprotection reaction. Therefore, it is concluded that the ester group remained intact during the hydrolysis of the acetonide ring.

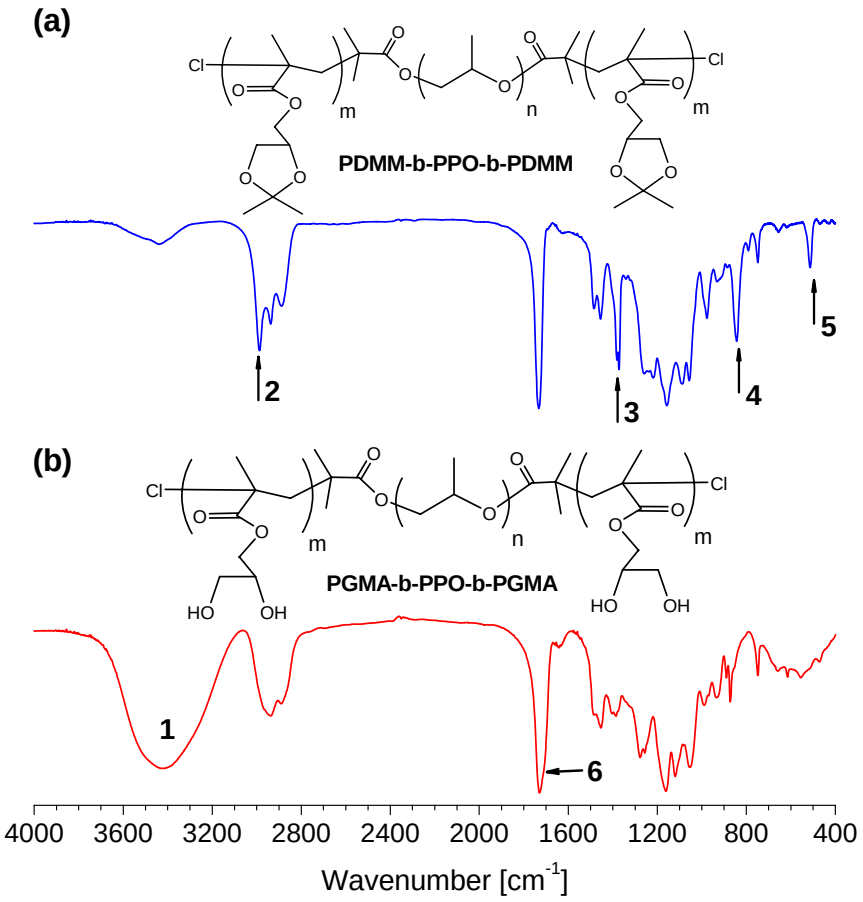

Figure 2.5: FTIR spectra in KBr (a) $(PDMM_{36})_2$-PPO_{34} triblock copolymer (b) $(PGMA_{36})_2$-PPO_{34} after the deprotection reaction (HCl 1N, 24 h at room temperature). The peaks marked are derived from: Diol group (**1**, 3000-3750 cm^{-1}); Geminal methyl groups on acetonide ring (**2**, 2988 cm^{-1}) and (**3**,1372,1382 cm^{-1}); Acetonide ring (**4**, 842 cm^{-1}) and (**5**, 513 cm^{-1}); Carbonyl group (**6**, 1728 cm^{-1}).

In conclusion, both NMR and FTIR results verify that the complete removal of the acetonide protecting group was achieved. All PGMA-*b*-PPO-*b*-PGMA copolymers obtained were soluble in water, methanol and DMSO and insoluble in hexane, THF, chloroform and ethanol. In contrast, PDMM-*b*-PPO-*b*-PDMM copolymers were insoluble in water and soluble in THF and chloroform, which indicates that the presence of the two hydroxy groups on the repeating unit of PGMA-*b*-PPO-*b*-PGMA enhanced the hydrophilicity significantly.

2.4.2 Association of PGMA-*b*-PPO-*b*-PGMA in Water

2.4.2.1 GPC Measurements.

GPC has already been used to detect aggregates and study micellization, due to its ability for detecting hydrodynamic size distributions, based on the differences in hydrodynamic radii. In particular, GPC has been applied for the determination of the relative amounts of micelles and unimers (single chains) as well as the size distribution of micelles.[35] However, it must be kept in mind that GPC suffers from the complex problem of solution dilution inside the columns, which can disturb micellization equilibriums during the measurement and causes misleading results.

The GPC chromatograms in water for the deprotected PGMA-*b*-PPO-*b*-PGMA triblock copolymers (1% w/w aqueous solutions) are shown in Figure 2.6. The chromatograms of all samples show two separated peaks, which unfortunately lay outside the calibration range of the columns. The peak at shorter elution times (higher molar masses) might correspond to associated species, micelles or aggregates. The second peak corresponds probably to triblock copolymers unimers. However, a further analysis coming from more suitable techniques such as DLS was necessary to interpret quantitatively these results. Nevertheless, micellization or association in water was already evidenced by these GPC measurements.

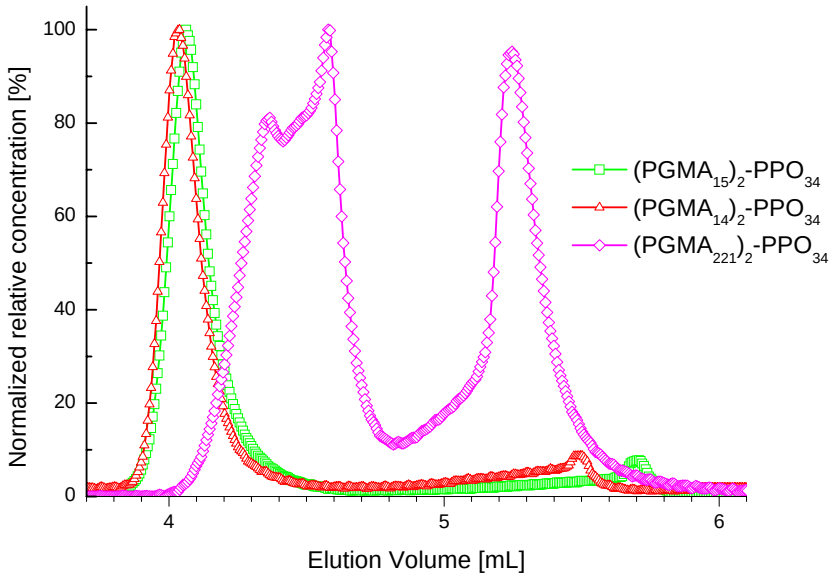

Figure 2.6: GPC chromatograms in water for the deprotected PGMA-*b*-PPO-*b*-PGMA triblock copolymer. Concentration 1% w/w.

2.4.2.2 DLS Studies.

GMA homopolymer is highly hydrophilic and exhibits no lower critical solution temperature (LCST) in aqueous solution. [19,28] It is also water-soluble over the whole pH range at room temperature.[18] On the other hand, the PPO block exhibits LCST phase behavior with the cloud point temperature being dependent on its molar mass. In the case of PPO_{34}, the cloud point is at around 10°C. At this temperature the PPO block becomes less soluble in water, and is expected to trigger a self-assembly process which should lead to the formation of micelles with PPO cores and PGMA coronas. In spite of this, the PPO block is still sligthly soluble even at 20 °C, so well-defined micelles are not expected to form at ambient temperature. Moreover, also other aggregation morphologies are possible. It has already been shown, for triblock copolymers with ABC architecture, that an outer PGMA block is effective in minimizing inter-micellar fusion at high polymer concentrations, however some micellar aggregation phenomena at elevated temperatures (>40°C) have been reported and are believed to involve inter-micelle hydrogen bonding.[17]

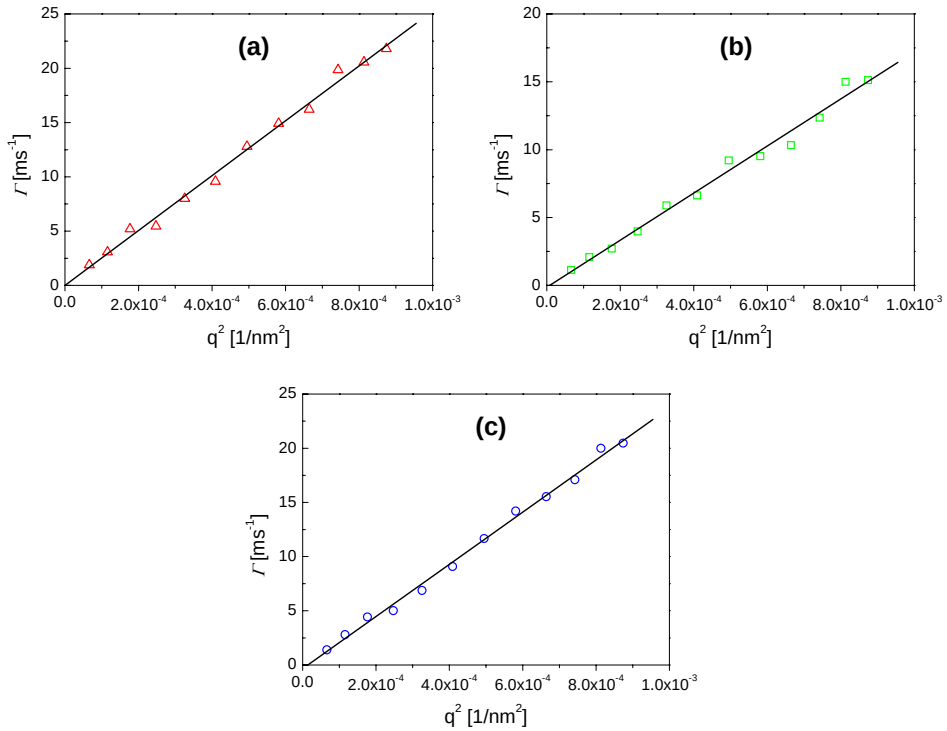

Figure 2.7: Relaxation rate (Γ) as a function of the square of the magnitude of the scattering vector (q^2) at 30°C for aqueous solutions of: (a) $(PGMA_{14})_2$-PPO_{34}, 1.4 mM ; (b) $(PGMA_{15})_2$-PPO_{34} , 1.5 mM; and (c) $(PGMA_{36})_2$-PPO_{34} , 1.0 mM.

From these considerations the PGMA-*b*-PPO-*b*-PGMA triblock copolymers were expected to be thermoresponsive in aqueous solution since the GMA block is permanently hydrophilic, whereas the PPO block becomes increasingly insoluble at higher temperatures. The specific behavior would depend on the ratio of molar masses between both types of blocks.

From the DLS measurements, the distributions of apparent hydrodynamic radii (R_h) were obtained by nonlinear fitting of the intensity correlation functions. In order to confirm that the signals detected are really caused by translational diffusion processes, angular dependent measurements of the decay rates (Γ) between 30° and 140° were performed at 30°C. The linear relationships obtained between Γ and the square of the scattering vector, q^2 (see Figure 2.7), confirm that the observed peaks are due to diffusive processes. Figure 2.8 shows the scattered intensity per particle size class for the $(PGMA_{14})_2$-PPO_{34} and $(PGMA_{15})_2$-PPO_{34} triblock copolymers at concentrations of around 12×CMC and 40×CMC, respectively (see below for CMC determination). In the high temperature range (Figure 2.8a) the distributions for micelles exhibit well defined and relatively narrow peaks. This contrasts to a recent report by Rannard *et al.*[17], who found a huge size decrease with increasing temperature (from R_h=35 to 15 nm for 30°C and 70°C respectively) for micelles formed by a $PGMA_{50}$-$PDMA_{20}$-PPO_{36} triblock copolymer. They explained such contraction as due to progressive dehydration of the PPO core. In the case of $(PGMA_{14})_2$-PPO_{34} the size of the micelles remains approximately constant in the high temperature range, R_h=10.2±1.4 nm. For $(PGMA_{15})_2$-PPO_{34}, R_h=14.0±3.0 nm. No evidence of remarkable micelle contraction was found.

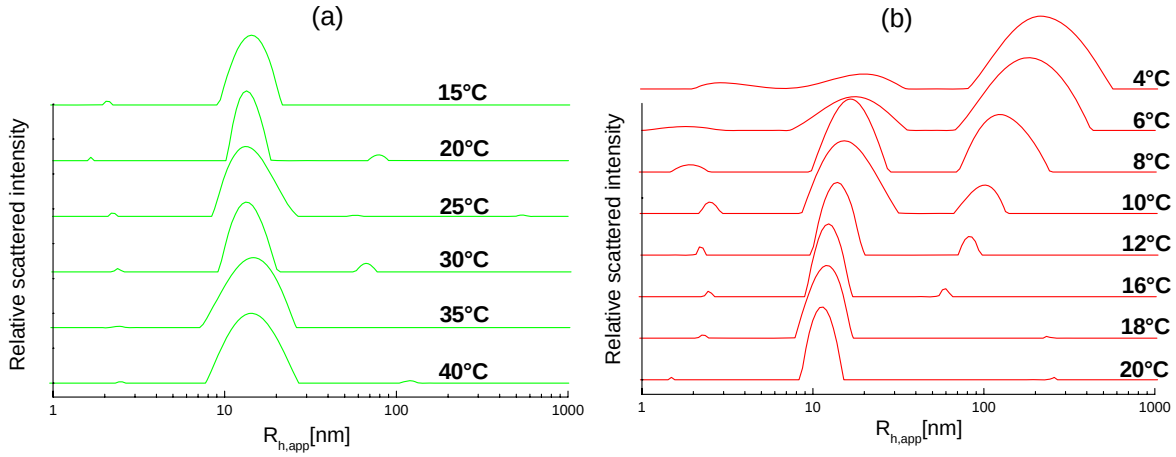

Figure 2.8: Distributions of apparent hydrodynamic radii (R_h) for (a) $(PGMA_{15})_2$-PPO_{34} triblock copolymer, 7.0 mM, temperature range 15-40°C and (b) $(PGMA_{14})_2$-PPO_{34}, 1.4 mM, between 4-20°C.

Nevertheless the weight fraction of the copolymer present as micelles (see the corresponding mass weighted distributions of R_h in Appendix 8.3) does change significantly with increasing temperature growing from 30.0% w/w at 15°C up to 91.4% w/w at 40°C for $(PGMA_{14})_2$-PPO_{34} and from 19.6% w/w at 15°C up to 75.5% w/w at 40°C for $(PGMA_{15})_2$-PPO_{34}. This temperature-dependent micellization is attributed to the increasing insolubility of the PPO block with increasing temperatures, which favours micelle formation. Besides, unimers sizes were approximately the same for both copolymers: R_h=2.1±0.5 nm for $(PGMA_{14})_2$-PPO_{34} and R_h=2.1±0.4 nm for $(PGMA_{15})_2$-PPO_{34}. In the low temperature range (Figure 2.8b), when the temperature is lowered down to 4°C the micelle peak disappears almost completely (when the mass weighted distribution is considered). It amounts to less than 1% w/w of the total copolymer, which indicates that most of the triblock copolymer was molecularly dissolved in water at this temperature. The mass fraction of micelles in comparison to unimers was significant only above 8°C (3.4% w/w) and increased steadily up to 32.4% w/w at 20°C. Therefore, 8°C corresponds approximately to the critical micellization temperature (CMT) for $(PGMA_{14})_2$-PPO_{34} at a concentration of 1.4 mM.

In the case of $(PGMA_{36})_2$-PPO_{34} (Figure 2.9), although an approximately constant value of R_h=11.4±1.8 nm for the micelles is observed between 20-40°C, at lower temperatures the micelles peak decreases drastically and amounts to only 1.7% w/w of the total copolymer at 15°C. The CMT for $(PGMA_{36})_2$-PPO_{34} at a concentration of 1mM was found to be around 19°C. For the unimers peak R_h=2.5±0.4 nm, which is slightly higher than the value obtained for the shorter triblocks.

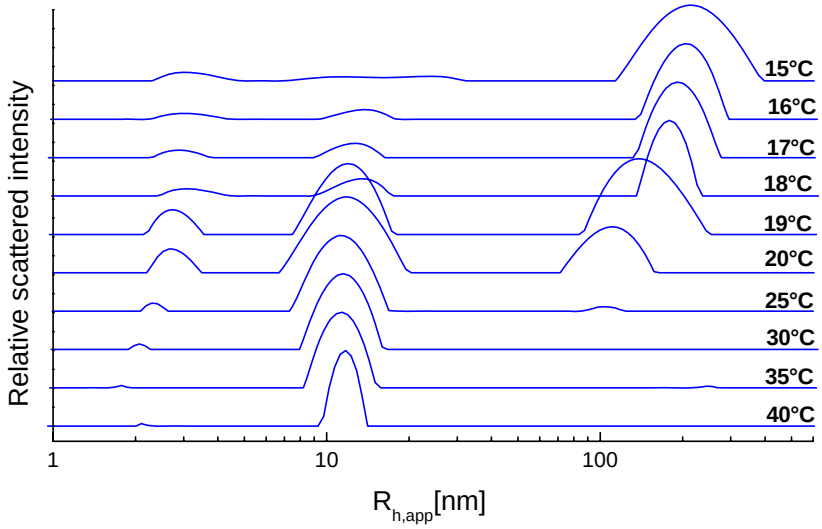

Figure 2.9: Distributions of apparent hydrodynamic radii (R_h) in the temperature range 15-40°C for $(PGMA_{36})_2$-PPO_{34} triblock copolymer at 1 mM concentration.

On the other hand, one additional population with R_h~175-215 nm is observed between 15-20°C, which is not be attributed to micelles but to some kind of aggregates. This population corresponds to a fraction of 1.0-1.5% w/w of the total and disappears completely above 20°C, simultaneously with a significant increase in the micelle population. This observation suggests that above the CMT micelles are formed, at least partially, at expense of the dissociation of the aggregates. Armes and co-workers proposed that in the case of PPO-PGMA diblock copolymers the presence of similar aggregates might be due to clustering of micelles.[28] On the contrary, the aggregation process might be due to intra- and intermolecular hydrogen bonding of adjoining hydroxy groups, in a way similar to what is observed for other highly hydroxylated polymers such as poly(vinyl alcohol) (PVA).[36] For PVA the strong hydrogen bonding causes a remarkable decrease in its solubility in water.[37] Consequently, DLS experiments were performed on aqueous solutions of PGMA homopolymer ($PGMA_{75}$ and $PGMA_{104,}$ 1mM). Aggregates with R_h ranging from 60 to 100 nm depending on temperature were found. However such aggregates corresponded to around 0.05% w/w of the total homopolymer present and therefore only a tendency to aggregation could be evidenced for the homopolymers.

For $(PGMA_{221})_2$-$PPO_{34,}$ bearing a considerably larger PGMA block, a multimodal distribution with two or even three populations was observed depending on temperature. In the whole temperature range (15-45°C) mostly unimers (R_h~4.5 nm) were present. However, also aggregates (R_h~240 nm) below 30°C and micelles (R_h~50 nm) above 25°C, corresponding to a maximum of 0.5% w/w of the total population, were found. This temperature dependent process is similar to the one described for $(PGMA_{36})_2$-PPO_{34}, but micelles and aggregates fractions are minor compared to unimers for the largest PGMA block, while the CMT is about 25°C for $(PGMA_{221})_2$-PPO_{34} at a concentration of 1.1 mM.

The weight average contour length (L_w) of the PGMA blocks can be estimated by multiplying the degree of polymerization per block derived from ^{1}H-NMR measurements by the polydispersities found from GPC (2.1) and the extended length of a monomeric vinyl unit (2.546 Å).[38] One obtains 4.65, 5.16, 11.9 and 78.3 nm, for 14, 15, 36 and 221 PGMA units respectively. The radius of the PPO core can be estimated, under the assumption that the micelles are spherical in shape and their core is formed by condensed (liquid like) PPO blocks, from the equation [39]:

$$R_{core} = \sqrt[3]{\frac{3nN_{agg}M_{PO}}{4\pi N_A \rho_{po}}} \qquad (2.1)$$

Where n is the degree of polymerization of the PPO block (n = 34), M_{PO} is the molar mass of the oxypropylene unit (M_{PO} = 58 g/mol), ρ_{PO} is the density of liquid PPO (ρ_{PO} = 1.01 g/cm^3), N_A is the Avogadro's constant, and N_{agg} is the micellar aggregation numbers derived from Asymmetrical Flow Field-Flow Fractionation (AF4) measurements (see Appendix 8.2 for details). N_{agg} = 31, 40 and 32 respectively. A value of about 3 nm for R_{core} is obtained for all samples. This estimate neglects the possible penetration of water and PGMA into the micelle core and gives therefore a lower limit for the core size. Adding this value to the L_w of the PGMA blocks one obtains 7.7, 8.2, 14.9 and 81.3 nm as radii for the micelles having 14, 15, 36 and 221 PGMA units per block respectively. Comparing these values with the R_h values from DLS (10.2, 14.0, 11.4 and 50 nm, respectively), they are in agreement with the PGMA blocks being coiled to some extent in the corona of the micelle for the longest and intermediate PGMA blocks and would imply a highly improbable all-trans conformation for the two shortest blocks. Therefore, it must be concluded that the PPO core of the micelles is not found in the assumed condensed liquid-like state, but in a hydrated and expanded state, which can also be expected due the partial, although slight solubility of the PPO block in water. Similar conclusions have been drawn from studies of Poloxamer 184, a PEO-*b*-PPO-*b*-PEO ABA triblock copolymer having a PPO middle block of ~30 propylene oxide units.[40]

The length of the propylene oxide unit in a fully extended configuration, assuming bond angles of 110° together with the characteristic bond length for carbon-carbon bonds (1.54Å) and for carbon-oxygen bonds (1.43Å), is calculated as 3.60Å and the contour length of a PPO chain with n/2 units (n=34) equals 6.12 nm which is an upper limit for the core size. Adding this value to the L_w of the PGMA blocks, one obtains 10.8, 11.3, 18.0 and 84.4 nm for the radii of micelles having 14, 15, 36 and 221 PGMA units per block respectively. Although these values are in better agreement with the experimental DLS R_h values, they are still a little too small especially for the shorter triblocks. There are various possible explanations for this discrepancy between L_w and experimental R_h values:

(i) In the first place, the occurrence of a transition from spherical micelles to cylindrical micelles for the shorter members of this homologous series is possible. Such a transition has been described and discussed before for dilute solutions of ABA triblock copolymers of the type PEO-*b*-PPO-*b*-PEO, for

example EO_{27}-PO_{39}-EO_{27}.[41] The transition occurs when, as a consequence of an increase in N_{agg} , the radius of the micelle core exceeds the stretched length of half the hydrophobic core and is favoured if the hydrophilic blocks are short (which leads to high association numbers) and if the hydrophobic blocks are also short (which sets a low limit on the radius of a spherical micelle).[42] In this study the highest discrepancy between L_w and R_h is shown precisely by the $(PGMA_{15})_2$-PPO_{34} triblock which is also the one having the biggest association number (N_{agg}=40, *versus* 31 and 32 for $(PGMA_{14})_2$-PPO_{34} and $(PGMA_{36})_2$-PPO_{34} respectively).

(ii) The second factor playing a role is molar mass polydispersity. By studying the factors influencing the anomalous micellization behavior of Poloxamer 184, it has been unambiguously concluded by Zhou *et al.*[42] that the origin of such perturbations is the polydispersity of the copolymers.

The combination of these two effects could explain the considerable difference in R_h between the $(PGMA_{15})_2$-PPO_{34} and $(PGMA_{14})_2$-PPO_{34} triblocks: the former has also the highest polydispersity of all samples, 1.40 *versus* 1.32 for the latter.

2.4.3 CMC Determination

2.4.3.1 Surface Tension Measurements

This method relies on the fact that an increase in surfactant concentration leads to a decrease in the surface tension; the micelle formation at the CMC causing a break in this dependence. The measured surface tension values were plotted as a function of logarithm of surfactant concentration and the CMC value was determined by the crossing point of the straight lines that continue the surface tension vs log concentration curves before and after the break. A representative plot of surface tension (γ) vs logarithm of surfactant concentration (log C) for $(PGMA_{36})_2$-PPO_{34} is shown in Figure 2.10. The CMC values determined according to this method are given in Table 2.2.

2.4.3.2 Adsorption Kinetics at the Air-Water Interface

To obtain information about the adsorption behavior of the triblock copolymers at the air/water interface, different volumes of an aqueous solution of the copolymer were injected into the water-filled trough, and the subsequent increase in surface pressure was monitored.[43] The surface tension γ is directly measured using the Wilhelmy plate method and relates to the surface pressure Π by $\Pi=\gamma_0-\gamma$ where γ is the surface tension for a monolayer-covered water surface and γ_0 is the surface tension of the neat water surface (γ_0 =69.6 mN/m at 40°C). This method can also be used to determine the CMC.

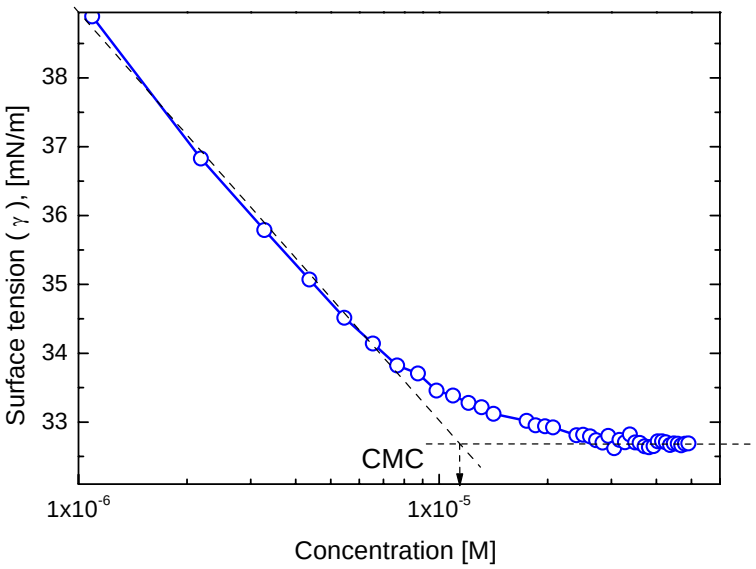

Figure 2.10: Determination of CMC from the experimental surface tension (γ) vs logarithm of surfactant concentration (log C) for $(PGMA_{36})_2$-PPO_{34} in water at 40°C.

Figure 2.11 shows the time-dependent surface pressure increase during the adsorption process of $(PGMA_{14})_2$-PPO_{34} (Figure 2.11a) and $(PGMA_{221})_2$-PPO_{34} (Figure 2.11b) at the air water interface after being injected at the bottom of the circular trough with stirring at 40°C.When only a small volume of the polymer solution was injected, there was an induction period where no significant increase in surface pressure occurs. For higher concentrations such induction period does not exist and a steep increase of Π is observed. In all cases a constant Π value is reached at the plateau region of the isotherms. The time for reaching this value depends on the concentration and on the length of the PGMA blocks. For $(PGMA_{14})_2$-PPO_{34} it varies between 6 min (for a total concentration in the trough of 36 μM) and around 4 h (for a total concentration of 73 nM). As could be expected the absorption at the air-water interface for the bulkier $(PGMA_{221})_2$-PPO_{34} takes longer, ranging from 40 min (for a total concentration of 91 μM) and around 5 h (for a total concentration of 920 nM). It can be seen from Figure 2.11 that above a certain concentration the plateau values are constant due to the fact that the CMC is reached. Therefore the CMC can also be determined from this type of measurement. The values obtained from these experiments are in agreement with those obtained by the first method.

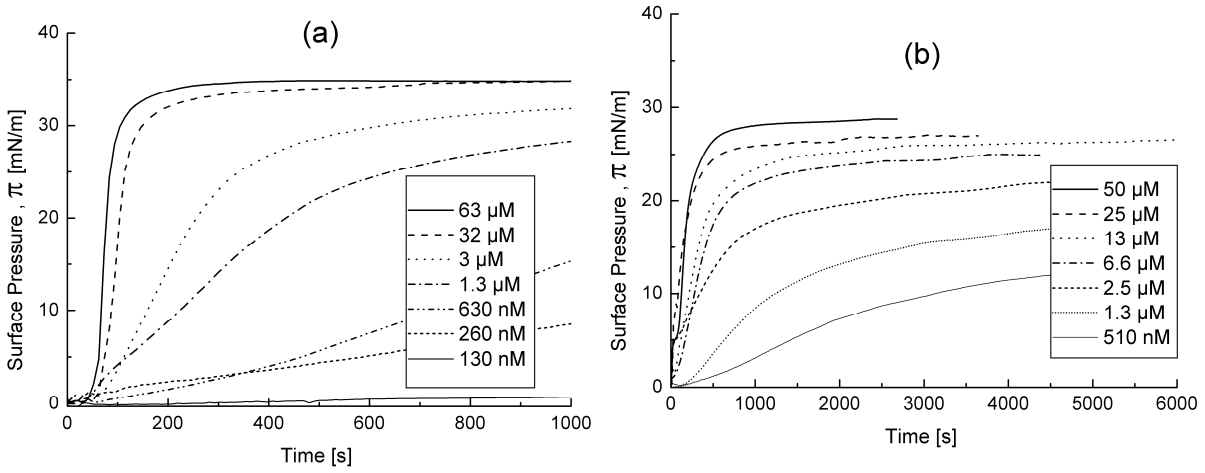

Figure 2.11: Time-dependent surface pressure increase during the adsorption process of (a) $(PGMA_{14})_2$-PPO_{34} and (b) $(PGMA_{221})_2$-PPO_{34} at the air water interface after being injected at the bottom of a circular trough with stirring at 40°C. The corresponding total concentration of the triblock copolymer in the trough for each experiment is given in the legend.

2.4.3.3 Fluorescence Studies

The pyrene solubilization technique has been used previously for the determination of the CMC in block copolymer solutions.[39,44] The pyrene fluorescence is sensitive to changes in the microenvironment which permits monitoring its incorporation into micelles at concentrations exceeding CMC. Figure 2.12 shows typical emission spectra of pyrene (5.4×10^{-7} M) in the presence of different concentrations of $(PGMA_{15})_2$-PPO_{34}. Figure 2.13 shows the corresponding pyrene excitation spectra. Both kinds of spectra, emission and excitation, are characteristic of pyrene monomer fluorescence in specific microenvironments. With increasing PGMA-*b*-PPO-*b*-PGMA concentration in the aqueous solution of pyrene, the intensity ratio between the first and the third vibrational band (I_1/I_3) in the emission spectra decreases from 1.9, typical of pyrene in water, down to around 1.3 indicating the location of pyrene in a hydrophobic environment. On the other hand, a shift of the (0,0) band in the excitation spectra from 334 nm to 336 nm is observed. This shift accompanies the transfer of pyrene molecules from a water environment to the hydrophobic micellar cores and thus provides information on the location of the pyrene probe in the system. Thus, the intensity ratio I_{336}/I_{334} of the (0,0) band of pyrene serves as a measure of the polarity of the environment and therefore is sensitive to the onset of micellization.[27] This ratio varied from 0.86 for water to 0.98 for PGMA and 1.20 for a PPO aqueous solution, all measured at 40°C.

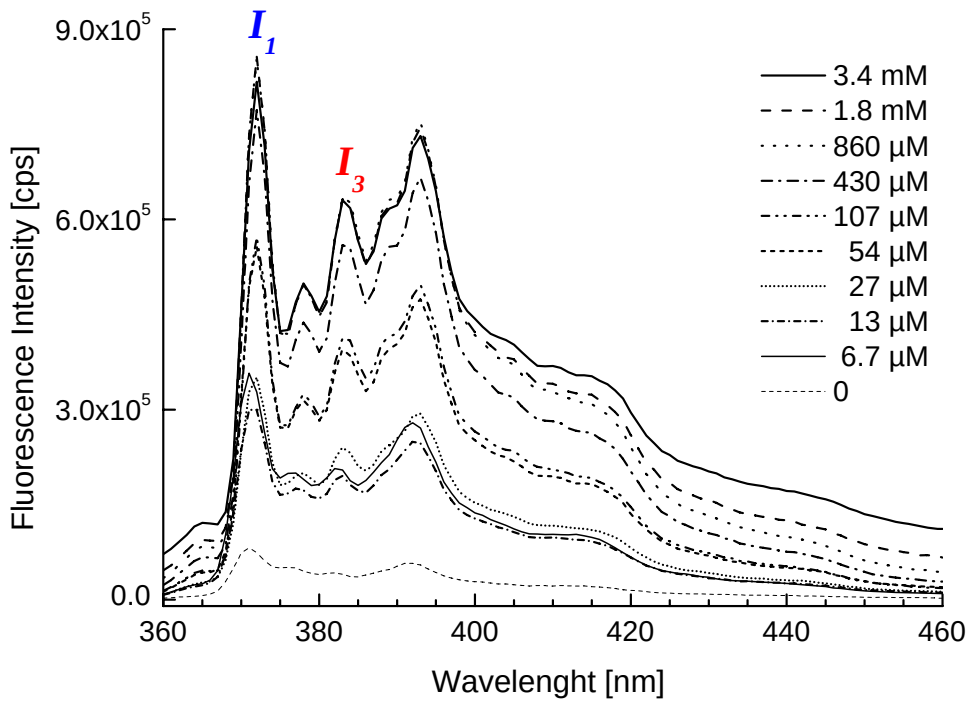

Figure 2.12: Emission spectra of pyrene (5.4×10^{-7} M) in aqueous solutions in the presence of different concentrations of $(PGMA_{15})_2$-PPO_{34}. Noteworthy is the change in the intensity ratio of the first (I_1) and third (I_3) pyrene vibrational bands. λ_{ex}=333 nm.

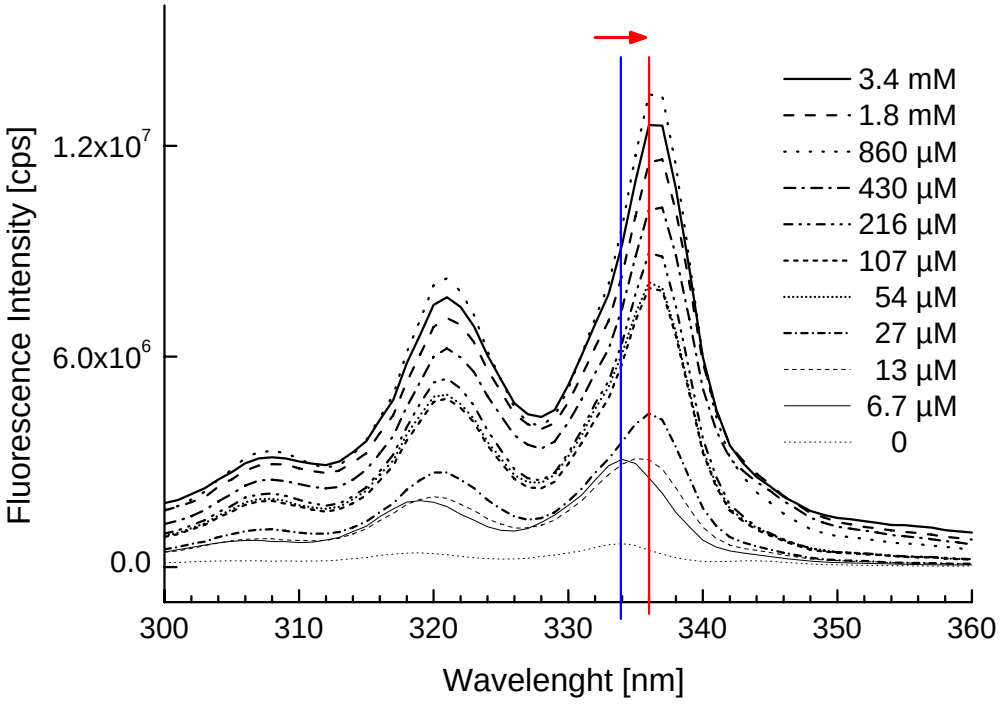

Figure 2.13: Excitation spectra of pyrene (5.4×10^{-7} M) in aqueous solutions, monitored at λ_{em}=390 nm, in the presence of different concentrations of $(PGMA_{15})_2$-PPO_{34}, showing the shift in the (0,0) band as pyrene partitions between aqueous and micellar environments.

A plot of the intensity ratio I_{336}/I_{334} from the excitation spectra as a function of $(PGMA_{221})_2$-PPO_{34} concentration is shown in Figure 2.14. The CMC values were taken as the intersection of straight line segments, drawn through the points at the lowest polymer concentrations, which lie on a nearly horizontal line, with that going through the points on the rapidly rising part of the plot. (see Figure 2.14). The CMC values found are given in Table 2.2.

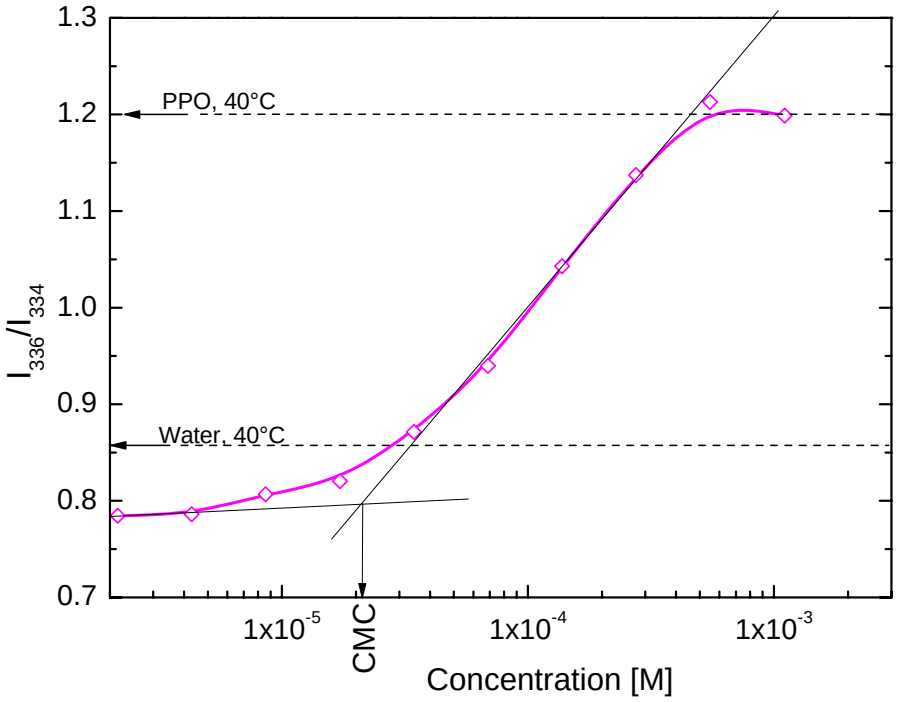

Figure 2.14: Intensity ratio I_{336}/I_{334} from pyrene excitation spectra as a function of $(PGMA_{221})_2$-PPO_{34} concentration at 40°C.

Table 2.2: Comparison of CMC Values as Determined from Surface Tension, Isothermal Titration Calorimetry and Fluorescence Measurements along with Thermodynamic Parameters for the Micellization of PGMA-*b*-PPO-*b*-PGMA Triblock Copolymers Derived from ITC Data at 40°C.

			ITC			
Sample	**CMC Wilh.-Platte [M]**	**CMC [a] Fluoresc. [M]**	**CMC ITC [M]**	**ΔH^o micell. [kJ/mol]**	**ΔG^o micell. [kJ/mol]**	**ΔS^o micell. [kJ/mol·K]**
$(PGMA_{221})_2$-PPO_{34}	-	2.1×10^{-5}	-	-	-	-
$(PGMA_{36})_2$-PPO_{34}	1.1×10^{-5}	8.1×10^{-6}	1.9×10^{-5}	44.99	-38.78	0.27
$(PGMA_{15})_2$-PPO_{34}	1.7×10^{-4}	$<6.7\times10^{-6}$	1.1×10^{-4}	7.25	-34.18	0.13
$(PGMA_{14})_2$-PPO_{34}	1.1×10^{-4}	$<2.1\times10^{-6}$	5.2×10^{-5}	11.57	-36.13	0.15

[a] Determined from the intensity ratio I_{336}/I_{334} in pyrene excitation spectra

2.4.4 Isothermal Titration Calorimetry (ITC) Studies

2.4.4.1 Analysis of the ITC Enthalpograms

ITC is a widely used method to determine CMC values of surfactants. Its advantage is the parallel determination of the micellization enthalpy and the CMC, from which the free energy of micellization can be determined.[45-47]

Normally asymmetric sigmoidal titration curves are obtained and the enthalpy of micellization is obtained from the step height. As the enthalpograms obtained here did not present clear sigmoidal features, the enthalpy of demicellization, $\Delta H_{demic.}$, is more difficult to determine. The difference between the linearly extrapolated upper curve into the CMC region and the first values of the titration enthalpy was taken as the demicellization enthalpy $\Delta H_{demic.}$ (see Figure 2.15). The CMC value was estimated by taking the concentration value at the half height of the enthalpogram.

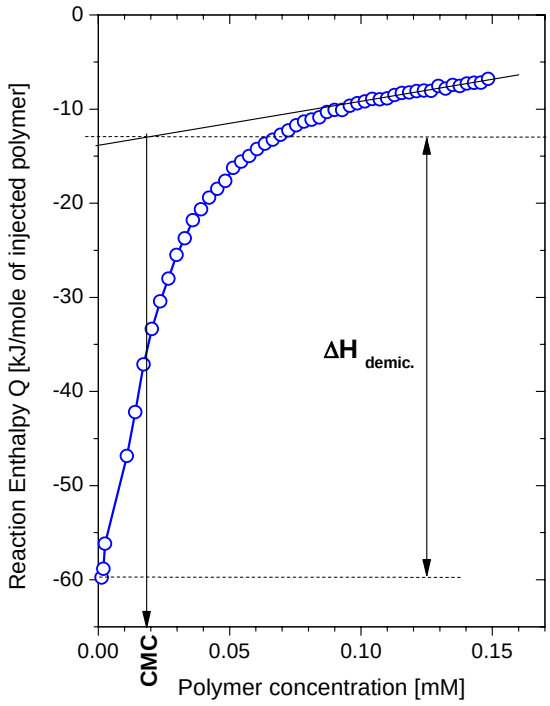

Figure 2.15: Determination of the enthalpy of demicellization, $\Delta H_{demic.}$ and the CMC from the experimental enthalpograms obtained by titration of a 1 mM $(PGMA_{36})_2$-PPO_{34} solution into water at 40°C (step size 5 µL).

All demicellization enthalpies were negative. For the demicellization of low molar mass surfactants a strong temperature dependence of the demicellization enthalpy is usually observed with a specific temperature where ΔH_{demic} is zero.[45] This specific temperature is higher for surfactants with large polar groups and the demicellization enthalpy at constant temperature becomes more negative for surfactants with larger polar groups. A similar effect seems to apply for the block copolymers, *i.e.* $(PGMA_{36})_2$-PPO_{34} has a more negative demicellization enthalpy than the block copolymers with the shorter PGMA segments.

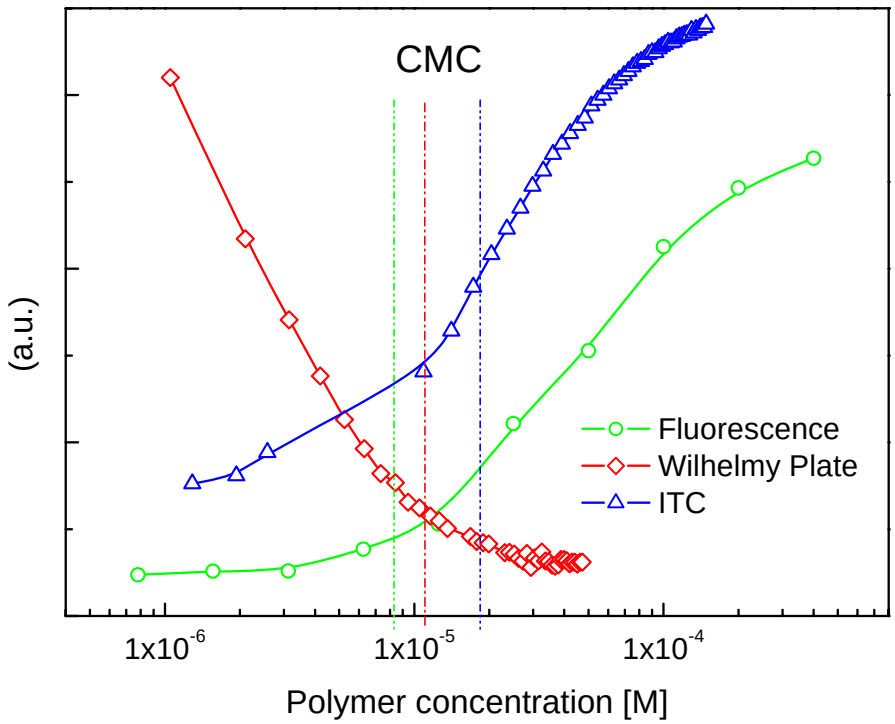

Figure 2.16: Determination of CMC by different techniques for $(PGMA_{36})_2$-PPO_{34} in water at 40°C. Method / Measured quantities: Fluorescence / Intensity ratio I_{336}/I_{334} from pyrene excitation spectra (green curve); Wilhelmy Plate / Surface tension (γ) (red curve); and ITC / ΔH demicellization (blue curve).

2.4.4.2 Determination of the Thermodynamic Parameters.

The value of the critical micellization concentration (CMC) of a nonionic surfactant in aqueous solution has been widely used to determine the free energy of micellization of the surfactant, $\Delta G_{mic.}$, that is, the standard Gibbs free energy of transfer of a polymer chain from the water phase into a micelle, using the relationships:[48]

$$\Delta G^{o}_{mic.} = RT\,(\ln CMC) \qquad (2.2)$$

The change in entropy, $\Delta S_{mic.}$, can easily be obtained using the Gibbs-Helmholtz equation:[49]

$$\Delta S^{o}_{mic.} = (\Delta H^{o}_{mic.} - \Delta G^{o}_{mic.})/T \qquad (2.3)$$

The term $\Delta G^{o}_{mic.}$ was calculated from the CMC values, expressed in polymer mole fraction, and Eq. 2.2, and ΔS^{o}_{mic} was derived from Eq. 2.3. The measured CMC values and the corresponding thermodynamic parameters are given in Table 2.2. When comparing the CMC values obtained from the different techniques used (see Figure 2.16), a satisfactory agreement is found, with all values lying within an order of magnitude of the CMC scale. The differences can be partially ascribed to the inherent different sensitivity of each method, the fluorescent probe method being more sensitive to the association onset.

2.5 Conclusions

Novel water soluble PGMA-*b*-PPO-*b*-PGMA triblock copolymers were successfully synthesized via ATRP technique. The blocks comprised a thermoresponsive poly(propylene oxide) (PPO) middle block with a molar mass of around 2000 $g \cdot mol^{-1}$ and two hydroxy-functional poly(2,3-dihydroxypropyl methacrylate) (PGMA) outer blocks with lengths varying from 14 to 221 monomeric units per block. Gel permeation chromatography analysis confirmed unimodal molar mass distributions with polydispersity indexes ranging between 1.29 and 1.40 for different lengths of the PGMA block.

The association behavior of PGMA-*b*-PPO-*b*-PGMA in aqueous solutions was studied. The size of the micelles formed and the thermal dependence of the micellization process were followed by dynamic light scattering at different temperatures. Depending on the length of the PGMA blocks, micelles showed an average hydrodynamic diameter in the range from 20 to 30 nm. Triblock copolymers having PGMA blocks with a degree of polymerization around half of that of the PPO block formed micelles with a well defined and practically constant size with apparent hydrodynamic radii R_h~10-15 nm in the temperature range of 15-40°C and exhibited a critical micellization temperature at about 8°C, above which micelles could be formed.. Copolymers having PGMA blocks of length comparable to that of the PPO block exhibited a critical micellization temperature at about 19°C. Also aggregates with sizes in the range of R_h~175-215 nm were formed at temperatures below CMT. Triblock copolymers having much longer PGMA blocks were present mostly as unimers.

Critical micellization concentrations (CMC) were determined using surface tension measurements, fluorescent probe technique with pyrene as probe molecule and isothermal titration calorimetry. CMCs were found to be in the range from 8×10^{-6} to 2×10^{-4}M depending on the length of the PGMA block and on the method used. A relatively good agreement was found between the CMC values obtained from the different methods.

2.6 References

[1] Alexandridis, P.; Lindman, B. In *Amphiphilic block copolymers,* 1st ed.; Alexandridis, P.; Lindman, B., Eds.; Elsiever Science, The Netherlands, 2000; p 10.

[2] Kabanov, A.; Alakhov, V. In *Amphiphilic block copolymers,* 1st ed.; Alexandridis, P.; Lindman, B., Eds.; Elsiever Science, The Netherlands, 2000; p 349 .

[3] Erukova, V.; Krylova, O.; Antonenko, Y.; Melik-Nubarov, N. *Biochim. Biophys. Acta* **2000**,1468, 73-86.

[4] Kabanov, A.; Batrakova, E.; Alakhov, V. *Advanced Drug Delivery Reviews* **2002**, *54*, 759-779.

[5] Sunhee, C.; Jhon, M. S.; Andrade, J. D. *J. Colloid Interface. Sci.* **1977**, *61*, 1-8.

[6] Gates, G.; Harmon, J.P.; Ors, J.; Benz, P. *Polymer* **2003**, *44*, 207-214.

[7] Gates, G.; Harmon, J.P.; Ors, J.; Benz, P. *Polymer* **2003**, *44*, 215-222.

[8] Leung B. K.; Robinson, G. B. *J. Appl. Polym. Sci.* **1993**, *47*, 1207-1214.

[9] Beers, K. L.; Boo, S.; Gaynor, S. G.; Matyjaszewski, K. *Macromolecules* **1999**, *32*, 5772-5776.

[10] Spanswick, J.; Matyjaszewski, K. *Materials today.* **2005**, *12*, 901-915.

[11] Patten, T. E.; Matyjaszewski, K. *Adv. Mater.* **1998**, *8*, 26-33.

[12] Coessens, V.; Pintauer, T.; Matyjaszewski, K. *Prog. Polym. Sci.* **2001**, *26*, 337-377.

[13] Beinert, G.; Hild, G.; Rempp, P. *Makromol. Chem.* **1974**, *175*, 2069-2077.

[14] Mori, H.; Hirao, A.; Nakahama, S. *Macromolecules* **1994**, *27*, 35-39.

[15] Mori, H.; Hirao, A.; Nakahama, S.; Senshu, K. *Macromolecules* **1994**, *27*, 4093-4100.

[16] Liu, F.; Liu, G. *Macromolecules* **2001**, *34*, 1302-1307.

[17] Pilon, N. L.; Armes, S. P.; Findlay, P.; Rannard, S. P. *Langmuir* **2005**, *21*, 3808-3813.

[18] Zhu, Z.; Armes, S. P.; Liu, S. *Macromolecules* **2005**, *38*, 9803-9812.

[19] Weaver, J. V.; Bannister, I.; Robinson, K. L.; Bories-Azeau, X.; Armes, S. P.; Smallridge, M.; McKenna, P. *Macromolecules* **2004**, *37*, 2395-2403.

[20] Liu, S.; Weaver, J. V.; Save, M.; Armes, S. P. *Langmuir* **2002**, *18*, 8350-8357.

[21] Zhang, Z.; Liu, G.; Bell, S. *Macromolecules* **2000**, *33*, 7877-7883.

[22] Oguchi, K.; Sanui, K.; Ogata, N.; Takahashi, Y.; Nakada, T. *Polym. Eng. Sci.* **1990**, *30*, 449-452.

[23] Wang, X. S.; Jackson, R. A.; Armes, S. P. *Macromolecules* **2000**, *33*, 255-257.

[24] Jankova, K.; Chen, X. Y.; Kops, J.; Batsberg, W. *Macromolecules* **1998**, *31*, 538-541.

[25] Liu, S.; Armes, S. P. *J. Am. Chem. Soc.* **2001**, *123*, 9910-9911.

[26] Hussain, H.; Busse, K.; Kressler, J. *Macromol. Chem. Phys.* **2003**, *204*, 936-946.

[27] Astafieva, I; Zhong, X. F.; Eisenberg, A.. *Macromolecules* **1993**, *26*, 7339-7352.

[28] Save, M.; Weaver, J. V.; Armes, S. P.; McKenna, P. *Macromolecules* **2002**, *35*, 1152-1159.

[29] Wang, J.; Grimaud, T.; Matyjaszewski, K. *Macromolecules* **1997**, *30*, 6507-6512.

[30] Matyjaszewski, K.; Wang, J.; Grimaud, T; Shipp, D. *Macromolecules* **1998**, *31*, 1527-1534.

[31] Matyjaszewski, K.; Shipp, D.; Wang, J. A.; Grimaud, T.; Patten, T. E. *Macromolecules* **1998**, *31*, 6836-6840.

[32] Matyjaszewski, K.; Wang, J.; Grimaud, T; Shipp, D. *Macromolecules* **1998**, *31*, 1527-1534.

[33] Craven, J.R.; Tyrer, H.; Booth, C.; Jackson, D. *J. Chromatogr.* **1987**, *387*, 233-240.

[34] Feng, X.; Pan, C.; Wang, J. *Macromol. Chem. Phys.* **2001**, *202*, 3403-3409.

[35] Hadjichristidis, N.; Pispas, S.; Floudas, G. In *Block copolymers,* 1st ed.; Wiley-Interscience, New Jersey, **2003**; p 214.

[36] Garnaik, B.; Thombre M. S. *J. Appl. Polym. Sci.* **1999**, *72*, 123-133.

[37] Okaya, T. In *Polyvinylalcohol developments,* 1st ed.; Finch, C. A., Ed.; John Wiley & Sons, Chichester, **1992**; p 4.

[38] Gerle, M.; Fischer, K.; Roos, S.; Müller, A.; Schmidt, M. *Macromolecules* **1999,** *32*, 2629-2637.

[39] Kavanov, A.; Nazarova, I.; Astafieva, I. *Macromolecules* **1995,** *28*, 2303-2314.

[40] Zhou, Z.; Chu, B. *Macromolecules* **1988,** *21*, 2548-2554.

[41] Glatter, O.; Scherf, G.; Schillén, K.; Brown, W. *Macromolecules* **1994,** *27*, 6046-6054.

[42] Booth, C.; Attwood, D. *Macromol. Rapid Commun.* **2000,** *21*, 501-527.

[43] Hussain, H.; Kerth, A.; Blume, A.; Kressler, J. *J. Phys. Chem. B* **2004**, *108*, 9962-9969.

[44] Wilhelm, M.; Zhao, C. L.; Wang, Y.; Xu, R.; Winnik, M. A. *Macromolecules* **1991,** *24*, 1033-1040.

[45] Paula, S.; Süs, W.; Tuchtenhagen, J.; Blume, A. *J. Phys. Chem*. **1995**, *99*, 11742-11751.

[46] Garidel, P.; Hildebrand, A.; Neubert, R.; Blume, A. *Langmuir* **2000**, *16*, 5267-5275.

[47] Majhi, P.R.; Blume, A. *Langmuir*, **2001**, *17*, 3844-3851.

[48] Zana, R. *Langmuir* **1996**, *12*, 1208-1211.

[49] Bai, G.; Wang, J. ; Yan, H.; Li, Z.; Thomas, R. K. *J. Phys. Chem. B* **2001**, *105*, 3105-3108.

3 Adsorbed and Spread Films of PGMA-*b*-PPO-*b*-PGMA at the Air-Water Interface

3.1 Introduction

In Chapter 2 the synthesis of PGMA-*b*-PPO-*b*-PGMA triblock copolymers via atom transfer radical polymerization, and the physicochemical characterization of their aqueous solutions were described. The present Chapter focuses on the features of PGMA-*b*-PPO-*b*-PGMA triblock copolymer adsorption at the air-water interface, its adsorption kinetics, its molecular arrangement at the interface, and the application of theoretical models for the analysis of its adsorption behavior. The fact that these polymers are water-soluble but at the same time are able to form stable films after spreading at the water surface offers the exceptional opportunity of comparing the characteristics and behavior of both adsorbed and pseudo-Langmuir films. At the end of the chapter some considerations are given about the possible relevance of non-equilibrium effects during the adsorption process.

3.1.1 Particularities of the Adsorption of Amphiphilic Polymers

The adsorption behavior of amphiphilic polymers at the air-water interface differs substantially from that of low molar mass surfactants. Among the many differences, some of the most relevant for the present study are:

(i) Polymers molar areas are larger and are not a constant. They can vary with surface pressure, especially for flexible polymers that are able to adopt different conformations.

(ii) At very low polymer bulk concentrations, surface tension decreases from that of pure water to a limiting value (typically about 40-50 mN/m for nonionic surface active water-soluble polymers) very steeply, *i.e.* in a narrow concentration range.

(iii) Further concentration increases affect only slightly the surface tension; there is only a weak dependence of surface tension on bulk concentration.

(iv) Adsorption equilibrium is achieved within hours, not in a matter of seconds or minutes as it is the case for low molar mass surfactants. Since desorption proceeds even slower, adsorption can be regarded approximately as being nonreversible within a short frame of time.

Early studies dealing with the adsorption of water-soluble polymers at the air-water interface made use of the same adsorption models that had been successfully applied in the past to low molar mass surfactants. Particularly, the well-known Gibbs adsorption equation has been extensively applied,[1-3] mostly in its simple form, which does not take into account the polydispersity in size inherent to polymers. Especially the weak dependence of surface tension at intermediate concentrations, mentioned above in point (iii), makes difficult the application of Gibbs adsorption equation and even leads to the following paradox not fully understood yet.[4, 5] Taking Gibbs' equation to be valid in this range, the large molar area of polymer chains results in a small adsorption, therefore the increase in surface tension with decreasing logarithmic concentration should be rather gradual. Moreover, adsorption must decrease upon dilution; thus, according to Gibbs' equation, a plot of surface tension *versus* the logarithmic concentration must be always concave downwards. Given the low limiting surface tension values discussed above in point (ii) it would be impossible for the surface tension to reach the value for pure water in a narrow concentration range, as it is in fact observed experimentally. Several explanations have been proposed for this paradox, including a depletion of the bulk concentration due to adsorption at the surface,[6] the effect of size polydispersity,[5] also of composition polydispersity in the case of copolymers,[1, 7] and the occurrence of a phase transition in the adsorbed film.[3]

Whatever the reasons for the difficulties of Gibbs model to explain water-soluble polymers adsorption, an alternative theoretical approach that includes the mentioned particularities of polymeric systems would be specially useful. Recently, Fainerman *et al.* proposed a model for describing adsorption of proteins to liquid-fluid interfaces.[8] Their model takes into account a distribution of protein conformations having different molar areas depending on monolayer coverage. This multiple conformation model was shown to reproduce satisfactorily the experimental behavior of both flexible and globular proteins.[8] Being proteins nothing but macromolecules, it is not surprising that their adsorption shares several common features with the adsorption of synthetic polymers. Thus, the multiple conformation model might also be suitable for describing the adsorption of the latter.

3.2 Experimental

3.2.1 Materials

The synthesis of the block copolymer $(PGMA_{14})_2$-PPO_{34} is discussed in detail in section 2.2. A 10 mM phosphate buffer solution (pH = 7) prepared in ultrapure water (SG Wasseraufbereitung und Regenerierstation GmbH, Germany) was used as subphase for all experiments.

3.2.2 Adsorption Kinetics at the Air-Water Interface

Adsorption experiments at constant surface area were performed in a circular Teflon trough with 30.0 mm diameter, 13.9 mm depth, and a subphase volume of 10.25 mL. A given volume of an aqueous polymer solution enough for reaching the desired end polymer concentration was injected into the subphase with a glass microsyringe through a channel just above the bottom of the trough. The trough was stirred with a rolling sphere to ensure a fast and homogeneous distribution of the polymer throughout the subphase without perturbing the surface. For monitoring the change in surface pressure due to the polymer adsorption, the surface tension was measured using a Wilhelmy film balance with a filter paper as plate. The surface tension γ is related to the surface pressure, Π, by $\Pi = \gamma_0 - \gamma$, where γ is the surface tension of the water surface after copolymer adsorption and γ_0 is the surface tension of pure water (γ_0 = 72.75 mN/m at 20°C). The surface pressure was measured with a precision of 0.01 mN/m. The reproducibility of adsorption experiments was estimated to be ± 0.2 mN/m. The temperature of the trough was maintained constant at 20°C by circulating thermostated water through the jacketed vessel containing the solution and inside the walls of a covering box designed to minimize water evaporation.

3.2.3 Desorption Kinetics from the Air-Water Interface

Desorption experiments at constant surface area were performed in the same circular Teflon trough. In this case, a polymer solution in a mixture of methanol/ chloroform 1:9 v/v was spread with a glass microsyringe onto the surface. The maximum observation time was approximately 23 h. The subphase was stirred during the whole experiment.

3.2.4 Surface Pressure (Π) - Area (A_m) Isotherms

Variable area experiments were carried out in a rectangular Teflon trough (Riegler & Kirstein, Berlin, Germany) with dimensions 792.0 mm × 68.5 mm equipped with a Wilhelmy film balance. The mean area available per molecule (A_m) was varied during the experiment by changing the distance between two mobile Teflon barriers positioned symmetrically to the trough center at a constant compression rate set between 2.5-7.3 Å^2 per polymer molecule per min, so that the total compression time was about 3.5 h. The temperature of the trough was maintained constant at 20°C.

3.3 Results and Discussion

3.3.1 Adsorption Kinetics at the Air-Water Interface

In order to gain information about the adsorption behavior of the triblock copolymers at the air-water interface, a series of experiments with total polymer concentrations in the trough, C_0, ranging from 25 nM to 2 μM was carried out.

Figure 3.1 shows the time-dependent surface pressure increase during the adsorption process of $(PGMA_{14})_2$-PPO_{34} at the air-water interface at different bulk concentrations, after being injected at the bottom of the circular trough with stirring. Zero time corresponds to the injection of the copolymer into the subphase. Even for the highest concentration there was an initial period of no evident increase in surface pressure, e.i. no polymer adsorbs to the interface up to at least 3.4 min after injection for C_0 = 2 μM. This period allows verifying that the surface is not disturbed during the injection procedure, and that the curves correspond indeed to the adsorption of the copolymer to a bare air-water interface. The occurrence of this delay in adsorption, in spite of being injected under stirring, may be related to the lifetime of micelles before they breakup. In previous calorimetry experiments involving the injection of a micellar solution into water under stirring it was found that a five minutes period was necessary to ensure the complete breakup of the injected micelles.[9] It must be pointed out that although a micellar concentrated solution is injected, within the investigated concentration range the polymer is present predominantly as single chains as the critical micellization concentration (CMC) for $(PGMA_{14})_2$-PPO_{34} is around 50 μM.[9]

The total observation time was at least 21 h, which is found to be long enough for ensuring adsorption equilibrium for total polymer concentrations above 100 nM. It is assumed than the interface is equilibrated when the increase in surface pressure is ≤ 0.1 mN/m per hour, and at that point the equilibrium surface pressure, Π_{eq}, is reached. For concentrations in the range 50-100 nM equilibrium is not achieved within the maximum observation time of 24 h and a progressive surface pressure increase is still observed.

The minimum concentration required to induce surface activity lies between 25 and 50 nM. For C_0 = 25 nM no effect on surface tension is evidenced. The surface activity of $(PGMA_{14})_2$-PPO_{34} is found to be considerably higher than that of analogous triblock copolymers of poly(ethylene oxide) and poly(propylene oxide) (PEO-*b*-PPO-*b*-PEO), also known as Poloxamers. The critical micellization concentration for $(PGMA_{14})_2$-PPO_{34} is almost two orders of magnitude smaller than for $(PEO_{13})_2$-PPO_{30} (CMC ~ 3.8×10^3 μM),[10] in spite of having a middle block of comparable length. Likewise, the maximum surface pressure reached due to $(PGMA_{14})_2$-PPO_{34} adsorption is around Π_{max} ~ 38.1 mN/m, while for $(PEO_{13})_2$-PPO_{30} this value is only Π_{max} ~ 29.4 mN/m.[10] These differences in surface activity might be partially caused by the increased bulkiness and rigidity of the glycerol monomethacrylate blocks located in the sublayer as compared with less voluminous and more flexible ethylene oxide blocks.

The shape of the time-dependent surface pressure curves in Figure 3.1 varies with the solution bulk concentration, indicating that the structure and dynamics of the adsorbed layer change with the surface coverage. The observed slowdown of the adsorption process suggests the appearance of a high energy barrier hindering further adsorption above certain surface concentration. The lowest concentration for which this change in adsorption kinetic is observed is C_0 = 100 nM. For this concentration the equilibrium surface pressure is Π_{eq} = 22.7 mN/m. A similar type of bimodal adsorption kinetics has been reported for PEO-*b*-PPO-*b*-PEO.[11,12] It has been explained as due to the change of the adsorption mechanism from diffusion controlled at dilute concentrations to a mixed diffusion-kinetic controlled one at higher bulk concentrations. The additional adsorption barrier was attributed to the completion of a brush layer at the interface.[12] However, there are several other factors that could cause similar barriers to adsorption, *e.g.* the work required to overcome the increasing surface pressure; or the requirement for a chain to adopt a specific orientation/conformation before adsorption, which is particularly the case for the long chains of surface active polymers and proteins.[13] An extensive discussion about possible adsorption mechanisms compatible with the presence of an adsorption barrier can be found elsewhere.[13]

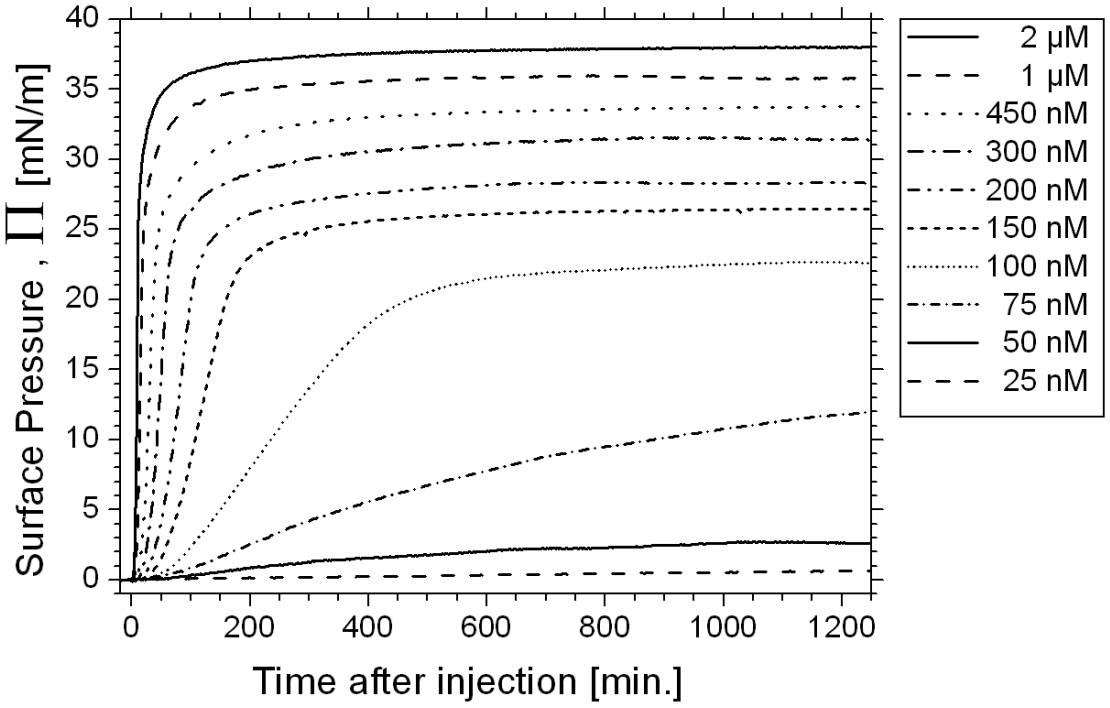

Figure 3.1: Time-dependent surface pressure increase induced by $(PGMA_{14})_2$-PPO_{34} adsorption at the air-water interface after being injected at the bottom of the circular trough with stirring at 20°C. The corresponding total concentration of the triblock copolymer in the trough (C_0) for each experiment is given in the legend.

3.3.2 Desorption Kinetics from the Air-Water Interface

Since $(PGMA_{14})_2$-PPO_{34} is highly soluble in water, it is not supposed to build insoluble Langmuir films at the air-water interface. A spread film of the polymer is expected to desorb into the subphase and to reach an equilibrium surface pressure similar to that of an adsorbed Gibbs film at the same total polymer concentration. In order to check this assumption a series of experiments with total polymer concentrations in the trough ranging from 10 nM to 600 nM were carried out. Figure 3.2 shows the time-dependent surface pressure during the desorption process of $(PGMA_{14})_2$-PPO_{34} after being spread onto the surface. When comparing the Π_{eq} values obtained for adsorbed films (Figure 3.1) with those obtained for spread films (Figure 3.2) at the same C_0, it is clear that the equilibrium surface pressures of spreads films are far higher than those of adsorbed films, *e.g.* for C_0 = 100 nM the Π_{eq} for spreads and adsorbed films are respectively 33.6 and 22.7 mN/m. It is concluded that polymer desorption from spread films is so severely retarded, that the surface layer finds itself in a kinetically hindered non-equilibrium state. Similar almost irreversible adsorption has also been recently reported for other water-soluble polymers.[14] It has been suggested that the formation of entanglements within the monolayer could be the cause; however, the detailed mechanism is still unclear. Thus, $(PGMA_{14})_2$-PPO_{34} spread films behave in fact as pseudo-Langmuir insoluble films, in spite of being composed of water-soluble molecules. Such films are stable for at least 23 h even at the lowest surface concentration investigated.

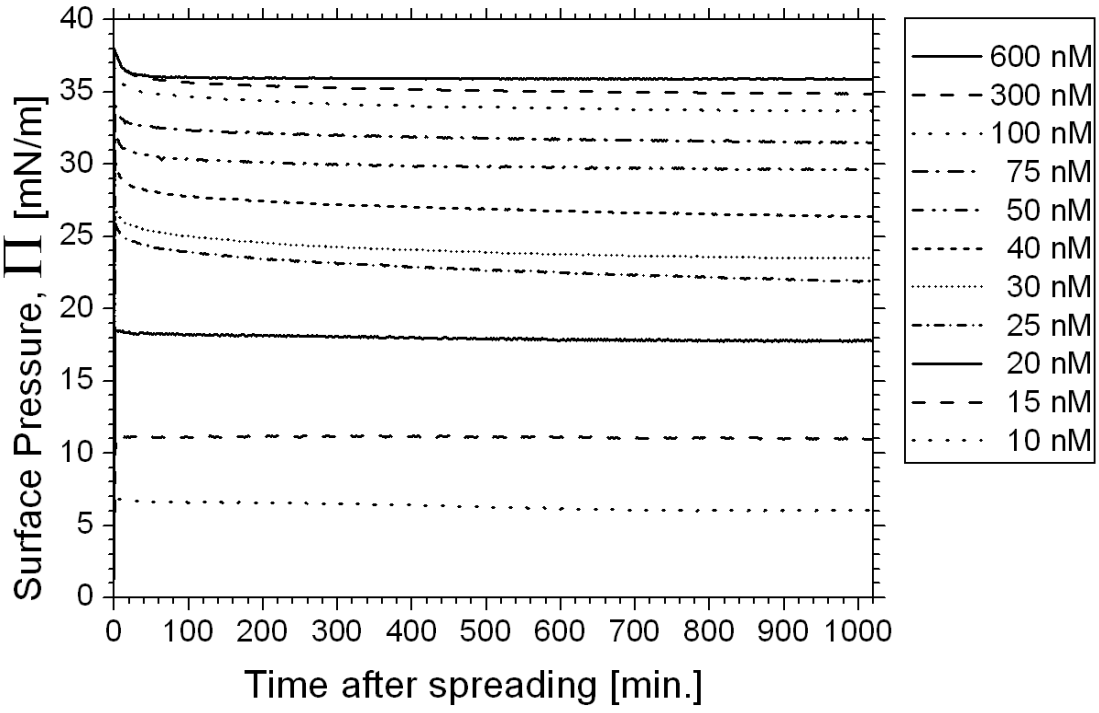

Figure 3.2: Time-dependent surface pressure during the desorption process of $(PGMA_{14})_2$-PPO_{34} after being spread onto the air-water interface with stirring of the subphase at 20°C. The total concentration of the triblock copolymer in the trough for each experiment is given in the legend

3.3.3 Polymer Compression Isotherm and Surface Dilatational Modulus

In spite of its simplicity, interfacial tensiometry under surface compression is a valuable method for studying the different physical states that can be adopted by polymer molecules adsorbed at the air-water interface. By progressively reducing the available area per polymer molecule, and consequently increasing the film lateral pressure, the polymer chains are forced through different physical states, which are in turn caused by variations of the molecular conformation and/or orientation. Figure 3.3 illustrates the surface pressure (Π) / mean area available per molecule (A_m) isotherm of $(PGMA_{14})_2$-PPO_{34} films at the air-water interface.

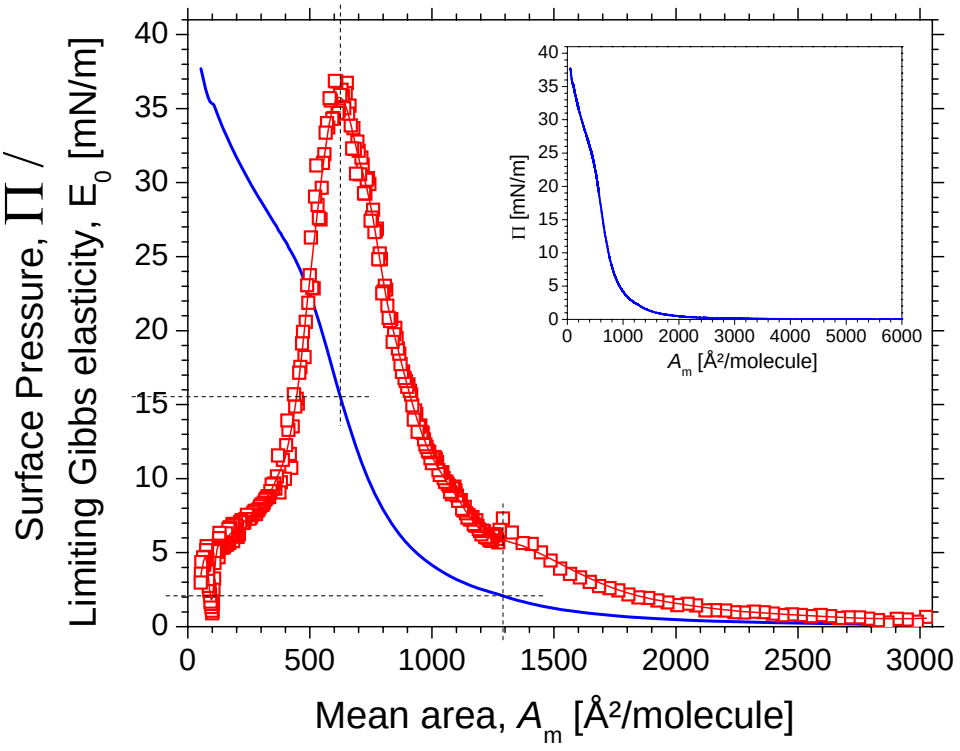

Figure 3.3: Surface pressure (Π) *vs.* mean area available per molecule (A_m) isotherm for $(PGMA_{14})_2$-PPO_{34} at the air-water interface at 20°C (blue curve). The film limiting Gibbs elasticity (E_0) derived from the Π-A_m isotherm is also shown (□). The inset shows the variation of Π within the full range of areas investigated.

An important parameter for the characterization of soluble adsorbed films is their surface dilatational modulus (also known as Gibbs elasticity) defined as the resulting change in surface tension caused by a change of the air-water interfacial area (A): $E = d\gamma / d\ln A$. It provides information about the rheological properties of a soluble film, which are intimately connected with the conformational distribution of molecules within the adsorbed layer.[11,15]

For the particular case of measurements where no relaxation process by diffusional exchange takes place in the time scale of the measurement, *i.e.* there is no significant exchange of molecules between the adsorbed layer and the bulk solution, desorption is not extensive and the mass of the adsorbed layer is approximately constant.[16] This stability

condition has been found to be valid for compressed surface layers of various PEO-*b*-PPO-*b*-PEO copolymers having a PPO block of similar length as in this study.[10] Besides, taking into account that the total duration of the compression experiments was set at around 3.5 h, which is a relatively short time compared to the long period of stability found for $(PGMA_{14})_2$-PPO_{34} spread films (of at least 23 h), it can be assumed that desorption is also not extensive for the considered $(PGMA_{14})_2$-PPO_{34} pseudo-Langmuir films. In that case, a limiting high-frequency surface dilatational modulus E_0 (also known as limiting Gibbs elasticity) is defined as:[17]

$$E_0 = \left(\frac{d\Pi}{d \ln \Gamma} \right)_T \qquad (3.1)$$

Where Γ is the polymer adsorption (equivalent to the surface excess concentration) defined as $\Gamma = N_S/A$, being N_S the number of moles adsorbed at the interface and A the total surface area. The value of E_0 coincides precisely with that of the surface compressional modulus, K, used to characterize the properties of insoluble Langmuir monolayers and given by:[18]

$$K = -A\left(\frac{d\Pi}{dA} \right)_T \qquad (3.2)$$

Thus, the variation of the Gibbs elasticity with film compression is derived from the slope of the Π-A_m isotherm according to Eq. 3.2, and it is shown in Figure 3.3 (units and scale are the same as for surface pressure).

Before proceeding with the analysis of the compression isotherm, it is important to consider the conditions for the equivalence of adsorbed and spread layers. In principle, the inherent polydispersity of polymer samples would give rise to differences in the composition of the layer. For spread layers, the most hydrophilic fractions would desorb preferentially into the subphase leaving the layer enriched in the more hydrophobic fractions. On the other hand, for adsorbed layers, the most hydrophobic fractions would adsorb preferentially. Therefore, only for long enough measuring times the initial difference in composition between both kinds of layers tends to disappear, as long as the bulk concentrations for the adsorption experiments are high enough to avoid depletion of the more hydrophobic fractions in the solution bulk due to their preferential adsorption at the surface. However, in recent comparative studies involving spread layers under compression and adsorbed layers of triblock copolymers of PEO-*b*-PPO-*b*-PEO type,[11,19] striking similarities between them were found, leading to the conclusion that the surface structure was determined solely by the surface concentration, *i.e.* it is independent of the solution bulk concentration and also of the path to reach that pressure; as long as exchange of already adsorbed chains between surface layer and the bulk solution can be considered unimportant.[11] According to the small extent of desorption expected under the chosen experimental conditions, as already pointed out in the previous discussion, this conclusion most probably applies to $(PGMA_{14})_2$-PPO_{34} adsorbed and spread layers as well.

3.3.4 Structural Changes of Spread Monolayer During Compression

There are several regimes, through which the interfacial layer may go during compression. Its particular structure, and also the surface pressure, is a function of the surface concentration. It is customary to analyze the equilibrium state of such two-dimensional system according to the scaling theory for polymer solutions, which states that all physical properties can be expressed as simple power laws of molar mass and concentration.[20] Within the frame of this theory, the relation between polymer adsorption and surface pressure is given by:[21]

$$\Pi = k\Gamma^{y} \qquad (3.3)$$

The value of the exponent y depends on the solvent quality and on the structure of the surface layer, *i.e.* two- or three-dimensional. Normally a dilute, a semidilute and a concentrated regime are considered.

3.3.4.1 Dilute Regime

In the dilute regime, polymer chains are adsorbed far away from each other on the surface. They do not overlap and contribute to the surface pressure as individual objects. Measurable changes in surface pressure were obtained only for areas smaller than 5000 Å²/molecule (see inset in Figure 3.1). In this regime the ideal gas law gives a good approximation for the variation of the surface pressure as a function of the adsorption (y = 1). At higher compression, chains are forced to overlap laterally and a semidilute regime is entered. Figure 3.4 is a log Π -log Γ plot derived from the compression isotherm in Figure 3.3. The experimental adsorption at the crossover between dilute and semidilute regimes is about $\Gamma^{*} \sim 3.75 \times 10^{-8}$ mol/m^2, and it is marked by an arrow in Figure 3.4.

3.3.4.2 Semidilute Regime

Chain overlap is expected to occur when the mean area available for a chain is of the order of the surface occupied by one isolated chain. Accordingly, the beginning of the semidilute regime is determined from the theoretical area occupied by a polymer chain, A^{*}, which is calculated from the individual contributions of its blocks. The PPO block is assumed to be located totally at the air-water interface. Thus, its conformation is assumed to be a two-dimensional self-avoiding walk, and its approximate size is calculated as that of a two-dimensional extended flexible chain:[22] $A_{PPO} \approx \pi(R_{g,PPO})^2 = (\pi/4)(R_{F,PPO})^2$, where $R_{g,PPO}$ is the radius of gyration and $R_{F,PPO}$ is the two-dimensional Flory's radius of the chain in good solvent conditions given by:[21] $R_{F,PPO} = l_{PPO}(N_{PPO})^{3/4}$. l_{PPO} is the Kuhn length of one monomeric unit ($l_{PPO} \sim 3.60$ Å),[9] and N_{PPO} is the degree of polymerization of the PPO block ($N_{PPO} = 34$).

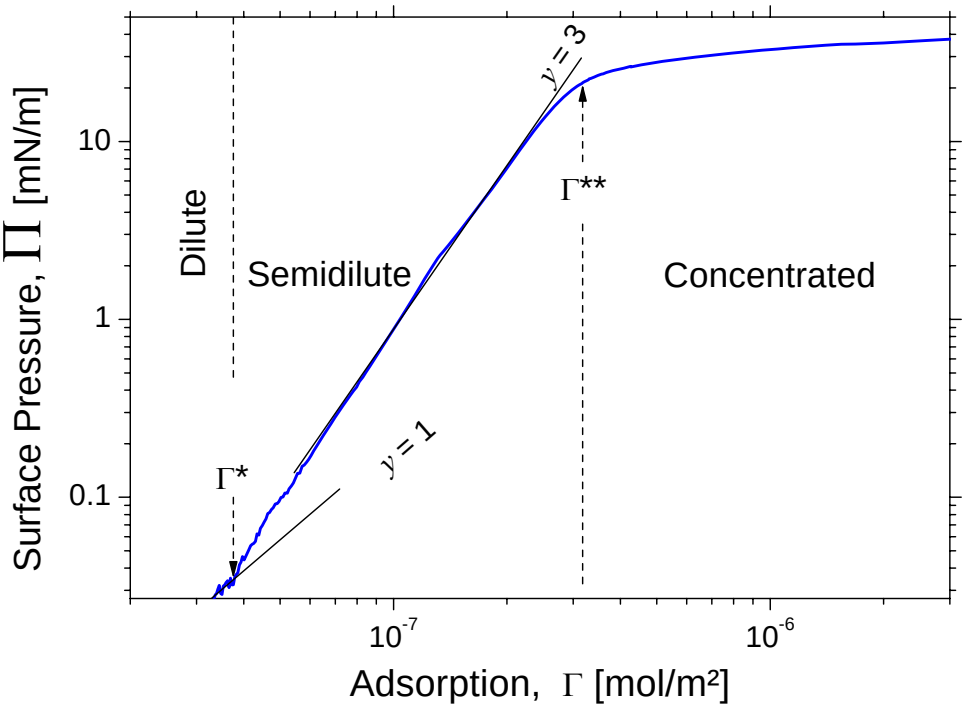

Figure 3.4: Log-Log plot of the surface pressure (Π) as function of the $(PGMA_{14})_2$-PPO_{34} adsorption (Γ) at the air-water interface at 20°C. The different scaling regimes considered are: dilute ideal gas-like behavior at $\Gamma < \Gamma^*$; semidilute two-dimensional solution between $\Gamma^* < \Gamma < \Gamma^{**}$; concentrated three-dimensional layer at $\Gamma > \Gamma^{**}$.

The PGMA blocks, being more hydrophilic, are assumed to be in a more three-dimensional conformation extending towards the subphase. In that case, the exponent for the Flory's radius takes the value 3/5 in good solvent conditions,[21] and $R_{F,PGMA} = l_{PGMA}(N_{PGMA})^{3/5}$, with $l_{PGMA} \sim 2.55$ Å [9] and $N_{PGMA} = 14$. The area of the whole chain is calculated by adding the contributions of the individual blocks as $A_{th}^* \sim 2260$ Å²/molecule. At this relatively large area the corresponding surface pressure has already increased measurably from zero ($\Pi^* = 0.33$ mN/m); confirming that at $A_m = A^*$ the structure of the interfacial layer changes from the dilute into the semidilute regime. The experimental molecular area at the crossover between dilute and semidilute regime is approximately $A^* \sim 4424$ Å²/molecule ($\Pi^* = 0.03$ mN/m), which is almost twice the theoretical overlapping area for two-dimensional coils calculated before.

For the two-dimensional arrangement of constant thickness expected in the semidilute regime, the surface pressure is a function of the third power of the surface concentration ($y = 3$),[21] and the exponent y in Eq. 3.3 is now given by: $y = 2\nu/(2\nu - 1)$, where ν is the Flory exponent , which takes values between 0.77 for good solvent conditions and 0.57 for theta solvent conditions.[19] For $(PGMA_{14})_2$-PPO_{34}, the linear region found in Figure 3.4 for adsorptions below $\Gamma = 2.53 \times 10^{-7}$ mol/m² ($\Pi = 13.7$ mN/m; $A \sim 657$ Å²/molecule), with a slope of $y = 2.860 \pm 0.004$, confirms that within that range of adsorptions the layer has a two-dimensional structure. The corresponding value of the Flory exponent, $\nu = 0.769$, indicates good solvent conditions for the polymer chains.

On the other hand, changes in the structure of the layer can be confirmed by concomitant changes in the viscoelastic properties of the layer (see Figure 3.3). Due to the flat two-dimensional conformation of the chains the film is purely elastic within the semidilute regime. At high mean molecular areas within this regime the surface dilatational modulus increases gradually with compression due to the increasing chain overlap repulsion, and reaches a maximum at about 1291 Å²/molecule (Π = 2.1 mN/m) followed by a short decrease. With decreasing molecular area the modulus exhibits a steep increase and reaches a second maximum at around 625 Å²/molecule (Π = 15.5 mN/m).

The following changes in the structures of the surface layers are proposed as explanation to this behavior. The first maximum corresponds to the saturation of the surfaces by a layer having a flat extended conformation. At the elasticity maximum, around Π = 2.1 mN/m, PGMA segments begin to change from a flat conformation to loops and tails protruding into the subphase. This relaxation process causes only a small decrease in dilatational modulus, since the PGMA blocks are relatively short. With further compression a swollen layer is formed by the PGMA blocks in the subphase and the PPO blocks remain at the interface. Upon further compression the repulsion between PPO segments causes a steep increase in dilatational modulus, and towards the end of the semidilute regime (Π = 13.7 mN/m) the interfacial layer becomes increasingly condensed. The subsequently decrease of the modulus, above Π = 15.5 mN/m, may have different explanations. On the one hand, it could be due to an exchange relaxation process via diffusional exchange between the surface and the bulk phase. It could also be due to a conformational change within the surface layer without involving diffusional exchange with the bulk phase.

The specific nature of the second peak can be elucidated by comparison with results obtained for other macromolecular systems. In studies dealing with surface active flexible proteins, which share several common features with amphiphilic polymers,[8] it has been proposed that the occurrence of a maximum in elasticity at intermediate surface pressures is due to the fact that the protein molecules have a distribution of conformations that depends on the film coverage, and therefore the average molecular area is not a constant, but it changes and gets smaller with increasing adsorption.[17] Results from studies involving various PEO-*b*-PPO-*b*-PEO copolymers having a PPO block of similar length than in this study,[11] point in the same direction. It has been concluded that the second peak in dilatational modulus occurring at around Π = 15 to 23 mN/m (for PEO blocks shorter and far larger than the PPO block, respectively) is due to the onset of a conformational change for the PPO block.[11] The corresponding molecular areas were 800 and 400 Å²/molecule, respectively. For $(PGMA_{14})_2$-PPO_{34}, both the molecular area and surface pressure of the second maximum of the dilatational modulus (A ~ 625 Å²/molecule, Π = 15.5 mN/m) agree well with these values. Therefore it is concluded that this peak is also caused by the onset of a conformational change for the PPO block.

The maximum value of the modulus at the second peak (E_0 ~ 36.9 mN/m) is rather high when compared to the value reported for PEO-*b*-PPO-*b*-PEO copolymers in the study

mentioned,[11] which was in the range of 14 to 27 mN/m depending on the length ratio between PEO and PPO blocks. Similarly, a value of $E_0 \sim 21.5$mN/m has been reported for $(PEO_{13})_2$-PPO_{30}.[23] Such increased rigidity of the $(PGMA_{14})_2$-PPO_{34} interfacial layer is attributed to a stronger repulsion between bulky PGMA blocks in the sublayer as compared to more flexible PEO blocks.

3.3.4.3 Concentrated Regime

With further compression the layer enters a three-dimensional concentrated regime, where the thickness increases with adsorption, and the surface pressure is proportional to the surface concentration ($y = 1$ in Eq. 3.3).[21] For $(PGMA_{14})_2$-PPO_{34}, the concentrated regime is entered in the region between $\Gamma \sim 3.18 \times 10^{-7}$ mol/m^2 ($\Pi \sim 21.4$ mN/m, $A_m = 522.0$ Å²/molecule), and $\Gamma \sim 3.55 \times 10^{-7}$ mol/m^2 ($\Pi \sim 23.8$ mN/m, $A_m = 468.08$ Å²/molecule), where the slope $y = 0.97$ is three times smaller than the slope of the semidilute regime, in agreement with the scaling theory of adsorption. This transition to a three-dimensional arrangement is confirmed by the sharp decrease in the dilatational modulus (Figure 3.3) after the second maximum, since the relaxation mechanisms involving desorption of PPO block segments are increasingly facilitated.

The particular kind of the tridimensional arrangement adopted is not unique for all block copolymers; it depends basically on the water affinity of the blocks and their length. Besides the trivial case of layer collapse, typical for highly insoluble molecules, some proposed arrangements include surface micelles, mixture of tails and loops, and brushes.[19] Two-dimensional micelles have been considered as less favored than brush formation for PEO-*b*-PPO-*b*-PEO polymers having a PPO block of similar length than in this study.[19] Normally a brush structure, *i.e.* a dense layer formed by stretched chains, has been assumed for ethylene/propylene oxide based block copolymers.[7,11,19,24] However, the extent of PO segments desorption, the PPO block conformation and its orientation are still unclear. Muñoz *et al.*[19] have proposed that the PPO block remains anchored to the interface and protrude in a folded conformation into the air phase forming a stratified brush above a swollen PEO brush (see Figure 3.12a). By contrast, Blomqvist *et al.*[11] proposed a partial solubilization of PPO blocks into the sublayer. Also Viera *et al.*,[7] based on neutron reflectivity measurements on PEO-*b*-PPO-*b*-PEO, have postulated an extensive mixture of desorbed PO segments with the hydrophilic PEO blocks within the adsorbed layer, forming a homogeneous swollen brush (Figure 3.12b). In conclusion, in spite of the various proposals based on experimental results, neither the exact conformation of the PPO block nor the possibility of two-dimensional micelles or other aggregation forms can be entirely confirmed or discarded without additional investigations of the structure and morphology of the interfacial layer; preferably by *in situ* techniques at the air-water interface with a spatial resolution in the nanometer range.

3.3.5 Determination of Polymer Adsorption at the Air-Water Interface

The dependence of the equilibrium surface pressure (Π_{eq}) on the total $(PGMA_{14})_2$-PPO_{34} concentration (C_0) as obtained from the adsorption experiments is presented in Figure 3.5, together with the surface pressure/mean area available per molecule isotherm. For the determination of the polymer adsorption (Γ) at a given C_0 it is assumed that when the surface pressure in both adsorption and compression experiments reaches equal values, the corresponding adsorptions are also equal for both. The overall agreement between spread layers under compression and adsorbed layers of analogous triblock polymers of PEO-*b*-PPO-*b*-PEO[11] already mentioned, leading to the conclusion that the surface structure is determined solely by the surface concentration, under conditions of negligible desorption, justify this assumption. The determination procedure, indicated by arrows in Figure 3.5, is carried out as follows: for each concentration C_0 on the surface pressure isotherm the experimental Π_{eq} is obtained. Then, the corresponding mean molecular area at the same surface pressure is determined on the Π-A_m curve. Finally, polymer adsorption is calculated as $\Gamma = (N_A A_m)^{-1}$, where N_A is Avogadro's number. The described procedure enables to estimate experimentally the amount of polymer absorbed at the interface through measuring techniques that are much simpler than the commonly used neutron or X-ray reflection techniques. The same procedure could also be applied to other systems for which the approximation of a pseudo-Langmuir film could be justified.

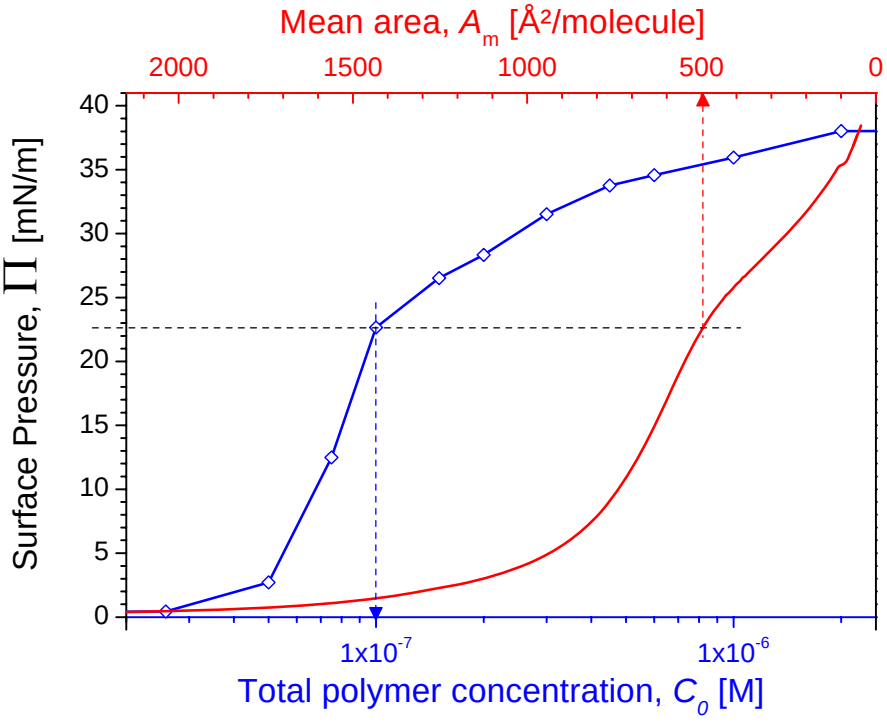

Figure 3.5: Dependence of equilibrium surface pressure (Π_{eq}) on total polymer concentration (C_0) for adsorption of $(PGMA_{14})_2$-PPO_{34} at the air-water interface (◊). The arrows illustrate the procedure for determining the adsorbed amount of polymer (Γ) corresponding to a given C_0 from the surface pressure (Π) / mean area available per molecule (A_m) isotherm (red curve).

Figure 3.6a shows the resulting evolution of $(PGMA_{14})_2$-PPO_{34} adsorption with increasing concentration, after introducing a correction for depletion in the solution bulk concentrations explained below. The plot can be divided into four regions. In region (i) there is a gradual increase in the amount of polymer adsorbed with concentration up to 1.1×10^{-8} M that is accompanied by a steep increase in surface pressure up to $\Pi \sim 22.7$ mN/m (see Figure 3.6b). The maximum slope of the Π *vs.* Γ curve is reached around $\Pi \sim 14.0$ mN/m, where the second derivate $(d^2\Pi/d\Gamma^2) = 0$. In region (ii) polymer adsorption remains almost unchanged up to 6.0×10^{-8} M. Throughout region (iii) there is a steep increase in adsorption. It is interesting to note that in the upper part of this region, between 2.4×10^{-7} M and 1.1×10^{-6} M, the adsorption increases 2.5 times, while the surface tension increases only slightly, $\Delta\Pi \sim 3.5$ mN/m (see Figure 3.6b). At even higher concentrations, the polymer adsorption reaches a plateau as the system approaches its CMC. A similar adsorption pattern including all regions mentioned has been reported for the adsorption behavior of PEO-*b*-PPO-*b*-PEO.[7] For that system, the steep increase in adsorption observed in region (iii) was not accompanied by significant changes in the monolayer thickness and was attributed to a structural rearrangement within the monolayer already in a rather condensed state.[7] As for these triblock copolymers the layer structure at high surface pressures depends strongly (but not exclusively) on the behavior of the PPO middle block,[7] it is expected that a similar structural rearrangement for $(PGMA_{14})_2$-PPO_{34} is the reason for the adsorption increase in region (iii). According to the discussion of the previous section, in region (iii) the surface layer is in a state equivalent to a rather condensed spread layer already in the middle of the concentrated regime; thus, the structural rearrangements would mainly be caused by conformational changes of the PPO block segments towards conformations having smaller molecular areas, and could include partially desorbed PPO segments dangling into the aqueous phase.

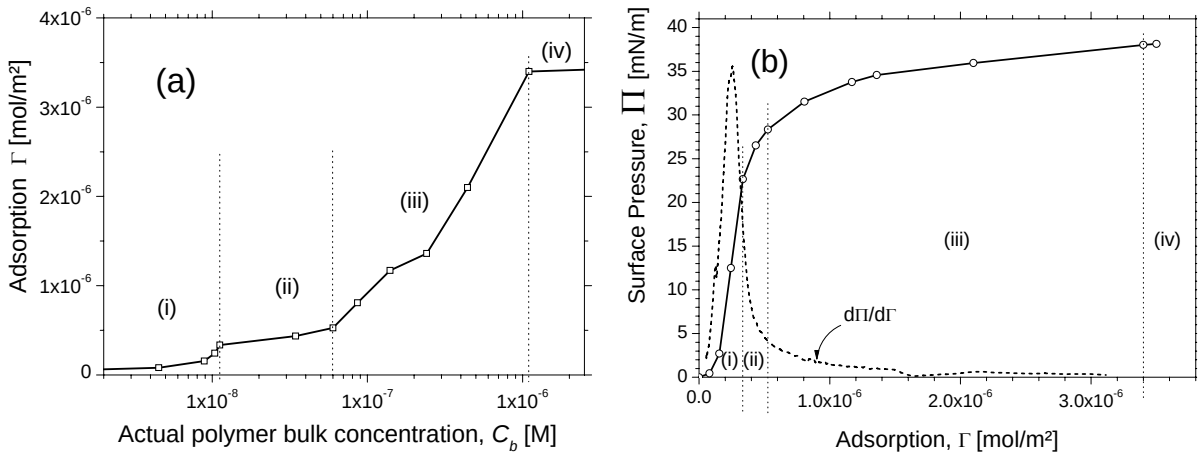

Figure 3.6: (a) Adsorption isotherm. Dependence of $(PGMA_{14})_2$-PPO_{34} adsorption (Γ) at the air-water interface on actual polymer bulk concentration (C_b). (b) Dependence of surface pressure (Π) on $(PGMA_{14})_2$-PPO_{34} adsorption. The dashed curve corresponds to the first derivate ($d\Pi/d\Gamma$).

3.3.6 Polymer Layer Surface Tension Isotherm

The surface tension isotherm for $(PGMA_{14})_2$-PPO_{34}, *i.e.* the dependence of surface tension at equilibrium (γ_{eq}) on total polymer concentration in the trough (C_0), obtained from adsorption experiments, is shown in Figure 3.7 (right curve). The shape of the curve exhibits some peculiarities not shown by ordinary low molar mass surfactants, but sometimes found for triblock copolymers of PEO-*b*-PPO-*b*-PEO type. In particular, the presence of two breaks: one at low concentrations ($C_0 \sim 1.0 \times 10^{-7}$ M, $\gamma_{eq} \sim 50.1$ mN/m) and a second at higher concentrations ($C_0 > 2.0 \times 10^{-6}$ M, $\gamma_{eq} \sim 34.6$ mN/m). While the second break has been reliably attributed to the bulk polymer concentration reaching the polymer's CMC, the nature of the first break is still elusive. Some of the proposed explanations include a depletion of the bulk concentration due to adsorption at the surface,[25] the effect of polymer polydispersity,[1, 7] a phase transition in the bulk,[2] and the occurrence of a conformational change in the adsorbed film above the break point.[3] Between both breaks there is a transition region exhibiting a weaker dependence on concentration, *i.e.* a smaller slope compared to the low concentration range.

3.3.6.1 Effect of Depletion on Polymer Layer Surface Tension Isotherm

Prior to further analysis of the surface tension isotherm, special consideration must be given to a significant and often ignored side effect of polymer adsorption. During measurements at sufficiently low polymer bulk concentrations, adsorption at the surface will deplete the polymer from the bulk reducing its original concentration. This phenomenon was first realized by Linse *et al.*[25] and its importance depends on the volumen-to-surface ratio (V/S) of the system. It is present for all systems of finite volume, and can be neglected only for very large solution volumes (V/S ~100 mm).[26] Since for the circular Teflon trough where the measurements were performed the volumen-to-surface ratio amounts to only to 3.8 mm (taking into account the whole trough surface), and for some measurements the concentrations are almost in the nanomolar range, a correction of the polymer bulk concentrations for depletion is necessary. The surface of the trough must be included in these calculations because depletion stems from the polymer adsorbing not only at the air-water interface, but also at the walls of the trough, *i.e.* at the Teflon-water interface. It must be taken into account that, the lipophobic nature of highly fluorinated surfaces causes a repulsion of the hydrocarbon portions of the polymer that opposes the driving force for adsorption.[5] Therefore, polymer adsorption at the walls must be lower than at the air-water interface. In absence of concrete values it is assumed that adsorptions at both, the walls of the trough and at the air-water interface, are equal. This assumption considers the worst possible case. The actual polymer bulk concentration after equilibration (C_b) is calculated from the total $(PGMA_{14})_2$-PPO_{34} concentration (C_0) and the corresponding adsorption (Γ) according to the equation:

$$C_b = C_0 - \Gamma\left(\frac{S}{V}\right) \qquad (3.4)$$

The correction procedure is indicated by arrows in Figure 3.7. The curve to the left corresponds to the corrected actual polymer concentrations in the solution bulk, C_b. The corrected concentrations are the only used for further analyses, including those leading to Figure 3.6a. The relative value of the calculated correction for depletion is very significant at low polymer bulk concentrations, and becomes negligible only at high concentrations, near or above the CMC.

Although after allowing for depletion the surface tension isotherm has been expanded on the concentration axis, the steep upwards-region at low concentrations not only remains, but becomes steeper. Therefore, such upturn in surface tension cannot be solely attributed to surface depletion effects. An additional factor that might also contribute to this phenomenon is the polymer polydispersity. As already pointed out by Ann *et al.*,[5] the variation of surface activity of the different species present in a polydisperse sample is probably strong enough for affecting the dependence of surface tension on concentration, even for fairly narrow molar mass distributions. An extensive discussion about the possible interplay between polydispersity, depletion and diffusion effects can be found elsewhere.[5-7] On the other hand, some experimental facts point in another direction. First, the value of the surface pressure at the first break ($\Pi \sim 22.7$ mN/m or $\gamma \sim 50.1$ mN/m) lies within the narrow range where the concentrated regime starts for the compressed surface layer, signaling the transition to a three-dimensional arrangement due to the desorption of PPO block segments. Second, according to the adsorption kinetics (Figure 3.1) around this pressure the adsorption mechanism changes and kinetics is slowed down due to a structural change in the adsorbed layer. Therefore, it is concluded that the occurrence of a conformational change within the adsorbed layer is most probably the origin of the low concentration break point in the $(PGMA_{14})_2$-PPO_{34} surface tension isotherm.

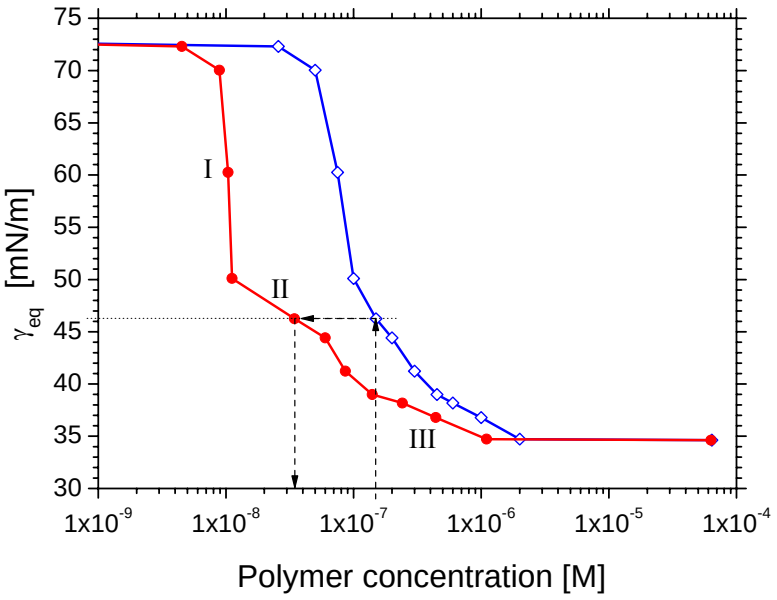

Figure 3.7: Dependence of equilibrium surface tension (γ_{eq}) on total polymer concentration (C_0) (◊), and on actual polymer bulk concentration (C_b) (●) for the adsorption of $(PGMA_{14})_2$-PPO_{34} at the air-water interface. The arrows illustrate the procedure to correct the effect of surface depletion on the original surface tension isotherm.

3.3.7 Theoretical Modeling of Polymer Adsorption

As mentioned previously, the weak dependence of surface tension on bulk solution concentration shown by many polymers in a broad intermediate concentration range results in an unusual shape of their surface tension isotherms, which is not compatible with adsorption models usually applied to low molar mass surfactants. Thus, most common isotherm models are not adequate for describing macromolecular adsorption, and the application of the broadly used Gibbs' equation to polymer adsorption leads to large errors.[27]

3.3.7.1 Multiple Conformation Model Theory

As already discussed, polymer molecules within an adsorbed film have the possibility to adopt various conformations having different molar areas depending on the surface pressure. Thus, theoretical models intended to describe the adsorption of macromolecules must account for the significant increase in non-ideality of the surface entropy as a result of the large area and various conformations that an adsorbed macromolecule can adopt. Barentin *et al.*[24] have proposed a model for the adsorbed layers of telechelic PEO polymers end capped with hydrophobic alkane groups. This model assumes that, for partially soluble brushing systems within the concentrated regime a thermodynamic equilibrium exists between two different polymer conformations: fully adsorbed chains and partially desorbed chains dangling into the aqueous phase but still grafted to the interface by the ends. It is also assumed that the two kinds of chains are ideally mixed and that the surface pressure is the sum of their partial pressures.[24] However, this model fails to reproduce the experimental surface pressure *vs.* mean molecular area isotherm beyond the semidilute two-dimensional regime. The same model was also applied to interfacial layers of triblock copolymers of PEO-*b*-PPO-*b*-PEO type by Muñoz *et al.*[19] with similar results. From the several other theoretical models proposed to date, the model proposed by Fainerman *et al.*[8] seems to be most suitable for modeling the adsorption of the flexible-chain $(PGMA_{14})_2$-PPO_{34}. Within this model, the macromolecules can exist in a number of states (j) with different molar areas (or conformations) that are in equilibrium with each other, ranging from a maximum at very low surface coverage (ω_{max}) to a minimum at high coverage (ω_{min}). The molar area increment (ω_0) is defined as the area difference between two consecutive conformations and is chosen in the order of magnitude of the molar area of the solvent or of one monomeric unit. The equation of state, based on a first-order model for the non-ideality of both entropy and enthalpy of mixing for the surface layer, is given by:[8]

$$-\frac{\Pi\omega_0}{RT} = \ln(1-\omega\textstyle\sum_{i=1}^{n}\Gamma_i) + (\omega-\omega_0)\sum_{i=1}^{n}\Gamma_i + \alpha(\omega\sum_{i=1}^{n}\Gamma_i)^2 \qquad (3.5)$$

It can also be written in shorthand as:

$$-\frac{\Pi\omega_0}{RT} = \ln(1-\theta) + \theta\left(1-{\omega_0}/{\omega}\right) + \alpha\theta^2 \qquad (3.6)$$

Where R is the ideal gas constant, Γ_i is the polymer adsorption in the i^{th} state, $\Gamma = \sum_{i=1}^{n} \Gamma_i$ is the total adsorption, $\theta = \omega\Gamma$ is the fraction of surface covered by the polymer, $\omega = \left(\sum_{i=1}^{n} \omega_i \Gamma_i\right) \Big/ \Gamma$ is the average molar area, *i.e.* the molar area averaged over all j polymer states present in the surface layer. The last term corresponds to the enthalpic effect of mixing, α being the constant of intermolecular interaction. The adsorption isotherm for each state (j) is given by:

$$b_j C = \frac{\omega\Gamma_j}{(1-\theta)^{\omega_j/\omega}} \exp\left[-2\alpha\left(\omega_j/\omega\right)\theta\right] \qquad (3.7)$$

Where C is the macromolecule concentration in the solution bulk and b_j is the adsorption equilibrium constant for the j^{th} state. The probability distribution of adsorption over the various states of the macromolecule is a function of b_j and, under the assumption that the values of the b_j constants are equal, the value of the polymer adsorption for each state j, Γ_j, is a function of the total adsorption that can be expressed as:

$$\Gamma_j = \Gamma \frac{(1-\theta)^{(\omega_j-\omega_1)/\omega} \exp\left[2\alpha\theta\dfrac{\omega_j-\omega_1}{\omega}\right]}{\sum_{i=1}^{n}(1-\theta)^{(\omega_i-\omega_1)/\omega} \exp\left[2\alpha\theta\dfrac{\omega_i-\omega_1}{\omega}\right]} \qquad (3.8)$$

An interesting feature of this model implicit in Eq. 3.8 is that at high surface coverage by a mixture of molecules occupying different area, the adsorption of molecules having a smaller area is favored at the expense of molecules having larger area requirements. Thus, the average molar area decreases with increasing coverage and approaches ω_{min} at full coverage.[17]

The equation of state and adsorption isotherm, Eqs. 5 and 7, agree well with experimental results for proteins at low and intermediate ranges of bulk concentrations, for which no aggregation of the proteins takes place in the surface layer. It is also able to reproduce inflection points, as the one shown in Figure 3.6b, often found in experimental Π *vs.* Γ curves of systems that can exist in a number of different conformations. Such inflection points cannot be accounted for by single-state models.[8] Although this multiple conformation model was developed for proteins, it can also be extended to study the adsorption of synthetic polymers. The main issue in that case is that synthetic polymers do not show an adsorption threshold for the onset of the surface pressure increase as in the case of proteins. This feature is evidenced in the inset of Figure 3.3 by the lack of a range of zero surface pressure at relatively high mean molecular areas corresponding to very low adsorptions. This behavior can be taken into account by setting a value of zero for the enthalpic constant ($\alpha = 0$) in Eqs. 5 through 8.[8]

To determine the adsorption characteristics of $(PGMA_{14})_2$-PPO_{34} from the experimental dependence of surface pressure on polymer adsorption, an iterative procedure was implemented including Eqs. 5 through 8. The fitting is performed as follows: First, values for

ω_{max} and ω_{min} are assumed. For each experimental $\Pi_k = \Pi_k(\Gamma_k)$ data point the value of ω is varied between ω_{max} and ω_{min}, and with this ω value Γ_j is calculated for each of $n = 101$ states arbitrarily considered. The value of ω is considered to be correct when the difference between assumed and calculated ω is minimal. Then Π is calculated for each k data point. The set of ω_{max} and ω_{min} are considered to be optimal when the difference between experimental and calculated surface pressures for all k points, $\Delta\Pi$, is minimal:

$$\Delta\Pi = \sum_k \left| \Pi_{k,\text{exp.}} - \Pi_{k,calc.} \right| \qquad (3.9)$$

3.3.7.2 Multiple Conformation Model Results

The values obtained from the fitting routine for the different model parameters were the following: $\omega_{max} = 5.8 \times 10^6$ m^2/mol, $\omega_{min} = 4.1 \times 10^5$ m^2/mol, $\omega_0 = 5.4 \times 10^4$ m^2/mol. The calculated average area per polymer molecule and the corresponding surface coverage are presented in Table 3.1. Figure 3.8 shows the comparison between the experimental and theoretical dependencies of surface pressure on polymer adsorption. The theoretical data match closely the experimental data up to relatively high surface pressures ($\Pi \sim 30$ mN/m); however the applied multiple conformation model with the calculated set of parameters is not able to reproduce the plateau reached by Π at higher adsorptions and predicts a further increase in surface pressure.

Table 3.1: Average Surface Area occupied by $(PGMA_{14})_2$-PPO_{34} Molecules at the Air-Water Interface (ϖ) and the Corresponding Surface Coverage (θ) Calculated According to the Multiple Conformation Model (Eqs. 5-8) for Different Adsorptions (Γ).

$\Gamma \times 10^7$ [mol/m²]	Π [mN/m]	ϖ [Å^2/molec.]	θ
0.80	0.44	457.4	0.22
1.55	2.71	417.1	0.39
2.44	12.49	385.0	0.56
3.35	22.65	333.6	0.67
4.35	26.51	277.3	0.73
5.27	28.33	233.1	0.74
8.07	31.52	161.2	0.78

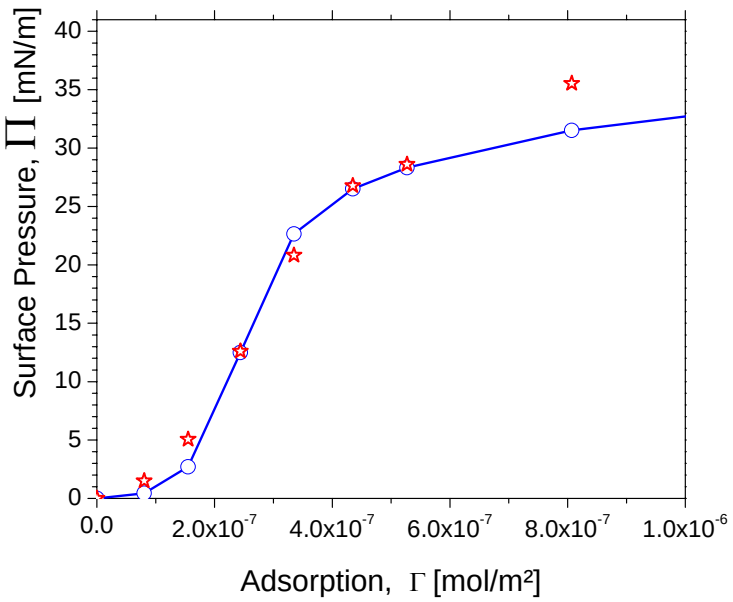

Figure 3.8: Dependence of surface pressure on (PGMA14)2-PPO34 adsorption at the air-water interface calculated according to the multiple conformation model (Eqs. 5-8) (✱). Experimental data (○). The solid curve is only a guide to the eye.

Figure 3.9 is a plot of the average surface area occupied by a $(PGMA_{14})_2$-PPO_{34} molecule ($\varpi = \omega/N_A$), calculated from the fitting procedure, as a function of surface pressure. It is shown together with a curve corresponding to the limiting case of full surface coverage ($\theta = 1$). As expected, the average molecular area decreases with increasing surface pressure in agreement with the picture of molecules having a smaller area requirement being favored at the expense of larger ones. It must be pointed out that, although the molar area ratio between the possible extreme conformations amounts to $\omega_{max}/\omega_{min} \sim 14$, the ratio between the average molar areas at very low coverage and at full coverage is only $\omega_{(\theta\to 0)}/\omega_{(\theta\to 1)} \sim 7.6$. The explanation for this is that at $\theta \to 0$ all states are equally probable, and therefore, contrary to what one would expect for conformations characterized by a large area, the limiting value for ω is not equal to ω_{max} but is given by:[17] $\omega_{(\theta\to 0)} = (\omega_{max}+\omega_{min})/2$. Using the parameters found for this system one obtains: $\varpi_{(\theta\to 0)} = 518$ Å^2/molecule. On the other hand, at $\theta \to 1$ the average molar area approaches ω_{min} as expected and $\varpi_{(\theta\to 1)} = 68$ Å^2/molecule. The inferred ability of $(PGMA_{14})_2$-PPO_{34} molecules to occupy at low concentrations molar areas almost eight times larger than at higher concentrations is the reason for its considerably high surface activity at low concentrations. It also confirms that the polymer chains are highly flexible and able to adopt different conformations during the transition of the adsorbed polymer film from a highly diluted to a nearly saturated state.

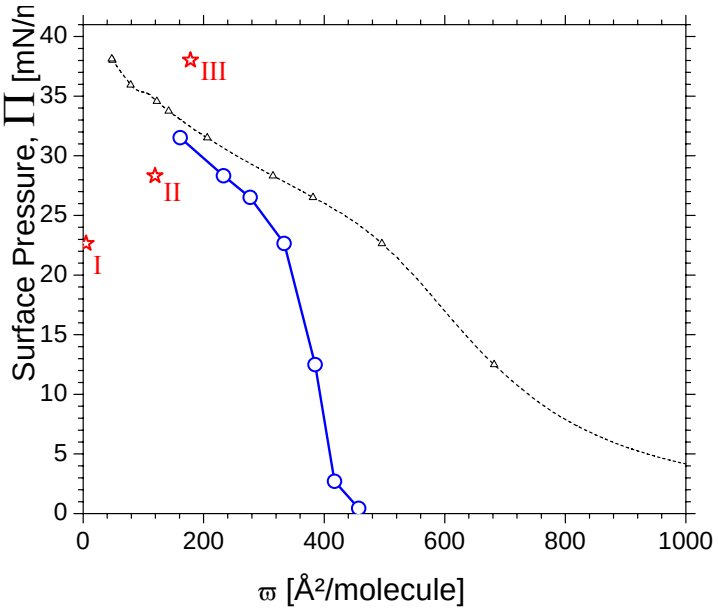

Figure 3.9: Dependence of surface pressure on the average surface area occupied by $(PGMA_{14})_2$-PPO_{34} molecules (ϖ) calculated according to the multiple conformation model (Eqs. 5-8) (○). Average area occupied per molecule for the limiting case of full surface coverage ($\theta = 1$) (Δ). Molecular surface area according to Gibbs adsorption equation (✱). Surface coverages are presented in Table 3.1.

In several investigations dealing with amphiphilic block copolymers[6,7,19,25] Gibbs adsorption equation has been traditionally used for analyzing the surface tension isotherms, which in the case of non-ionic surfactants is expressed as:

$$\Gamma = -\frac{1}{RT}\frac{d\gamma}{d\ln C} \qquad (3.10)$$

If the molecular surface area is calculated by applying Eq. 3.10 to the linear portions of the experimental surface tension isotherm, sections marked as I, II and III in Figure 3.7, the values obtained are 4.9, 119.4, and 178.1 Å²/molecule, respectively. A comparison with the values calculated by applying the multiple conformation model (Table 3.1) evidences that for sections I and II the molecular surface areas from Gibbs adsorption equation increase with increasing surface pressure, which is opposite to the expected tendency. Besides, they are unrealistically too small, and eventually lack of physical meaning, as it is the case for section I. These results exemplify the problems brought about by the application of Gibbs adsorption equation, which is otherwise perfectly applicable to the adsorption of common low molar mass surfactants, to a polymeric system exhibiting a rather complex adsorption behavior.

It is interesting to analyze the features of the distribution of adsorption over the various states/molecular areas allowed for the polymer within the multiple conformation model, and its variation with surface pressure/coverage. Figure 3.10a-c illustrates the distribution of the fractional adsorption (f_j), $f_j = \Gamma_j \Big/ \left(\sum_{i=1}^{n} \Gamma_i\right)$, over the n states considered, which have molar areas evenly spaced between ω_{min} (j=1) and ω_{max} (j=101).

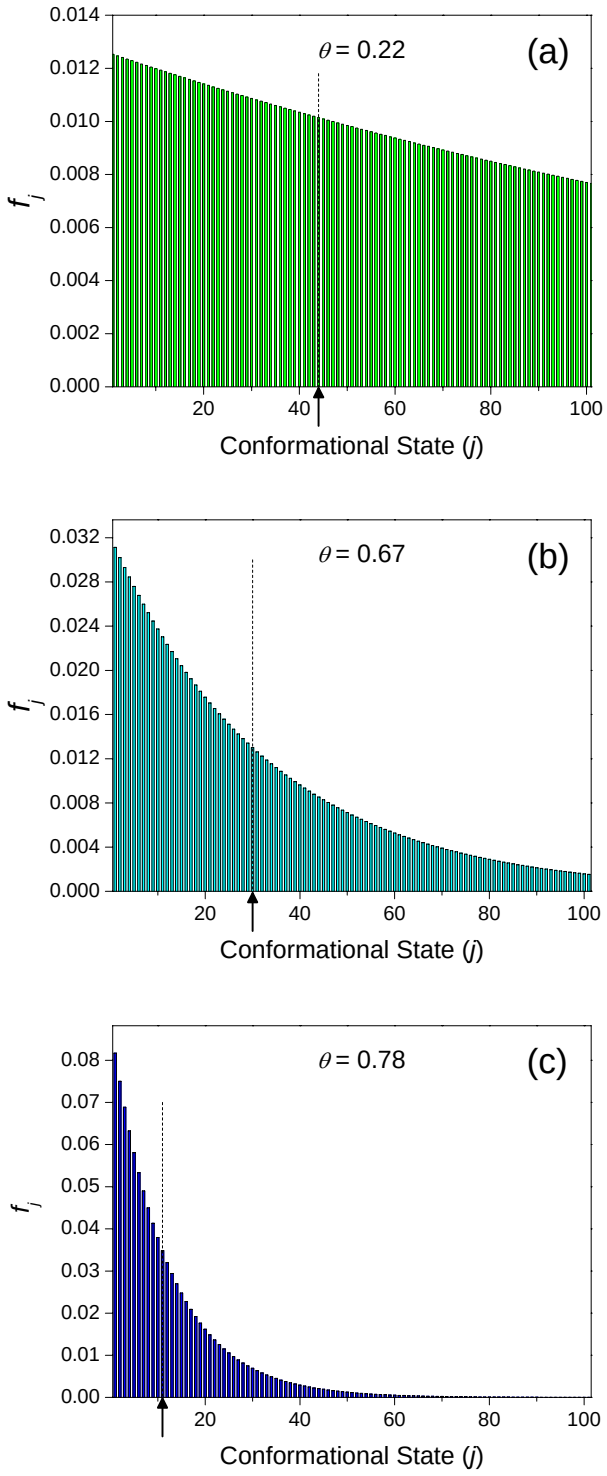

Figure 3.10: Distribution of the fractional adsorption (f_j), over the j conformational states having molar areas between ω_{min} (j = 1) and ω_{max} (j = 101) for the adsorption of $(PGMA_{14})_2$-PPO_{34} at the air-water interface at different surface coverages: (a) θ = 0.22 (green), (b) θ = 0.67 (cyan), and (c) θ = 0.78 (blue). An arrow marks the position of the conformation with molar area equal to the average molar area (ω) at the respective θ. Results derived according to the multiple conformation model.

At low surface coverage (Figure 3.10a) all states have a similar fractional adsorption. As a result, the average molar area is close to the limiting value $\omega_{(\theta\to 0)} = (\omega_{max}+\omega_{min})/2$. The position of the average conformation having a molar area equal to ω at the respective θ is indicated with an arrow in Figure 3.10. With increasing coverage (Figure 3.10b), states having a smaller area requirement are preferred and have a higher fractional adsorption. As the film approaches full coverage (Figure 3.10c) the fractional adsorption of states having smaller areas increases considerably. In consequence, the average molar area approaches ω_{min}. A schematic representation of the morphology of the adsorbed interfacial layer of $(PGMA_{14})_2$-PPO_{34} at high coverage, compatible with the distribution shown in Figure 3.10c, is shown in Figure 3.12b. It has been assumed that some PPO blocks partially solubilize and protrude into the aqueous phase, rather than into the air.

Finally, it must be pointed out that, although the applied multiple conformation model is able to reproduce satisfactorily the experimental curves at low and intermediate ranges of polymer bulk concentrations, the shape of the distribution of adsorption over the various conformational states present in the adsorbed layer, shown in Figure 3.10a-c, are not exactly what would be expected for a film in equilibrium. According to a scaling description of an equilibrium layer (in which an adsorbed chain is considered as a sequence of surface bond monomer-trains interspersed with tails and loops extending away from the surface) the equilibrium distribution based on a statistical analysis of loops and tails would be unimodal probability distribution. It exhibits a single narrow peak, whose broadness depends on chain length and solvent quality, and its mean value is located around the peak maximum.[28]

3.3.8 Equilibrium *versus* Non-equilibrium Models of Polymer Adsorption

In previous discussions, it has been implicitly assumed that adsorbed layers are in a fully equilibrated state after long times. However, from some years now several experimental observations have evidenced deviations from equilibrium, not only for polymers adsorbing from the melt or concentrated solutions to strong attractive surfaces, but also for neutral homopolymers adsorbing from dilute solutions to weakly attractive surfaces. A recent review on this topic can be found elsewhere.[28] Such observations raise concerns that non-equilibrium effects may play an important role in adsorption of flexible polymers to liquid-gas interfaces as well. Unfortunately, the body of knowledge on this topic is rather limited. The influence of non-equilibrium on the structure of an adsorbed polymer layer depends mainly on the relative magnitude of the equilibration time for an adsorbed chain in comparison to the time required for adsorption. If the polymer adsorbs faster than the surface equilibrates the resulting layer morphologies are governed by kinetic rather than equilibrium parameters, and the chains within the layer are found in kinetically frozen states that do not correspond to their equilibrium conformations. Such non-equilibrium morphologies can gradually relax, be long-lived, or even persist indefinitely depending on how severe the retardation on relaxation kinetics is.

Chain dynamics within the adsorbed layer, and in consequence the relaxation kinetics and equilibration time, is determined basically by the strength of chain interactions with the interface and with other chains (hydrogen bonds, dipole attractions, dispersion forces, etc.). Also steric constraints, in the form of entanglements or mutual pinning between loops, may slow down chain dynamics. Regarding the chain-interface interactions, it has been postulated that irreversibility becomes important whenever the sticking energy of a monomeric unit to the interface is larger than the thermal excitation kT, with k being the Boltzmann constant. This value is exceeded even for weakly adsorbing polymer systems, *e.g.* adsorbed through van der Waals interactions.[28] Moreover, for long adsorbed chains their motion is hindered by many segments stuck to the surface. Accordingly, their dynamics is typically very slow, and irreversibility is in consequence very common for long polymeric chains.

Irreversibility manifests itself more clearly in the distribution of chain conformations present in the adsorbed layer (similar to those shown in Figure 3.10). Within a fully equilibrated layer all polymer chains of a sufficient length become statistically identical. Thus, the distribution of the fractional adsorption exhibits a single narrow peak.[28] If the adsorbed layer is not in equilibrium, chains are not longer statistically identical and the distribution broadens. There might also be a great number of states, each characterized by a different fractional adsorption.[28] From these considerations it seems probable that for a flexible polymer the conformational distribution within an adsorbed layer is broad and history-dependent, whenever chains adsorb considerably faster than the layer structure equilibrates.[29] If equilibration is far slower, the process can be considered as an irreversible adsorption of molecules with flexible shape.[30] In that case, according to a model proposed by Schneider *et al.*,[30] the conformational distribution is bimodal. It exhibits one population of chains adsorbed early into a highly flattened conformation that occupy a large fraction of the initially bare surface and are strongly adsorbed; and a second population of chains attached more weakly due to the smaller surface area available at latter adsorption times.[29] Such kind of U-shaped conformational distribution is evidently quite different to the sharp unimodal distribution expected for equilibrium adsorption, and the whole adsorption process departs substantially from the equilibrium adsorption picture.

A first indication that deviations from equilibrium might be relevant for adsorbed layers of $(PGMA_{14})_2$-PPO_{34} comes from the variation in the adsorption kinetics at a bare air-water interface (Figure 3.1). The lowest concentration for which a sudden slowdown in adsorption kinetic is observed is C_0 = 100 nM (Π_{eq} = 22.7 mN/m). The equilibrium surface pressure at this concentration lies exactly within the narrow range of surface pressures where a compressed spread layer enters the concentrated regime ($\Pi \sim$ 21.4-23.8) mN/m, where the already highly condensed polymer layer adopts with further compression a three-dimensional conformation with the PPO blocks protruding into the subphase. Therefore, at the kink in the adsorption kinetic curves the surface gets saturated with PPO blocks that might have a very slow chain dynamics, or be even kinetically frozen in an extended conformation due to the interplay between the strength of the interactions with the interface and other chains, and steric constraints. Hence, the remaining free surface available for adsorption after the kink

would be far smaller than at lower surface pressures. Further chains arriving at the surface could not adsorb in an extended conformation, but they must adapt their conformations to the increasingly limited surface available, which retards considerably the adsorption process. In order to overcome this high energy barrier opposing adsorption, a strong increase in bulk concentration is necessary before adsorption could further proceed, which appears to be confirmed by the flatness of region (ii) in the Γ *vs.* C_b curve of Figure 3.6a (it is also reproduced in Figure 3.11 for comparison), showing almost constant polymer adsorption. Within this region the adsorption increases only by 60% when the bulk concentration is increased more than five times. The existence of the barrier to adsorption is also evidenced if one compares the value of the polymer adsorption at the surface at a given bulk concentration (Γ) with the equivalent two-dimensional concentration in the bulk of the solution (Γ_b), according to the equation:

$$\beta = \frac{\Gamma}{\Gamma_b} = \frac{\Gamma}{(C_b)^{2/3} \cdot N_A^{-1/3}} \qquad (3.11)$$

The value of the coefficient β is an indication of how the molecules are partitioned between the interface and the solution bulk. As can be see in Figure 3.11, at very low bulk concentrations the value of β increases steeply with increasing concentration up to C_0 = 100 nM (equivalent to C_b = 11 nM). With a further increase in bulk concentration β falls and stabilizes around an average value of $\beta = 3.2 \times 10^4$. The value of β before the fall is about twice this average, which confirms the increasing barrier to adsorption above this concentration limit.

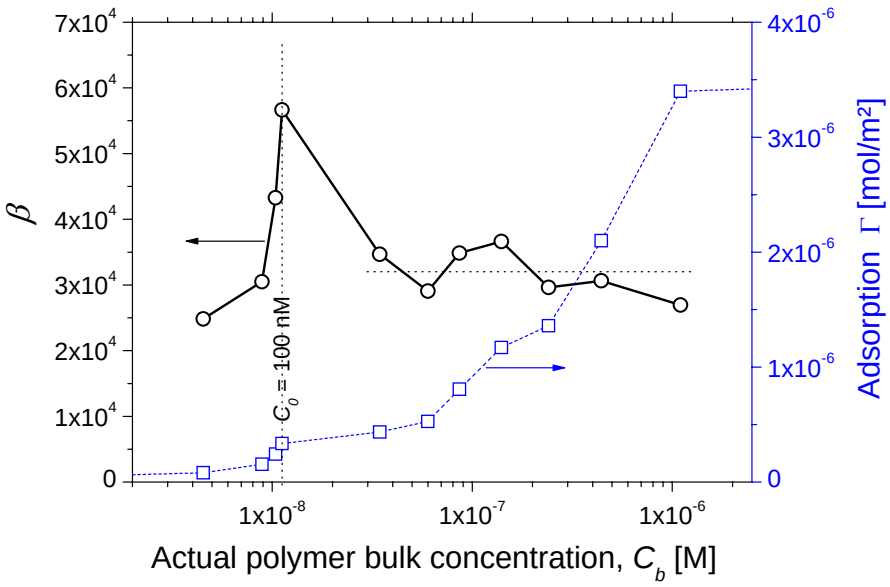

Figure 3.11: Dependence of β, defined as the ratio of $(PGMA_{14})_2$-PPO_{34} adsorption (Γ) at the air-water interface to the equivalent two-dimensional concentration in the bulk of the solution (Γ_b), on actual polymer bulk concentration (C_b). The adsorption isotherm Γ *vs.* C_b (---) is included for comparison.

Although these results are compatible with the occurrence of non-equilibrium adsorption effects during the adsorption of $(PGMA_{14})_2$-PPO_{34} at the air-water interface, they are not conclusive: the same results could be interpreted, with different assumptions, as due to the formation of a complete polymer brush layer in equilibrium. In that case, the energy barrier opposing adsorption is assumed to be created by excluded volume interactions with the already grafted chains,[12,24] and a true chemical equilibrium between fully adsorbed chains at the interface and grafted chains forming the brush would be postulated for surface concentrations in the concentrated regime.[19,24] In order to verify the relevance of non-equilibrium effects, it would be desirable to apply experimental techniques that allow for the determination of the actual distribution of chain conformations within the adsorbed layer, not only the average surface structure as is the case for neutron scattering or ellipsometry. However, this task is outside the scope of the present study.

Figure 3.12 illustrates schematically the expected morphologies for the adsorbed interfacial layer of $(PGMA_{14})_2$-PPO_{34} at the air-water interface, at surface concentrations equivalent to those of the concentrated regime ($\Gamma > \Gamma^{**}$) discussed for spread monolayers.

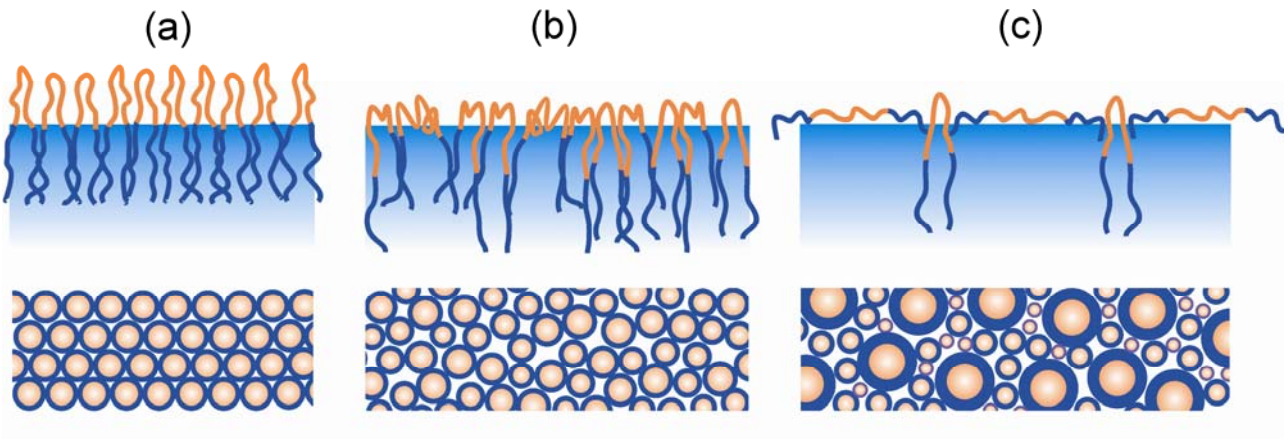

Figure 3.12: Schematic illustration of the lateral morphology of a $(PGMA_{14})_2$-PPO_{34} adsorbed layer at the air-water interface according to: (a) stratified polymer brushes model, (b) multiple conformation model, and (c) adsorption with strong non-equilibrium effects. The circles diagrams, below the lateral view of the surface, represent the area occupied by the different conformers, rather than their actual shape at the interface.

The simple model of stratified polymer brushes occupying a uniform molecular area is depicted in Figure 3.12a. In accordance to the equilibrium picture of the multiple conformation model (Figure 3.12b) there is a narrow distribution of conformations around an average conformation. This average conformation resembles, at the considered high coverage, the conformation having the minimal molar area (ω_{min}). It has been assumed that the PPO blocks partially solubilize and protrude into the aqueous phase, rather than into the air. In contrast, if non-equilibrium effects were important, as would be the case if the polymer adsorbs much faster than the surface equilibrates, mainly two populations of conformations

would be present at high surface concentrations (Figure 3.12c): one population of chains adsorbed early into a highly flattened conformation that occupy a large fraction of the initially bare surface and are strongly adsorbed; and a second population of chains attached more weakly to the interface due to the smaller surface area available at latter adsorption times.

3.4 Conclusions

Surface layers of the water-soluble amphiphilic triblock copolymers PGMA-*b*-PPO-*b*-PGMA were prepared by adsorption from the bulk and by spreading. For $(PGMA_{14})_2$-PPO_{34}, time-dependent measurements exhibit a bimodal adsorption kinetics related to the appearance of a high energy barrier against adsorption from the solution bulk. Monolayers deposited by spreading at the air-water interface are found to be stable enough to withstand compression up to high surface pressures, and to form pseudo-Langmuir films even though $(PGMA_{14})_2$-PPO_{34} is highly water-soluble at room temperature.

The following conformational transitions, identified from the changes in dilatational surface elasticity in combination with the compression isotherm, take place within the surface layer with increasing surface pressure for both adsorbed and spread layers:

(i) Transition from a dilute, bidimensional gas-like regime, to a semidilute regime occurs at a molecular area of ~ 4424 Å²/molecule (Π = 0.03 mN/m). $(PGMA_{14})_2$-PPO_{34} chains maintain a flat conformation with most segments in contact with the interface up to $\Pi \sim 2$ mN/m.

(ii) Above Π = 2.1 mN/m (1291 Å²/molecule) PGMA segments begin to change from a flat conformation to loops and tails protruding into the subphase, and form an increasingly condensed swollen layer with increasing pressures.

(iii) The onset of the conformational change for PO segments takes place at a molecular area of ~ 625 Å²/molecule (Π = 15.5 mN/m).

(iv) In the range $\Pi \sim 21.4$ to 23.8 mN/m the PPO blocks adopt a three-dimensional conformation, and the layer thickness increases accordingly. This process continues up to about $\Pi \sim 34.5$ mN/m, corresponding to an average area per PO monomeric unit of approximately 4 Å².

A new procedure was applied for the estimation of the amount of polymer absorbed at the interface as a function of the solution bulk concentration, based on tensiometry measurements. It is an alternative to more complex measuring techniques commonly used for this purpose such as neutron reflection, and can also be applied to other systems for which the approximation of a pseudo-Langmuir spread film could be justified. The obtained adsorption isotherm suggests the occurrence of a conformational change of the PPO block segments toward conformations having smaller molecular areas for actual bulk concentrations above 6.0×10^{-8} M. These changes are equivalent to those of a rather condensed spread layer already

in the middle of the concentrated regime. The surface tension isotherm exhibits, even after correction of the concentration for the depletion of the polymer from the bulk due to the polymer adsorption at the surface, a sharp break at low concentrations; besides another one at higher concentrations clearly corresponding to the bulk polymer concentration reaching the CMC. It is concluded that the low concentration break in the $(PGMA_{14})_2$-PPO_{34} surface tension isotherm (γ *vs* ln *C*) is probably due to a conformational change within the adsorbed layer.

A theoretical multiple conformation model is applied to describe the adsorption of $(PGMA_{14})_2$-PPO_{34} at the air-water interface. It reproduces satisfactorily the experimental dependency of surface pressure on polymer adsorption at low and intermediate ranges of bulk concentrations. A ratio of approximately eight between the average molecular areas at low coverage and at full coverage confirms that $(PGMA_{14})_2$-PPO_{34} molecules are highly flexible; and that they are able to adopt very different conformations during the transition of the adsorbed polymer film from a highly diluted to a nearly saturated state. It is also the reason for its considerably high surface activity at low concentrations. However, this model (with the calculated set of parameters) fails to reproduce the experimental isotherm in the upper part of the concentrated regime for $\Pi > 30$ mN/m and predicts a further increase in surface pressure instead of the plateau reached by Π.

Some experimental results indicate that non-equilibrium effects might be relevant for adsorbed layers of $(PGMA_{14})_2$-PPO_{34}. In that case, the conformational distribution would be bimodal. It exhibits one population of chains adsorbed early into a highly flattened conformation occupying a large fraction of the initial bare surface, and a second population of chains attached more weakly due to the smaller surface area available at latter adsorption times. However, those results are not conclusive, since they could also be interpreted, with different assumptions, as the formation of a complete polymer brush layer in equilibrium.

3.5 References

[1] Wanka, G.; Hoffmann, H.; Ulbricht, W. *Colloid Polym. Sci.* **1990**, *268*, 101.

[2] Wanka, G.; Hoffmann, H.; Ulbricht, W. *Macromolecules* **1994**, *27*, 4145.

[3] Alexandridis, P.; Athanassiou, V. ; Fukuda, S. ; Hatton, T.A. *Langmuir* **1994**, *10*, 2604.

[4] Noskov, B. A.; Akentiev, A. V.; Grigoriev, D. O. ; Loglio, G.; Miller, R. *J. Colloid Interface Sci*. **2005**, *282*, 38.

[5] Ann, S. W.; Thomas, R. K.; Forder, C.; Billingham, N. C.; Armes, S. P.; Penfold, J. *Langmuir* **2002**, *18*, 5064.

[6] Mu, Q. S.; Lu, J. R.; Ma, Y. H.; Paz de Banez, M. V.; Robinson, K. L.; Armes, S. P.; Lewis, A. L.; Thomas, R. K. *Langmuir* **2006**, *22*, 6153.

[7] Vieira, J. B.; Li, Z. X.; Thomas, R. K. *J. Phys. Chem. B* **2002**, *106*, 5400.

[8] Fainerman, V. B.; Lucassen-Reynders, E. H.; Miller, R. *Adv. Colloid Interface Sci*. **2003**, *106*, 237.

[9] Amado, E.; Augsten, C.; Maeder, K.; Blume, A.; Kressler, J. *Macromolecules* **2006**, *39*, 9486.

[10] Kiss, E.; Keszthelyi, T.; Kormány, G.; Hakkel, O. *Macromolecules* **2006**, *39*, 9375.

[11] Blomsqvist, B. R.; Wärnheim, T.; Claesson, P. M. *Langmuir* **2005**, *21*, 6373.

[12] Muñoz, M. G.; Monroy, F.; Ortega, F.; Rubio, R. G.; Langevin, D. *Langmuir* **2000**, *16*, 1094.

[13] Eastoe, J.; Dalton, J. S. *Adv. Colloid Interface Sci*. **2000**, *85*, 103.

[14] Díez-Pascual, A. M.; Compostizo, A.; Crespo-Colín, A.; Rubio, R. G.; Miller, R. *J. Colloid Interface Sci*. **2007**, *307*, 398.

[15] Díez-Pascual, A. M.; Monroy, F.; Ortega, F.; Rubio, R. G.; Miller, R. ; Noskov, B. A. *Langmuir* **2007**, *23*, 3802.

[16] Vollhardt, D.; Fainerman, V. B. *Adv. Colloid Interface Sci*. **2006**, *127*, 83.

[17] Lucassen-Reynders, E. H.; Fainerman, V. B.; Miller, R. *J. Phys. Chem. B* **2004**, *108*, 9173.

[18] Esker, A. R.; Kim, C.; Yu, H. *Adv. Polym. Sci.* **2007**, *209*, 59.

[19] Muñoz, M. G.; Monroy, F.; Ortega, F.; Rubio, R. G.; Langevin, D. *Langmuir* **2000**, *16*, 1083.

[20] Villanove, R.; Rondelez, F. *Phys. Rev. Lett.* **1980**, *45[18]*, 1502.

[21] Aguié-Béghin, V.; Leclerc, E.; Daoud, M.; Douillard, R. *J. Colloid Interface Sci*. **1999**, *214*, 143.

[22] Monroy, F.; Hille, H. M.; Ortega, F.; Rubio, R. G. *Phys. Rev. Lett.* **2003**, *91[26]*, 268302.

[23] Hambardzumyan, A.; Aguié-Béghin, V.; Daoud, M.; Douillard, R. *Langmuir* **2004**, *20*, 756.

[24] Barentin, C.; Muller, P.; Joanny, J. F. *Macromolecules* **1998**, *31*, 2198.

[25] Linse, P.; Hatton, A. T. *Langmuir* **1997**, *13*, 4066.

[26] Fainerman, V. B.; Lylyk, S. V.; Makievski, A. V.; Miller, R. *J. Colloid Interface Sci*. **2004**, *275*, 305.

[27] Noskov, B. A.; Akentiev, A. V.; Loglio, G.; Miller, R. *J. Phys. Chem. B* **2000**, *104*, 7923.

[28] O'Shaughnessy, B.; Vavylonis, D. *J. Phys.: Condens. Matter* **2005**, *17*, R63.

[29] Douglas, J. F.; Schneider, H. M.; Frantz, P.; Lipman, R.; Granick, S. *J. Phys.: Condens. Matter* **1997**, *9*, 7699.

[30] Schneider, H. M.; Frantz, P.; Granick, S. *Langmuir* **1996**, *12*, 994.

Part III. Triblock Copolymers of Poly(2,3-dihydroxypropyl methacrylate) and Poly(propylene oxide): Interactions with Model Lipid Membranes

4 Infrared Reflection Absorption Spectroscopy for Studying Adsorption of PGMA-*b*-PPO-*b*-PGMA at Phospholipid Monolayers

4.1 Introduction

In the second part of this investigation novel water soluble amphiphilic triblock copolymers of poly(glycerol monomethacrylate) and poly(propylene oxide)-*b*-poly(glycerol monomethacrylate) (PGMA-*b*-PPO-*b*-PGMA) were synthesized because of their expected enhanced ability to interact with biological membranes compared to the widely used poly(ethylene oxide)-*b*-poly(propylene oxide)-*b*-poly(ethylene oxide) (PEO-*b*-PPO-*b*-PEO) block copolymers. It is expected than their bulkier hydrophilic PGMA blocks might induce a disturbance in the packing of liquid-crystalline lipid bilayers in addition to the effect caused by the hydrophobic PPO block alone.

This part of the present investigation focuses on the features of PGMA-*b*-PPO-*b*-PGMA triblock copolymer adsorption to monolayers of the phospholipids dipalmitoyl-phosphatidylcholine (DPPC) and dimyristoylphosphatidylcholine (DMPC) located at the air-water interface. Such lipid monolayers found widespread application as simplified model of the outer leaflet of a cell membrane.[1] When the DPPC monolayer is initially in a liquid expanded (LE) fluid-like state the progressive adsorption of the polymer induces a first order transition of the monolayer into a more ordered liquid condensed (LC) state. In the transition region two kinds of lipid domains having different degrees of order coexist. Such domains are large enough for being visualized *in situ* by optical methods; therefore epifluorescence microscopy[2] and Brewster Angle Microscopy (BAM)[3,4] have been normally used for studying the changes in morphology of lipid monolayers brought about by surfactant adsorption. However, there is an obvious limit on the size of the structures that can be optically resolved. A useful complementary technique is infrared reflection absorption spectroscopy (IRRAS) which has proved to be a powerful tool for the *in situ* investigation of molecular structure information, such as molecular conformation and orientation, also in connection to lipid monolayers.[5] In this section the adsorption kinetics of PGMA-*b*-PPO-*b*-PGMA triblock copolymer to phospholipids monolayers and the concomitant interactions between them are discussed, as investigated by IRRAS coupled with BAM and surface pressure measurements in order to gain a better insight into the polymer-membrane interactions on the molecular level.

4.2 Experimental

4.2.1 Materials

1,2-Dimyristoyl-*sn*-glycero-3-phosphocholine (DMPC), 1,2-dipalmitoyl-*sn*-glycero-3-phosphocholine (DPPC) and the acyl chain perdeuterated analogous 1,2-dipalmitoyl-d62-*sn*-glycero-3-phosphocholine (DPPC-d_{62}) and 1,2-dimyristoyl-d54-*sn*-glycero-3-phosphocholine (DMPC-d_{54}) were purchased from Avanti Polar Lipids (Alabaster, AL) and used as received. The general chemical structure of the lipids is shown in Figure 4.4. A 10 mM phosphate buffer solution (pH = 7) prepared in ultrapure water (SG Wasseraufbereitung und Regenerierstation GmbH, Germany) was used as subphase for all experiments. The synthesis of the block copolymer PGMA-*b*-PPO-*b*-PGMA is discussed in detail in section 2.2.

4.2.2 Surface Tension Measurements

Adsorption experiments at constant surface area were performed in a square Teflon trough (Riegler & Kirstein, Berlin, Germany) with dimensions 59.8 mm × 59.8 mm × 3.2 mm, and a subphase volume of 15.7 mL. For preparation of a phospholipid monolayer a defined amount of fresh lipid solution in chloroform was spread with a glass microsyringe onto the subphase. After waiting for 15 min for complete solvent evaporation, an aqueous solution of the triblock copolymer was injected below the phospholipid monolayer through a channel just above the bottom of the trough. For reference measurement the polymer was injected into pure water without the lipid monolayer. The subphase was stirred with a small rolling sphere to ensure a homogeneous bulk concentration without large perturbations of the surface. For monitoring the change in surface pressure due to the injected copolymer, the surface tension was measured using a Wilhelmy film balance with a filter paper as plate. The surface tension γ is related to the surface pressure, Π, by $\Pi = \gamma_0 - \gamma$, where γ is the surface tension of the water surface after copolymer adsorption and γ_0 is the surface tension of pure water (γ_0 = 72.75 mN/m at 20°C). The surface pressure was measured with a precision of 0.01 mN/m. The reproducibility of adsorption experiments was estimated to be ± 0.2 mN/m. The temperature of the trough was maintained constant at 20°C by circulating thermostated water through a jacket surrounding the trough.

4.2.3 Surface Pressure (Π) - Area (A) Isotherms

Variable area experiments, namely phospholipid Π-A isotherms and polymer squeeze out experiments, were carried out in a rectangular Teflon trough (Riegler & Kirstein, Berlin, Germany) with dimensions 300 mm × 60 mm equipped with a Wilhelmy film balance for monitoring the surface pressure Π. The available area was varied during the experiment by changing the distance between two mobile Teflon barriers positioned symmetrically to the

trough center at a compression rate of 1 $Å^2$ per lipid molecule per min. The temperature of the trough was maintained constant at 20°C.

4.2.4 Infrared Reflection Absorption Spectroscopy Measurements

Experiments were performed in an IRRAS setup consisting basically of a Teflon trough (Riegler & Kirstein, Berlin, Germany) and an FT-IR spectrometer (Bruker Equinox 55, Karlsruhe, Germany) connected to an XA 511 reflection attachment (Bruker) equipped with an external narrow band mercury-cadmium-telluride (MCT) detector. The trough is divided into two compartments, one for the sample (59.8 mm × 59.8 mm × 3.2 mm) the other for the reference subphase. Both compartments are connected through a long Teflon tube in order to ensure that the liquids in the two troughs have the same height throughout the duration of the experiment, while effectively preventing diffusion of the sample into the reference compartment. The sample trough contained the Wilhelmy film balance for monitoring the surface pressure. The temperature of 20°C was kept constant by a circulating water bath. The experimental setup is covered by a plexiglas box in order to ensure constant air humidity. Procedures for lipid monolayer spreading and polymer injection are the same as for surface pressure measurements, including injecting through a channel and stirring of the subphase.For spectra acquisition, the IR beam is directed by means of a group of mirrors onto the liquid surface at an angle of incidence of 40° with respect to the surface normal. A KRS-5 polarizer (>98% degree of polarization) is used to generate perpendicular polarized light (*s*-polarized). The trough system is positioned on a moveable platform which allows shuttling between the sample and the reference trough. This shuttle technique diminishes the noise due to water vapor absorbing IR radiation in the beam path. After allowing for temperature and humidity equilibration inside the chamber, IRRA spectra were recorded continuously at a spectral resolution of 4 cm^{-1} using a Blackman-Harris 4-term apodization and a zero filling factor of two. One thousand scans were collected for a total acquisition time of around 5.2 min per spectrum. The IRRA spectrum was calculated as $\log(R/R_0)$, so called reflectance-absorbance (RA), where R_0 is the single beam reflectance spectrum from the water surface on the reference trough and R is the single-beam reflectance spectrum from the sample trough. Reflection-absorption spectra are usually presented as $-\log(R/R_0)$, however in this work inverted spectra are shown for the sake of clarity.

4.2.4.1 Angle Dependent IRRAS Measurements

IRRA spectra at several angles of incidence from 32° to 70° in 2° steps were recorded, using both *p*-(parallel) and *s*-polarized IR radiation with 2000 and 1000 scans per spectrum, respectively, and 6 cm^{-1} spectral resolution. After a baseline correction using the OPUS software (Bruker), the intensity of $\nu_{as}(CD_2)$ and $\nu_s(CD_2)$ vibrational bands of DPPC-d_{62} were determined by the standard method of the OPUS software package. Measurements with *p*-polarized light near the Brewster angle were eliminated because of their poor signal-to-noise ratio due to the minimum in reflectivity of *p*-polarized radiation at the Brewster angle. IRRAS

bands simulations were performed using a Visual Basic program, implementation of a formalism reported previously.[6,7] The corresponding optical theory[8-10] as well as the formulas necessary to calculate the respective IRRAS bands using a Lorentzian band[11,12] have been reviewed in detail elsewhere. In short, the required parameters for the average tilt angle θ simulation of the molecular axis relative to the surface normal are the following: the refractive indices of the film phase n_o and n_{eo}, the refractive index of the water subphase, the absorption coefficient of the water subphase, the angle of incidence, and the polarizer efficiency. The ordinary and extraordinary refractive indices n_o and n_{eo} of the lipid film were both set equal 1.41.[13] The necessary data for water were taken from literature[14] and interpolated to the desired step width over the required wavenumber range. The polarizer efficiency in the region of the $\nu(CD_2)$ stretching bands was 0.015.

4.2.5 Brewster Angle Microscopy Measurements

BAM is a probe-free technique for the visualization of monolayer domains. The contrast arises from differences in reflectivity of *p*-polarized light impinging under the Brewster angle onto the air-water interface. Such differences in reflectivity within a film stem basically from variations in the refractive index, thickness and optical anisotropy of the film.[3] In this study a commercially available BAM microscope (Nanofilm Technologie, Göttingen, Germany) was used to monitor changes in the morphology of lipid monolayers caused by adsorption of the amphiphilic polymer. The air-monolayer interface was illuminated at angle of incidence of ca. 53° by a *p*-polarized laser beam of wavelength 688 nm, the reflected light passes through an analyzer, and a lens system focuses an image on a CCD camera. The analyzer was *p*-positioned after spreading the lipid monolayer for filtering out the residual *s*-polarized light before polymer injection and was fixed at this position during the whole measurement. The system delivers images of a surface around 2.70 × 1.85 mm² with a resolution below 20 µm. Images were processed with the software Image-Pro Plus (Media Cybernetics, Bethesda, MD).

4.3 Results and Discussion

4.3.1 Π *versus* A Isotherms of Perdeuterated Phospholipid Monolayers

In spite of its simplicity, the monolayer technique is a valuable method for studying potential interactions between cell membranes and biological active substances as, *e.g.* antimicrobial peptides, proteins or drugs acting at the membrane level.[15] An insoluble lipid monolayer spread at the air-water interface serves as simplified model of the outer leaflet of the cell membrane. By varying the available area per lipid molecule, and consequently the monolayer lateral pressure, or changing temperature it is possible to force the monolayer

through different physical states which in turn simulate variations in the molecular packing and fluidity of the actual cell membrane.

For studying the interaction of the uncharged block copolymer zwitterionic phosphatidylcholines were chosen as the lipid component (see Figure 4.4 for chemical structure). Phosphatidylcholines are the most abundant lipids in the mammalian cell membrane;[16] among them DPPC is a critical determinant of the physiological function of pulmonary surfactant and makes up to one third of it.[17] For these reasons DPPC is frequently the phospholipid of choice for monolayer studies. On the other hand, not only the nature of the lipid headgroup but also the physical state of the acyl chains plays a crucial role in the penetration process. Therefore both DPPC, which exhibits at room temperature a first order phase transition between a fluid LE state and a more rigid LC state with increasing Π; and the dimyristoyl phospholipid (DMPC), whose monolayers do not exhibit an LE-LC phase transition and are more expanded than the corresponding DPPC ones, were chosen for studying the influence of the physical state of the lipid monolayer on block copolymer penetration.

Furthermore, due to the overlapping in the methyl/methylene stretching vibration region between several IRRA bands coming from the copolymer backbone with bands coming from the lipid acyl chains, both being of interest for this investigation, the acyl chain perdeuterated phospholipids DPPC-d_{62} and DMPC-d_{54} were used for IRRAS measurements, although some control measurements were also made with DMPC and DPPC. Figure 4.1 illustrates the surface pressure (Π) /area per molecule (A) isotherms of pure DPPC-d_{62} and DMPC-d_{54} monolayer films at the air-water interface at 20°C. Although for the plateau region in the DPPC-d_{62} isotherm, where both LC and LE phases coexist, a zero slope is ideally expected in accordance with a first order phase transition,[18] experimentally this is normally not the case. Only under conditions of extreme purity, very low compression rates, and film stability a zero slope is obtained.[19] For the same reasons DPPC isotherms obtained under slightly different experimental conditions vary considerably.[20] Besides the mean area per lipid molecule an important property of the monolayer is its compressibility, κ, defined as:

$$\kappa = -\frac{1}{A}\left(\frac{\partial A}{\partial \pi}\right)_T \qquad (4.1)$$

The corresponding compressibilities derived from the lipid isotherms according to Eq. 4.1 are shown in the inset. As can be seen in Figure 4.1, the isotherms of DPPC-d_{62} and DMPC-d_{54} are practically identical for low lipid densities until a surface pressure high enough for inducing a close packing of the lipid molecules in LC domains is reached. The exact value of this transition pressure, $\Pi_{LE\text{-}LC}$, can be determined from the corresponding transition area, $A_{LE\text{-}LC}$, located at the kink in the compressibility curve of DPPC-d_{62}.[21] With this procedure, the beginning of the LE-LC coexistence region is found to be $A_{LE\text{-}LC}$ = 71.0 Å²/lipid molecule and $\Pi_{LE\text{-}LC}$ = 10.4 mN/m. Since the effect of adsorption of a block copolymer into a DPPC monolayer has been found to be equivalent, to some extent, to a mechanical compression of the film,[22] the considerable compressibility difference between DPPC-d_{62} and DMPC-d_{54}

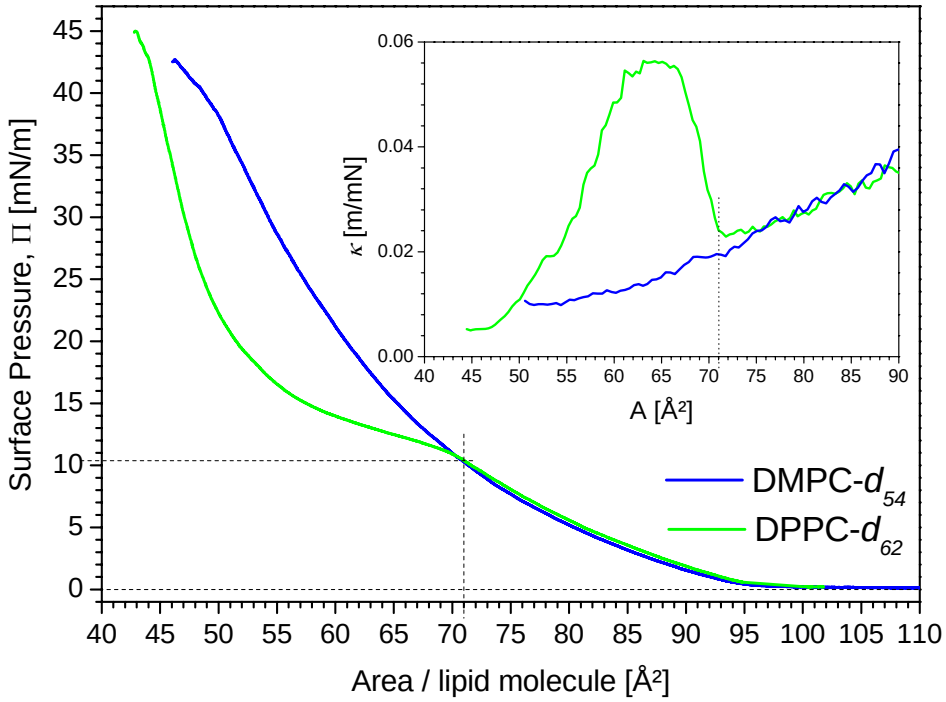

Figure 4.1: Surface pressure (Π) / area (A) isotherms of pure 1,2-dipalmitoyl-d62-*sn*-glycero-3-phosphocholine (DPPC-d_{62}, green curve) and 1,2-dimyristoyl-d54-*sn*-glycero-3-phosphocholine (DMPC-d_{54}, blue curve) monolayer films at the air-water interface at 20°C. The monolayer compressibilities (κ) derived from the corresponding Π-A isotherm are shown in the inset.

during compression isotherm measurements is expected to influence the adsorption process of $(PGMA_{14})_2$-PPO_{34} at constant surface area and to be reflected as kinetic and morphological differences between experiments with one or the other lipid.

4.3.2 Adsorption of Triblock Copolymer to Perdeuterated Phospholipid Monolayers at Constant Surface Area

4.3.2.1 Constant Copolymer Concentration and Variable Lipid Initial Surface Pressure

An example of the evolution of surface pressure during the adsorption of $(PGMA_{14})_2$-PPO_{34} to DPPC-d_{62} monolayers at different initial surface pressures (Π_0), which is equivalent to different lipid lateral packing densities (δ_0), is presented in Figure 4.2. The polymer concentration in the bulk of the solution is 8 μM for all measurements. Zero time corresponds to the injection of the copolymer into the subphase and although the time scale spans a period of only 5 h the total observation time is at least 12 h, which is found to be long enough for assuring adsorption equilibrium for the selected initial lipid surface pressures. The initial portion of the curves prior to polymer injection corresponds to the equilibration period of the lipid monolayers. The shape of the curve for adsorption of the copolymer to a pure air-water interface shows that in spite of being injected under stirring no polymer adsorbs to the interface up to about 22 min after injection. What is more important, contrary to the sharp

jump in Π that has been reported in some studies dealing with Poloxamers[23,24] immediately after injecting them through a lipid monolayer, no instantaneous increase in Π took place as a consequence of injection below lipid films even at the lowest initial packing density, which allows us to ensure that the film was not disturbed during the injection procedure, and that the curves correspond indeed to the adsorption of the copolymer into an intact lipid monolayer. A comparison of the adsorption behavior to monolayers initially in the liquid expanded regime (Π_0 < 10.4 mN/m) *versus* those in the liquid condensed regime evidences the role of monolayer compressibility in copolymer adsorption kinetics. With increasing adsorption of $(PGMA_{14})_2$-PPO_{34} to LE monolayers the available area per lipid molecule decreases gradually until a surface pressure corresponding to the onset of the LE-LC phase transition, $\Pi_{LE\text{-}LC}$, is reached. From this point the monolayer compressibility increases steeply (see inset in Figure 4.1). Consequently, further copolymer adsorption forces lipids from the liquid-expanded into the liquid-condensed state thereby creating accessible area for additional adsorption, which in turns accelerates markedly the adsorption process, as evidenced by a less steep slope in Figure 4.2. This adsorption mechanism, sometimes called "excluded area effect"[25] is typical for lipids undergoing an LE-LC monolayer phase transition. On the contrary, copolymer adsorption to lipid monolayers already in the LC regime cannot drive any further lipid condensation and no vertical slope is obtained. As the monolayer cannot accommodate copolymer molecules by the excluded area mechanism, also the extent of polymer adsorption is reduced.

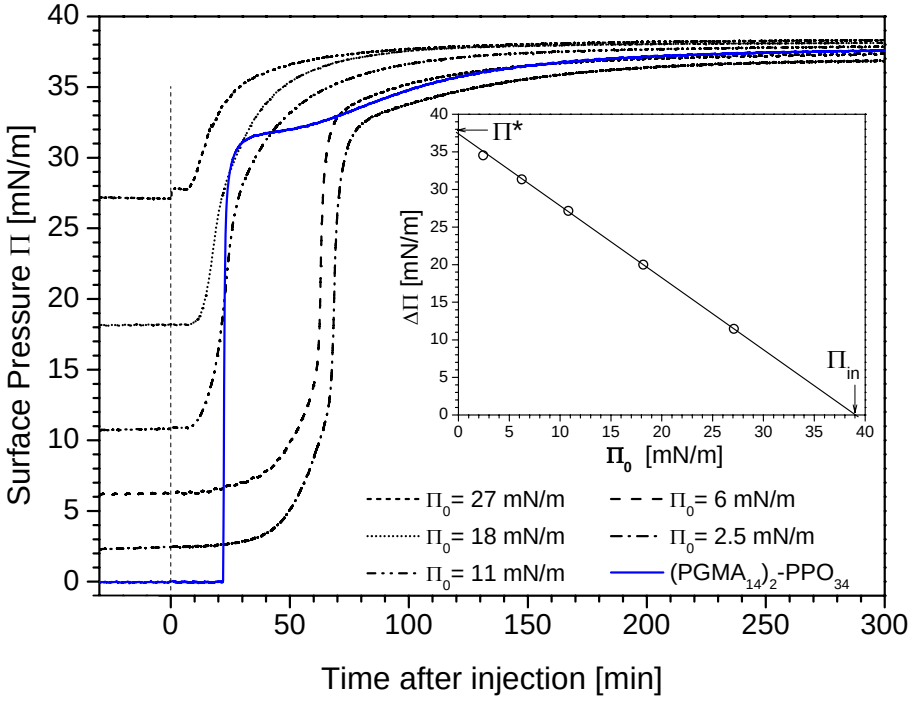

Figure 4.2: Time dependent increase in surface pressure induced by $(PGMA_{14})_2$-PPO_{34} adsorption to a pure air-water surface (blue curve) and to DPPC-d_{62} monolayers at different lipid initial surface pressures (Π_0) at 20°C. The polymer concentration was 8 µM for all experiments. The inset shows the dependence of the surface pressure increase at equilibrium ($\Delta\Pi = \Pi_{eq}$-Π_0) on Π_0. Π^* is the surface pressure at equilibrium when polymer is injected below pure water and Π_{in} is the lipid pressure above which the copolymer no longer penetrates the monolayer.

The inset in Figure 4.2 illustrates the dependence of the surface pressure increase ($\Delta\Pi = \Pi_{eq} - \Pi_0$) on Π_0, where Π_{eq} is the surface pressure once equilibrium was achieved. $\Delta\Pi$ is a linear function of Π_0, in agreement with previous results on to adsorption of the amphiphilic polypeptides δ-lysin and melittin to various phospholipid monolayers.[26] By extrapolating to higher values of Π_0 up to $\Delta\Pi = 0$ the maximum penetration surface pressure Π_{in}, defined as the lipid pressure above which the copolymer no longer penetrates the monolayer, is determined as 39.1 mN/m. The fact that Π_{in} is slightly higher than the equilibrium surface pressure when the copolymer adsorbs at a neat air-water interface ($\Pi_0 = 0$) at the same bulk concentration of 8 μM, $\Pi^* = 37.9$ mN/m, gives an indication of moderate affinity between copolymer and lipid. Because the surface pressure of a lipid monolayer for having a lateral packing density equivalent to that of a biologically relevant bilayer membrane, Π_M, is generally $\Pi_M \geq 28$ mN/m[16] (for comparison, Π_M~30 mN/m in the case of lipid bilayers used as membrane models[1]), the ability of $(PGMA_{14})_2$-PPO_{34} to penetrate up to a $\Pi_{in} = 39.1$ mN/m suggests that this copolymer would be able to insert into relevant biological membranes, such as in the blood-brain barrier (Π_M~35 mN/m) or erythrocyte membranes (Π_M = 31-35 mN/m).[16]

4.3.2.2 Constant Lipid Initial Surface Pressure and Variable Polymer Concentration

Examples of the surface pressure increase during the adsorption of $(PGMA_{14})_2$-PPO_{34} to DMPC-d_{54} monolayers at a constant initial surface pressure, Π_0~10.5 mN/m, are presented in Figure 4.3. The copolymer concentration, *C*, in the bulk of the solution was varied from 300 nM to 8 μM. Also the corresponding curves for copolymer adsorption to a pure air-water interface at the same bulk concentrations are shown. With increasing copolymer concentration, higher amounts are adsorbed at the interface up to a concentration, C_s, where saturation of the interface is reached. At this concentration the equilibrium surface pressure of the mixed monolayer, Π_{eq}, equals that of the copolymer adsorbed at an air-water interface, Π^*; consequently, the difference between them, defined as $\Delta\Pi^* = \Pi_{eq} - \Pi^*$, vanishes.

The inset in Figure 4.3 illustrates the dependence of $\Delta\Pi^*$ on copolymer concentration. For comparison, a set of equivalent measurements with DPPC-d_{62} was carried out, and the corresponding $\Delta\Pi^*$ *vs.* *C* curve is also shown in the inset. By extrapolation to higher concentrations up to $\Delta\Pi^* = 0$ the saturation concentration was determined to be 6.8 μM and 9.5 μM for DPPC-d_{62} and DMPC-d_{54} monolayers, respectively. The fact of C_s being lower for DPPC-d_{62} than for DMPC-d_{54} is clearly a consequence of DMPC-d_{54} lacking an LE-LC phase transition, and being therefore unable to accommodate copolymer molecules by the mentioned excluded area mechanism as is the case for DPPC-d_{62}.

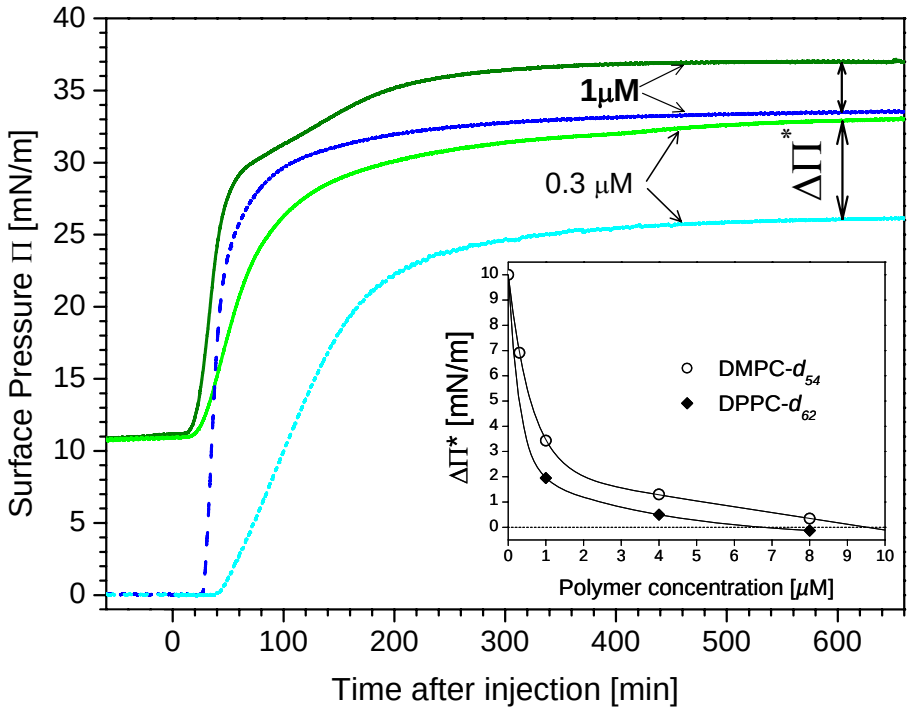

Figure 4.3: Time dependent increase in surface pressure due to the adsorption of $(PGMA_{14})_2$-PPO_{34} at DMPC-d_{54} monolayers (Π_0~10.5 mN/m, 20°C) with increasing copolymer concentrations (green full lines). Only two concentrations are shown for the sake of clarity. The corresponding curves for copolymer adsorption to a pure water surface ($\Pi_0 = 0$, blue dashed lines) are also shown. The inset shows the dependence of $\Delta\Pi^* = \Pi_{eq} - \Pi^*$ on polymer concentration, being Π^* the surface pressure at equilibrium when polymer is injected below pure water.

4.3.3 IRRAS Investigations

4.3.3.1 Pure Lipid / Triblock Copolymer Monolayers

Figure 4.4 illustrates the IRRA spectra of $(PGMA_{14})_2$-PPO_{34} (Π = 36.9 mN/m) adsorbed to the air-water interface and spread monolayers of pure DMPC-d_{54} (Π = 37.3 mN/m) and DPPC-d_{62} (Π = 37.5 mN/m). In order to enable the comparison of the main features of the IRRA spectra of the copolymer with those of the lipids, spectra were taken at around the same surface pressure. The most characteristic feature for all IRRA spectra is the strong broad band centered at around 3580 cm^{-1} corresponding to ν(O-H), the stretching vibration of the O-H bonds from water. In the case of $(PGMA_{14})_2$-PPO_{34} this band completely hides the band coming from the stretching vibration of the hydroxyl groups in the diol function of the PGMA blocks, which is expected to be found in this region. The intensity of the ν(O-H) band correlates in a complex way with the thickness, composition and surface density of the film.[5] The considerable difference in ν(O-H) band intensity between DPPC-d_{62} and DMPC-d_{54} in spite of their similar chemical composition is attributed on the one hand to DPPC-d_{62} acyl chains being longer, and consequently the monolayer being thicker, than for DMPC-d_{54}; and, on the other hand, to the higher lateral packing density, or lower available area per molecule, of DPPC-d_{62} (45.2 Å²/lipid molecule) compared to DMPC-d_{54} (50.4 Å²/lipid molecule, see Figure 4.1).

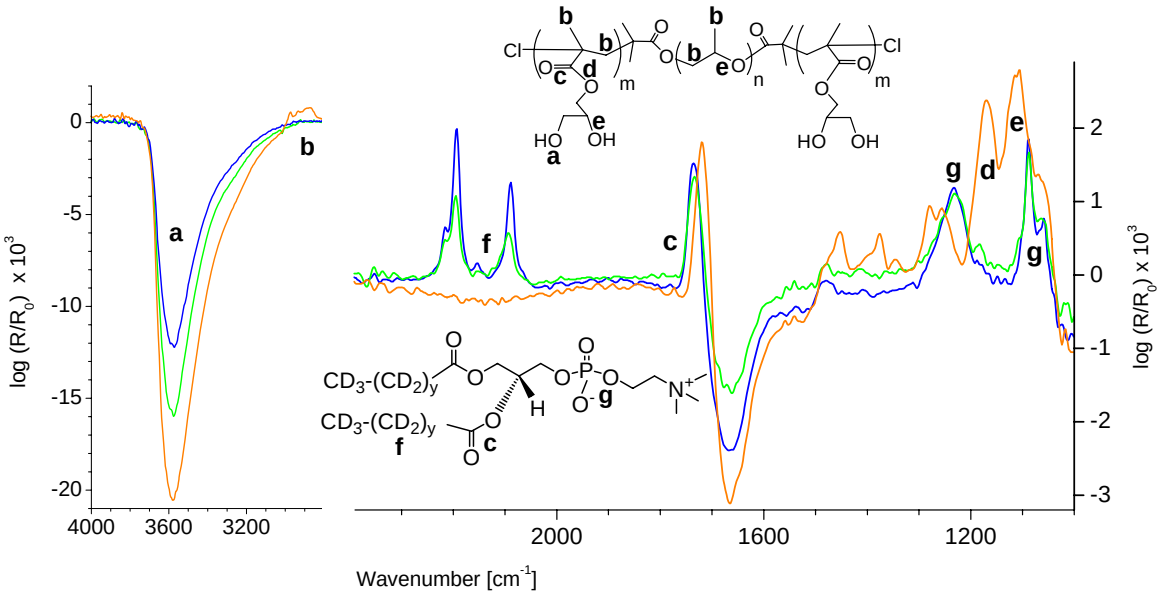

Figure 4.4: Inverted IRRA spectra of monolayer films of $(PGMA_{14})_2$-PPO_{34} at Π = 36.9 mN/m (orange curve); DMPC-d_{54} (y = 12) at Π = 37.3 mN/m (blue curve); and DPPC-d_{62} (y = 14) at Π = 37.5 mN/m (green curve) at the air- water interface at 20°C. The regions indicated correspond to the following vibrational modes: (a) hydroxyl stretching from water and dihydroxypropyl group; (b) methyl/methylene stretching; (c) carbonyl group stretching; (d) ester group stretching; (e) ether group stretching; (f) perdeuterated methyl/methylene stretching; and (g) phosphate group stretching. The ordinate corresponds to log(R/R_0) values.

Most bands in the IRRA spectrum of $(PGMA_{14})_2$-PPO_{34} are a combination of vibration modes coming from the middle PPO block overlapped with contributions from both PGMA outer blocks. The frequencies of the most characteristic IR vibrational bands, and its corresponding assignment are presented in Table 4.1. Regarding the lipid monolayers, the frequency of the methylene stretching vibration is sensitive to the conformational order of the lipid acyl chains, and responds to changes of the trans/gauche ratio in acyl chains.[27] Therefore, the shift of the $\nu_{as}(CD_2)$ and $\nu_s(CD_2)$ bands to lower frequencies for DPPC-d_{62} when compared to those of DMPC-d_{54} is an indication of a higher conformational order of the acyl chains of DPPC-d_{62}. On the other hand, the ester carbonyl stretching vibration is sensitive to hydrogen bonding and polarity distribution of the interfacial region; and due to hydrogen bonding to the oxygen atom the band frequency for a fully hydrated lipid is decreased as compared to that of a lipid in anhydrous state.[28] Consequently, the higher frequency of the ν(C=O) band for DPPC-d_{62} indicates a more dehydrated state when compared to that of DMPC-d_{54}. Further detailed assignment and discussion about infrared spectroscopy of lipid membranes can be found in several comprehensive reviews.[27-30]

Table 4.1: Assignment and wavenumber in cm^{-1} of IR vibrational modes observed in IRRA spectra of $(PGMA_{14})_2$-PPO_{34}, DMPC-d_{54} and DPPC-d_{62} films at the air-water interface at 20°C and Π~37 mN/m.

$(PGMA_{14})_2$ -PPO_{34}	DMPC-d_{54}	DPPC-d_{62}	IR vibrational mode
2972			$\nu_{as}(CH_3)$ methyl antisymmetric stretching
2933			$\nu_{as}(CH_2)$ methylene antisymmetric stretching
	2216	2215	$\nu_{as}(CD_3)$ perdeuterated methyl antisymmetric stretching
	2195	2194	$\nu_{as}(CD_2)$ perdeuterated methylene antisymm. stretching
	2093	2089	$\nu_s(CD_2)$ perdeuterated methylene symmetric stretching
1719	1734	1736	ν(C=O) carbonyl stretching
1452			$\delta_{as}(CH_3)$ methyl antisymmetric bending
1376			$\delta_s(CH_3)$ methyl symmetric bending
1280			$\delta(CH_2)$ twisting
1256			$\delta(CH_2)$ twisting
	1232	1233	$\nu_{as}(PO_2^-)$ phosphate antisymmetric stretching
1170			ν_{as}(CO-O-C) ester antisymmetric stretching
1115			ν(C-O) from 2° alcohol
1106			ν(C-O-C) ether stretching vibration
	1088	1089	$\nu_s(PO_2^-)$ phosphate symmetric stretching
1070			ν_s(CO-O-C) ester symmetric stretching / ν(C-O) from 1° alcohol
	1064	1059	ν(C-O-PO_2^-) phosphate-ester stretching
	971	973	ν(C-N^+-C) choline moiety stretching

4.3.3.2 Time Dependent Adsorption to Phospholipid Monolayers in an LE phase

Three dimensional representations of the time-dependent IRRA spectra collected during the adsorption of $(PGMA_{14})_2$-PPO_{34} to the air-water interface in the presence of a lipid monolayer offer a valuable overview of the changes in chemical composition, molecular conformation and orientation involved in the process (see Figure 4.5). For these measurements, an aqueous polymer solution is injected under moderate stirring at the bottom of the sample trough below a DPPC-d_{62} monolayer spread at $\Pi_0 = 2.5$ mN/m. The polymer concentration reached was 8 μM. The time evolution of the vibrational bands in the IRRA spectra is shown in the 3D-plots and contour plots in Figure 4.5.

The sudden decrease in intensity of the ν(O-H) band (Figure 4.5a) marks the onset of the copolymer adsorption, around 60 min after being injected (Note that reflection-absorption spectra are inverted and presented as $\log(R/R_0)$ for the sake of clarity). Spectra observed before this time correspond to a pure lipid monolayer. The time development of the methyl/methylene stretching bands is better visualized in the accompanying contour plot.

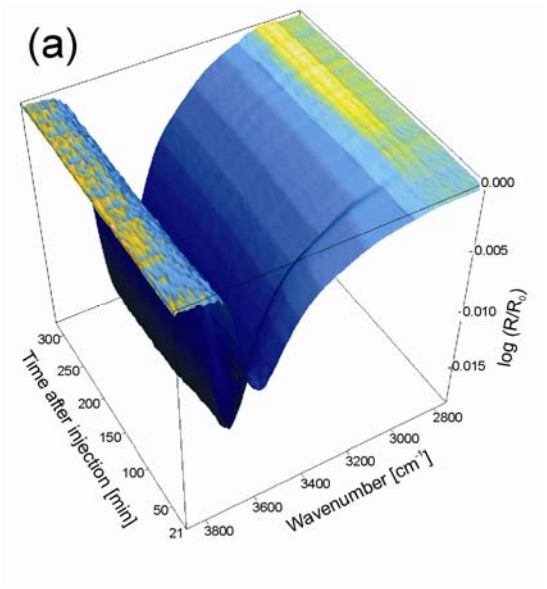
(a)
Time after injection [min]
Wavenumber [cm⁻¹]
log (R/R₀)

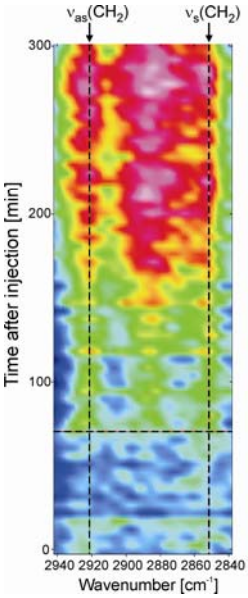
νas(CH2)
νs(CH2)
Time after injection [min]
Wavenumber [cm⁻¹]

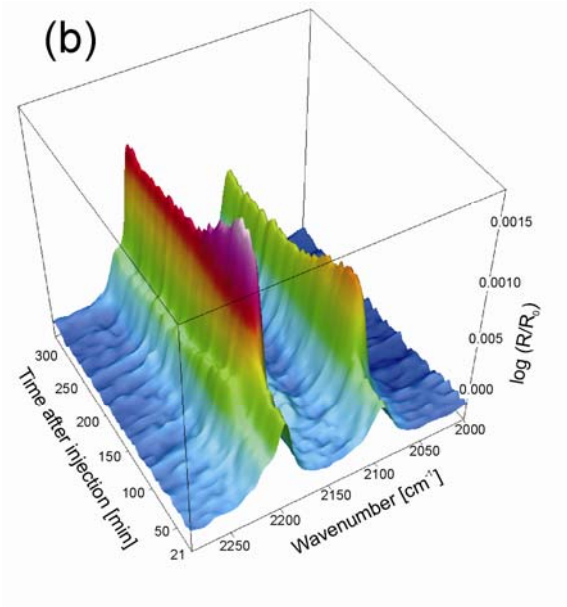
(b)
Time after injection [min]
Wavenumber [cm⁻¹]
log (R/R₀)

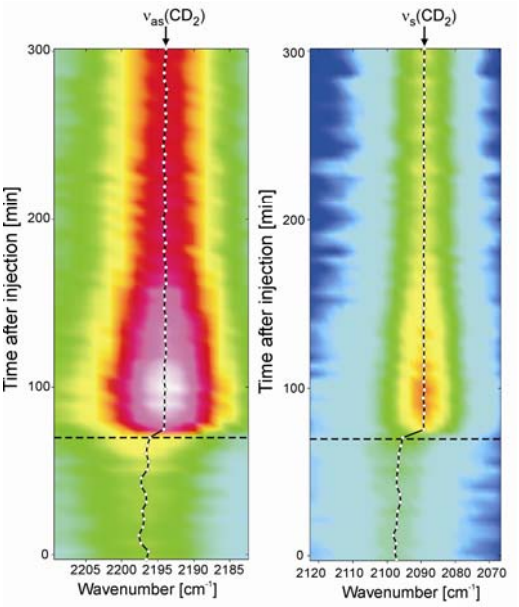
νas(CD2)
νs(CD2)
Time after injection [min]
Wavenumber [cm⁻¹]

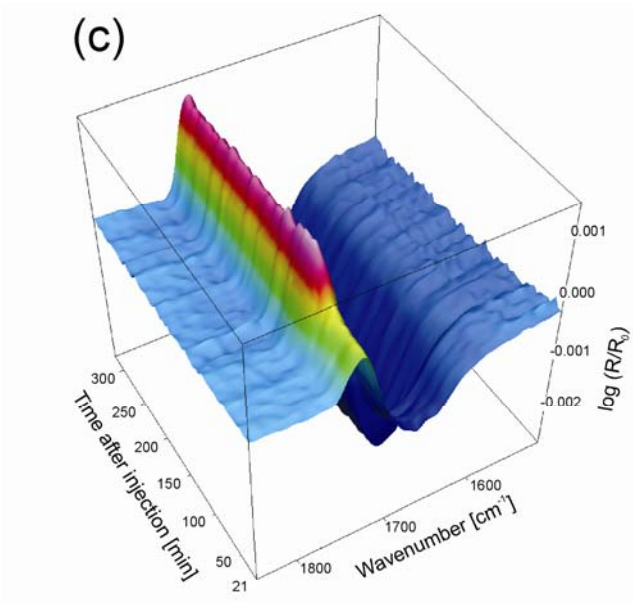
(c)
Time after injection [min]
Wavenumber [cm⁻¹]
log (R/R₀)

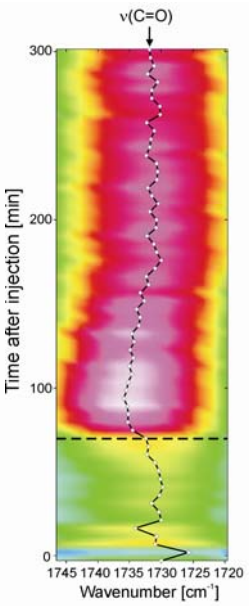
ν(C=O)
Time after injection [min]
Wavenumber [cm⁻¹]

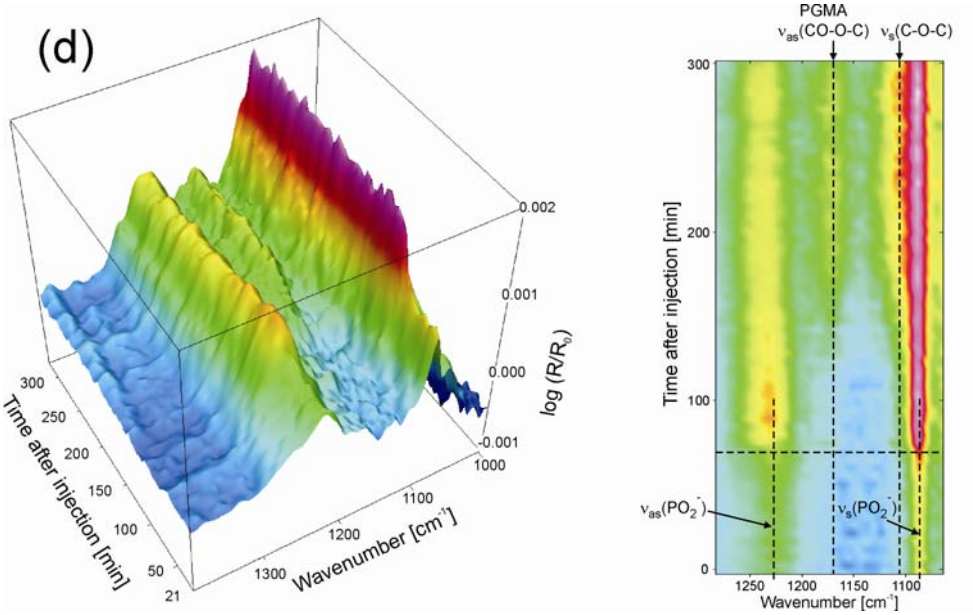

Figure 4.5: Time-dependent inverted IRRA spectra during the adsorption process of $(PGMA_{14})_2$-PPO_{34}, 8 µM, to a DPPC-d_{62} monolayer found initially in a liquid expanded (LE) phase (Π_0= 2.5 mN/m). The following vibrational modes are presented in the 3D plots: (a) ν(O-H) / $\nu(CH_2)$; (b) $\nu(CD_2)$; (c) ν(C=O) and (d) $\nu(PO_2^-)$ / ν(CO-O-C) / ν(C-O). The position of the most significant IRRA bands found in each region is indicated in the corresponding contour plots.

Although these bands probably appear simultaneously with the decrease in the ν(O-H) band, they are relatively weak and can be distinguished clearly from the baseline noise only some minutes later (for comparison purposes this time is indicated by a horizontal line in the contour plots at 69.5 min in Figures 4.5a-d). The most intense bands are the methylene group stretching bands, $\nu_{as}(CH_2)$ at 2921 cm^{-1} and $\nu_s(CH_2)$ at 2852 cm^{-1}, which originate predominantly from methylene groups in the PPO middle block with a minor contribution from the CH_2 moieties in the PGMA blocks. This assignment is based on reference IRRAS measurements carried out with homopolymers of PPO and PGMA. The pronounced frequency shift of the $\nu_{as}(CH_2)$ band from 2933 cm^{-1} for the copolymer adsorbed at the air-water interface to 2921 cm^{-1} for the copolymer inserted into the DPPC-d_{62} monolayer clearly evidences the presence of the PPO block in the more hydrophobic solid-hydrocarbon like environment that is found in the hydrophobic region of the lipid monolayer. Similar effects were observed before for the change in frequency of the CH_2 stretching bands of poly(*N*-*n*-propylmethacrylamide) and poly(*N*-isopropylmethacrylamide) observed during their coil-globule transition when the water is expelled from the interior of the globule making its inner core more hydrophobic.[31]

The spectral region shown in Figure 4.5b includes the perdeuterated methylene antisymmetric stretching $\nu_{as}(CD_2)$ and methylene symmetric stretching $\nu_s(CD_2)$ bands coming from the lipid perdeuterated acyl chains. As can be clearly seen from the curve on the contour plot connecting the band maximum for each spectrum, the progressive copolymer adsorption shifts the frequency of the $\nu_{as}(CD_2)$ band to lower wavenumber going from approximately

2197 cm^{-1} down to 2194 cm^{-1}. The latter value is typical for perdeuterated acyl chains with substantial conformational order.[32] The 3D plot shows also that simultaneously with the frequency shift, an increase in $\nu_{as}(CD_2)$ band intensity takes place; this can be better visualized in Figure 4.6a, where the time development of the intensity at band maximum for some selected bands is shown. The $\nu_{as}(CD_2)$ intensity increase is caused by the narrowing of the band, and by the reduction of the tilt angle of the acyl chains, *i.e.* the lipid molecules bring their tails axes closer to the surface normal. The subsequent slight decrease in $\nu_{as}(CD_2)$ band intensity (see Figure 4.6a) could be attributed to a relaxation in the tilt angle of the previously compressed acyl chains. However, this relaxation is only partial and the band intensity at equilibrium is considerable higher than before copolymer adsorption. The development of the symmetric $\nu_s(CD_2)$ band (see corresponding contour plot) follows a similar pattern as the antisymmetric band, regarding both band frequency shift and intensity variation. It shifts from approximately 2097 cm^{-1} down to 2089 cm^{-1} at equilibrium. This frequency shift of approximately 8 cm^{-1} is far more pronounced than for the $\nu_{as}(CD_2)$ band, making the $\nu_s(CD_2)$ band frequency more adequate for following the changes brought in by the copolymer adsorption.

The time evolution of the carbonyl group stretching band, ν(C=O), is illustrated in Figure 4.5c. Initially this band originates exclusively from the ester carbonyl stretching vibrations of both lipid acyl chains. Its low initial frequency, 1730 cm^{-1}, indicates a well hydrated state of the lipid interfacial region before polymer adsorption.[28] A progressive shift to higher frequencies is observed 55 min after injection signaling the onset of copolymer adsorption, a maximum frequency of 1736 cm^{-1} is reached 94 min after injection. This higher frequency corresponds to a less hydrated state of the lipid interfacial region, and its value is similar to that of pure DPPC-d_{62} in an LC phase at surface pressures well above the LE-LC phase transition. The actual Π at this point (from Π curve in Figure 4.6a) is 33.5 mN/m, which implies that at this pressure most of the lipid should already be found in the LC phase. Afterwards there is a frequency shift toward lower wavenumbers in agreement with the relaxation process observed for both $\nu_{as}(CD_2)$ and $\nu_s(CD_2)$ bands. However, in the case of the ν(C=O) band also copolymer adsorption plays a role in this shift, since as polymer adsorption proceeds there is an increasing contribution of the ester carbonyl group stretching vibration bands from the ester groups of PGMA blocks, centered at ~1719 cm^{-1}, that superpose on the ν(C=O) lipids band. At the final adsorption equilibrium state the ν(C=O) band is located at 1732 cm^{-1} and is a mixture of both contributions.

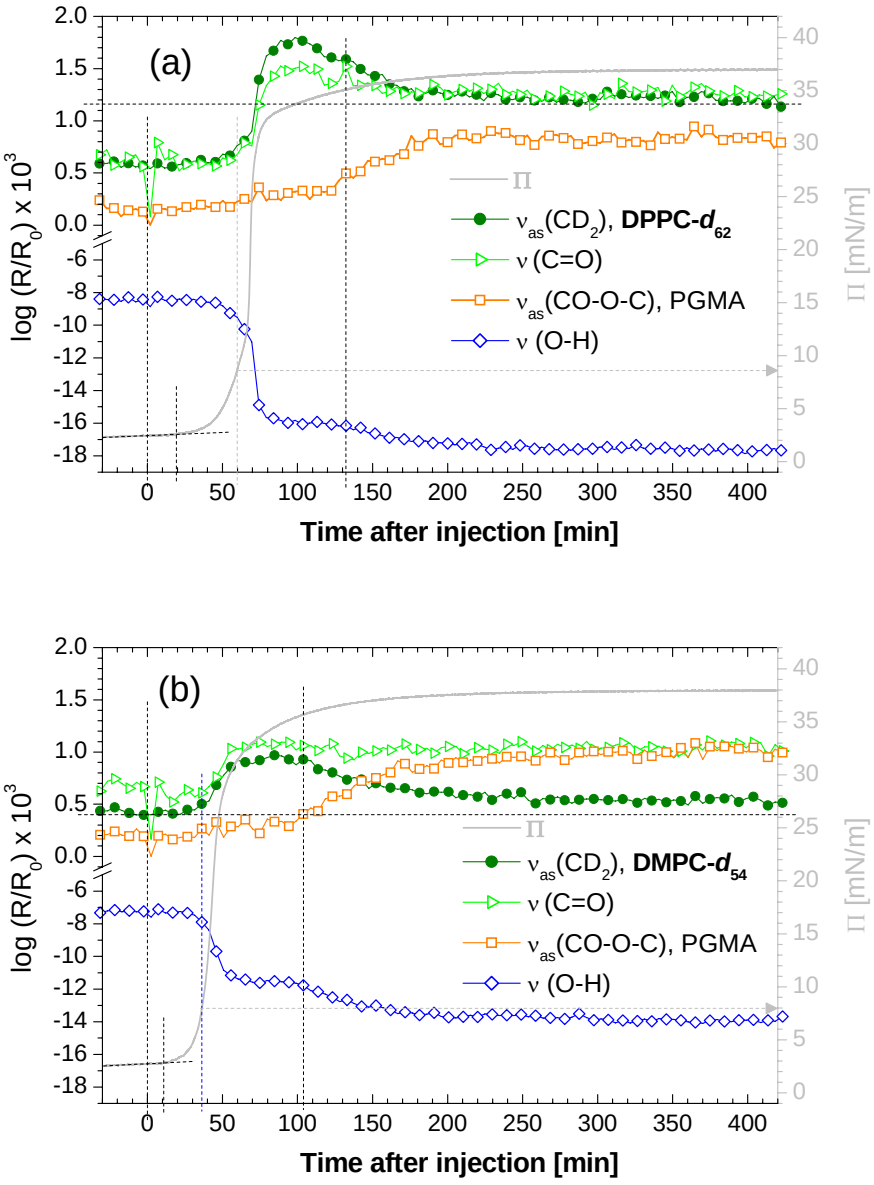

Figure 4.6: Time-dependent development of the intensity of the inverted IRRA bands ν(O-H), $\nu_{as}(CD_2)$, ν(C=O), and ν_{as}(CO-O-C) during the adsorption process of $(PGMA_{14})_2$-PPO_{34}, 8 µM, to a lipid monolayer initially at $\Pi_0 = 2.5$ mN/m: (a) DPPC-d_{62}, (b) DMPC-d_{54}. The corresponding surface pressures are shown on the right ordinate.

In the 1280-1060 cm^{-1} region, shown in Figure 4.5d, there is an extensive superposition of bands coming from the lipid headgroup and the copolymer ester and ether moieties. Phosphate group antisymmetric $\nu_{as}(PO_2^-)$ and symmetric $\nu_s(PO_2^-)$ stretching bands are initially found at 1228 cm^{-1} and 1087 cm^{-1}, respectively. Lipid phosphate groups bind water molecules more easily than carbonyl groups,[28] and since the phosphate group is strongly acidic and provides hydrogen bonding acceptors, its vibrational modes are very sensitive to hydrogen bonding.[29] Particularly the $\nu_{as}(PO_2^-)$ band frequency decreases from values above ~1240 cm^{-1} in the dry state to ~1230 cm^{-1} and below for a fully hydrated lipid.[28] Therefore, the initial $\nu_{as}(PO_2^-)$ frequency corresponds clearly to a very hydrated state of DPPC-d_{62}. In spite of its

sensitivity the $\nu_{as}(PO_2^-)$ band could not be further used for monitoring the hydration state of the lipid headgroups, since after adsorption onset this band is overlapping with contributions from the CH_2 bending vibrational modes of the copolymer blocks at 1280 cm^{-1} and 1256 cm^{-1}.

The most characteristic band of the copolymer is located at 1170 cm^{-1} and originates predominantly from the antisymmetric stretching vibration of the ester groups, ν_{as}(CO-O-C), of PGMA blocks; although it includes a contribution of the very broad symmetric ether stretching band from the PPO block, ν_s(C-O-C) centered at 1106 cm^{-1}. The ν_{as}(CO-O-C) band reaches a significant intensity only around 132 min after injection (marked by a dashed line in Figure 4.6a), well after the $\nu_{as}(CH_2)/\nu_s(CH_2)$ bands from the methylene groups of the PPO middle block appear. Also the band intensity *vs*. injection time curve for the ν(O-H) band exhibits an inflexion point at this time, indicating a change in the optical parameters of the monolayer brought about by the penetration of PGMA blocks.

All these facts put together suggest that once $(PGMA_{14})_2$-PPO_{34} has reached the subphase beneath the lipid monolayer, adsorption proceeds in a two-step mechanism:

(i) Initially only the more hydrophobic PPO middle block penetrates the lipid monolayer, while the hydrophilic PGMA blocks remain completely immersed in the subphase. With increasing adsorption of PPO blocks into the LE monolayer the available area per lipid molecule decreases gradually until a pressure equivalent to $\Pi_{LE\text{-}LC}$ is reached: Further copolymer adsorption forces lipids from the expanded into the condensed state.

(ii) Subsequently, after the LE-LC phase transition of the lipid has been almost completed, as indicated by the $\nu(CD_2)$ band frequency shifts, the bulky PGMA hydrophilic blocks are dragged into the headgroup region of the lipid monolayer as the PPO hydrophobic block inserts further into the acyl chain region. At this point, extended hydrogen bonding between the hydroxyl groups of the PGMA blocks and the phosphocholine lipid headgroups is expected to take place. However, this could not be verified due to the superposition of the lipid $\nu_{as}(PO_2^-)$ band with some copolymer $\delta(CH_2)$ bending modes. Such a hydrogen bonding would provide additional anchoring to the copolymer once adsorbed.

For comparison an analogous experiment with DMPC-d_{54} instead of DPPC-d_{62} was carried out, and its results are summarized in Figure 4.6b. The basic features of the adsorption processes are similar, but there are also clear differences. The first evidence of adsorption to the DMPC-d_{54} monolayer is found 10.9 min after injection, which is about 8 min before that with a DPPC-d_{62} monolayer. This indicates that the kinetics of adsorption is considerable faster to DMPC-d_{54}, although the headgroup, the initial lipid lateral packing densities and the monolayer compressibilities at low pressure are practically the same for both lipids. Therefore, this faster kinetics must be attributed to DMPC-d_{54} acyl chains being two perdeuterated methylene units shorter, which decreases the intermolecular van der Waals interactions between them. The influence of the acyl chain length on monolayer behavior

becomes clear when one realizes that at 20°C the DMPC-d_{54} monolayer is above its critical temperature, while DPPC-d_{62} is still far below it. It has already been pointed out that a DMPC monolayer close to its critical point is characterized by exhibiting highly dynamic domains and strong fluctuations in lateral thickness in the micrometer range.[21] In accordance with a higher monolayer fluidity during adsorption, DMPC-d_{54} $\nu_{as}(CD_2)$ and $\nu_s(CD_2)$ stretching bands exhibit a smaller frequency shift than for DPPC-d_{62}. With progressive copolymer adsorption the antisymmetric $\nu_{as}(CD_2)$ band frequency shifts from approximately 2197 cm^{-1} down to 2195 cm^{-1}, the symmetric $\nu_s(CD_2)$ band shifts from approximately 2099 cm^{-1} to 2092 cm^{-1}. There is also a progressive increase in $\nu_{as}(CD_2)$ band intensity of DMPC-d_{54} with copolymer adsorption, but as expected it is less pronounced than for DPPC-d_{62}. The carbonyl group stretching band, ν(C=O), shifts slightly to higher frequencies from 1733 cm^{-1} to a maximum frequency of 1736 cm^{-1} and decreases progressively to 1726 cm^{-1} at the final adsorption equilibrium state, indicating a larger contribution of the ester carbonyl group stretching vibration bands from PGMA blocks, which implies a higher $(PGMA_{14})_2$-PPO_{34} surface concentration than in the DPPC-d_{62} case, and is in agreement with the observed slightly higher equilibrium surface pressure for DMPC-d_{54} (Π_{eq} = 37.9 mN/m) than for a DPPC-d_{62} monolayer (Π_{eq} = 36.9 mN/m).

4.3.3.3 Adsorption to Phospholipid LC Monolayers

Adsorption experiments into lipid monolayers initially in a liquid condensed state allow the quantitative determination of the change in orientation of the lipid alkyl chains caused by copolymer adsorption. For these experiments a DPPC-d_{62} monolayer initially spread at an available molecular area A = 101.6 Å²/lipid molecule (Π_0~0 mN/m) was compressed to Π_0 = 20.2 mN/m, then angular dependent IRRAS measurements were carried out as described in the experimental section. Next, enough copolymer solution for reaching a concentration of 8 µM in the bulk of the solution was injected below the monolayer and allowed to reach adsorption equilibrium after ~16 h (Π_{eq} = 38.0 mN/m), then angular dependent IRRAS measurements were performed again. Figure 4.7 shows the intensity of the lipid $\nu_{as}(CD_2)$ and $\nu_s(CD_2)$ stretching bands with varying angle of incidence of *p*- and *s*-polarized IR radiation. Both *p*- and *s*- experimental data sets were fitted together, and from the fitting parameters the orientation of the DPPC-d_{62} alkyl chains was determined.

A comparison between the experimental and the calculated fitted values shows a good agreement, as shown in Figure 4.8. The average tilt angle with respect to the surface normal for the pure lipid at Π_0 = 20.2 mN/m was determined to be θ_0 = 30° ± 3°. After copolymer adsorption the average tilt angle reduces to θ_{eq} = 18° ± 3° at Π_{eq}= 38.0 mN/m. Comparing the latter value obtained for a mixed monolayer with reported values for pure DPPC-d_{62} monolayers under similar conditions (θ = 33°± 3° at Π = 42 mN/m and 18°C, from a neutron and x-ray reflectivity study),[33] it is concluded that $(PGMA_{14})_2$-PPO_{34} incorporation into a DPPC-d_{62} monolayer initially in LC condensed phase leads to a change in the monolayer packing by forcing the lipid alkyl chains into a more vertical orientation.

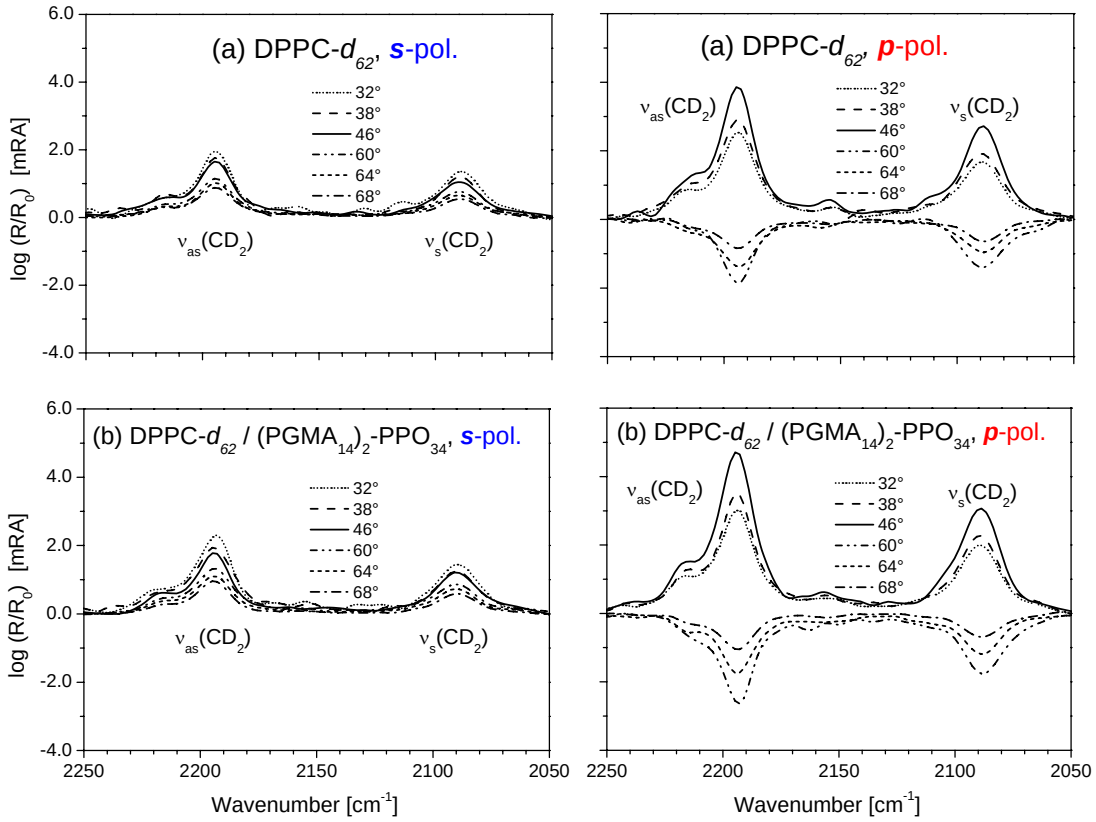

Figure 4.7: Inverted IRRA spectra of the methylene antisymmetric, $\nu_{as}(CD_2)$, and symmetric, $\nu_s(CD_2)$, stretching bands of DPPC-d_{62} lipid alkyl chains with *p*- and *s*-polarized IR radiation with varying angle of incidence for (a) pure DPPC-d_{62} monolayer at Π_0 = 20.2 mN/m, and (b) DPPC-d_{62} / $(PGMA_{14})_2$-PPO_{34} mixed monolayer at Π_{eq} = 38.0 mN/m. Only some selected angles are shown for the sake of clarity.

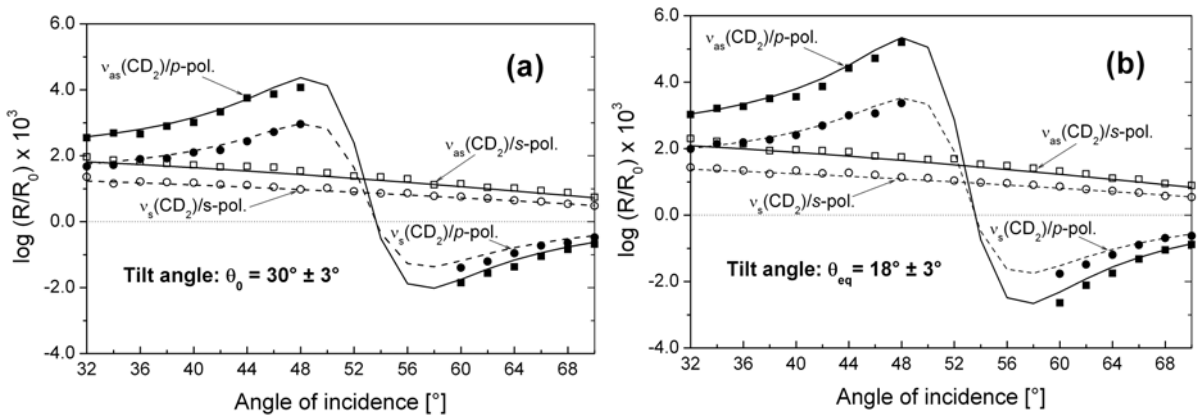

Figure 4.8: Intensity of the inverted methylene $\nu_{as}(CD_2)$ (squares) and $\nu_s(CD_2)$ (circles) stretching IRRA bands of DPPC-d_{62} lipid alkyl chains *versus* angle of incidence, with *p*-(full symbols) and *s*-(open symbols) polarized IR radiation. Tilt angle (θ) with respect to the surface normal: (a) θ_0 = 30° ± 3°, corresponding to pure DPPC-d_{62} at Π_0 = 20.2 mN/m; and (b) θ_{eq} = 18° ± 3°, corresponding to a mixed monolayer DPPC-d_{62} / $(PGMA_{14})_2$-PPO_{34} after adsorption equilibrium is reached at Π_{eq} = 38.0 mN/m. Both experimental data (symbols) and simulated values (full and dashed lines) are shown.

4.3.4 BAM Investigations

The IR beam in the IRRAS experiment focussed onto the water surface covers an ellipsoidal area of ca. 2 cm^2. Therefore, IRRA bands observed in the spectrum are an average over all molecules present in this area. In order to ensure that the lipid organization induced by the copolymer takes place indeed on the microscopic scale and to rule out any macroscopic phase separation at the surface, which would lead to misleading conclusions from IRRAS results, a simultaneous observation of the surface during IRRA spectra acquisition is necessary. Brewster angle microscopy images, such as those shown in Figure 4.9, allow for a direct observation of the changes in the morphology of the lipid monolayer brought about by adsorption of the copolymer. During these experiments, enough $(PGMA_{14})_2$-PPO_{34} solution for reaching a concentration of 1 μM in the subphase is injected below a DPPC-d62 monolayer and allowed to adsorb without stirring the subphase. These conditions are chosen in order to slow down the copolymer adsorption kinetics so that enough BAM images could be taken during the relatively short period of time when the LE and LC lipid domains coexist. Symbols on the Π-t curves presented in Figure 4.9 mark the time at which the corresponding image is acquired.

Liquid-condensed lipid domains appear in BAM as bright patches surrounded by a dark fluid phase. Domain morphology is basically determined by the interplay of three factors: (i) line tension at the domain boundary, (ii) dipolar repulsion between molecules, and (iii) molecular chirality.[34] Typically observed domains for an enantiomeric pure DPPC monolayer in the LE-LC transition region are either triskelions; 3-arms propeller-like structures originated in long-range dipolar repulsion interactions along the arms, whose turning direction is determined by the DPPC chirality; or kidney-shaped domains, which have been identified as the preferred shape at equilibrium.[35] However, during the adsorption of $(PGMA_{14})_2$-PPO_{34} to DPPC-d_{62} monolayers none of those regular forms was observed for the LC lipid domains (see Figure 4.9a-b), although a regular size was preserved. This deformation is likely a consequence of the preferential partitioning of the copolymer in the more fluid LE phase, which modifies the line tension between the LC and LE phases compared to that of a pure lipid monolayer, similar to the mechanism that has been reported for the incorporation of non-ionic surfactants of the poly(ethylene oxide) monodecyl ether type into DPPC monolayers.[36]

Although the formation of lipid LC domains above $\Pi_{LE\text{-}LC}$ is expected to proceed mostly through homogeneous nucleation, and therefore a random distribution of the nuclei should be observed, this is not the case independently of the lipid initial packing density. The quite regular lipid domain spacing observed (see Figures 4.9a1, 4.9b1) is the result of repulsive dipole interactions between them, a repulsive nature of DPPC LC domains has already been reported.[37,38]

With increasing lipid initial packing density the number of domain nuclei per area increases as well, and consequently their maximum size before domains impinge on each other and coalescence takes place is reduced, as well as the time elapsed before an optically isotropic mixed monolayer is obtained. When similar fluorescence microscopy studies are

performed using a fluorescence probe insoluble in the DPPC LC domains, such as the tail-labelled NBD-PC dye, a delay of the onset of domain fusion,[35] or the complete inhibition of fusion, even at high lipid packing densities are observed;[37,39] because with increasing area fraction covered by LC domains the insoluble dye is enriched in the remaining fluid phase. The fact that a coalescence actually takes place, and at relatively low surface pressures, Π = 22.9 mN/m for image b4 in Figure 4.9, suggest that $(PGMA_{14})_2$-PPO_{34} partitions not only into the fluid phase, but also into the LC lipid domains, at least partially.

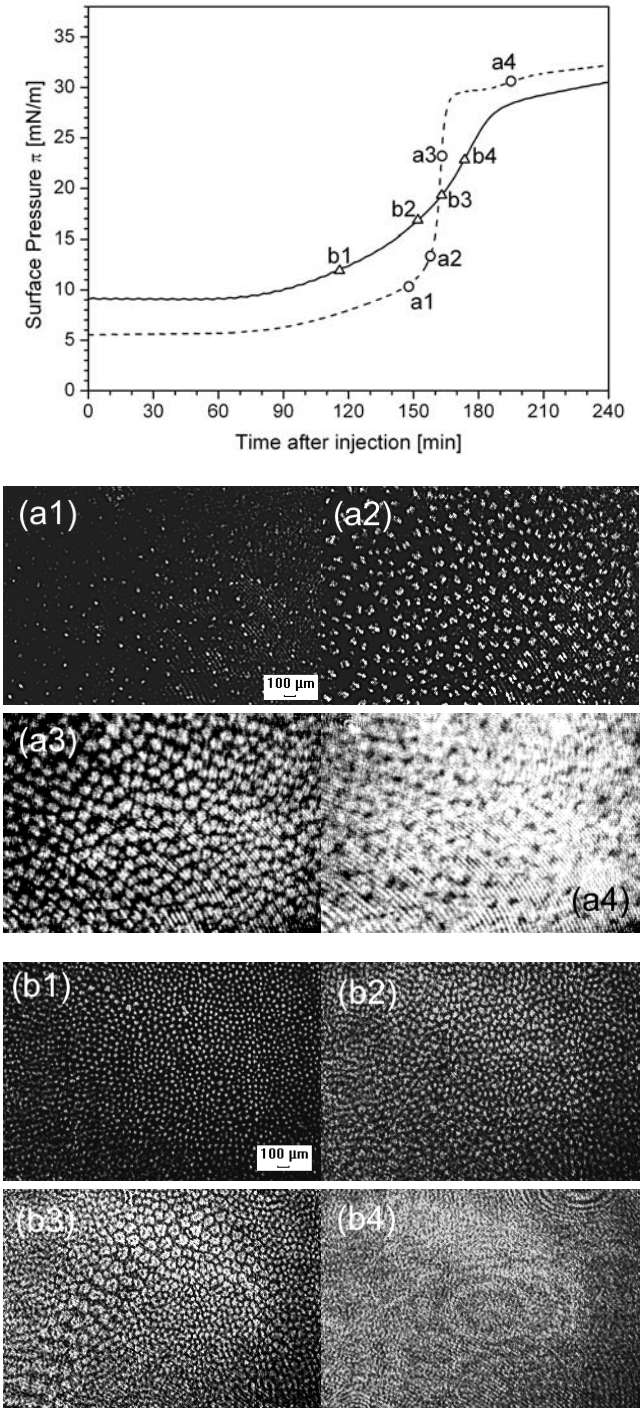

Figure 4.9: BAM sequences acquired during the LE to LC phase transition induced by the incorporation of $(PGMA_{14})_2$-PPO_{34}, 1 µM, into DPPC-d_{62} monolayers at two different initial surface pressures: (a) Π_0 = 5 mN/m (dashed line), and (b) Π_0 = 9 mN/m (full line). Measurements performed without stirring at 20°C.

4.3.5 Squeeze Out Experiments

In order to check the ability of $(PGMA_{14})_2$-PPO_{34} to remain inserted into the lipid monolayer with increasing compression, the following experiment is carried out: first a DMPC-d_{54} monolayer spread with an available molecular area A = 110.4 Å²/lipid molecule is compressed up to A_0 = 85.5 Å²/lipid molecule (Π_0~5.0 mN/m), then sufficient copolymer solution for reaching a concentration of 16 µM in the bulk of the solution was injected below the monolayer and allowed to reach equilibrium after ~21 h. Then the mixed monolayer was compressed stepwise by 1 Å² per lipid molecule at a time, and an IRRA spectrum is subsequently recorded for each compression step. Particularly adequate for following the compression process is the 1150-1350 cm^{-1} region, which includes the lipid phosphate group antisymmetric stretching band, $\nu_{as}(PO_2^-)$, at ~1229 cm^{-1} and the antisymmetric stretching vibration of the ester groups of the copolymer PGMA blocks, ν_{as}(CO-O-C), at ~1170 cm^{-1}. The evolution of the bands in this region with decreasing available area per lipid molecule is presented in Figure 4.10a. The methyl/methylene group stretching bands which originate predominantly from the PPO middle block follow a similar evolution than the ν_{as}(CO-O-C) band. In Figure 4.10b the intensity at band maximum for the lipid $\nu_{as}(CD_2)$ band and the copolymer ν_{as}(CO-O-C) band are plotted against the decreasing available area per lipid molecule, together with the corresponding surface pressure.

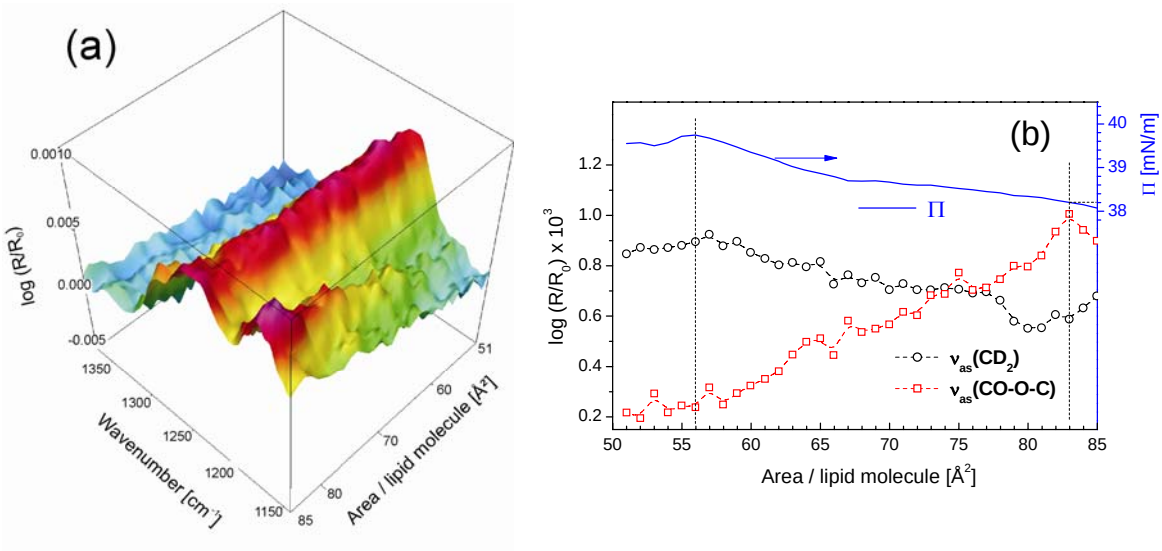

Figure 4.10: Squeeze out of $(PGMA_{14})_2$-PPO_{34} incorporated previously in a DMPC-d_{54} monolayer during compression from 85 to 50 Å²/lipid molecule. (a) Area-dependent IRRA spectra of the 1350 to 1150 cm^{-1} region, which includes the ν_{as} (PO_2^-) vibrational band (~1229 cm^{-1}) coming from the lipid head-group, and the ν_{as}(CO-O-C) band (~1170 cm^{-1}) coming from the polymer PGMA blocks. (b) Intensity of the IRRA bands $\nu_{as}(CD_2)$ and ν_{as}(CO-O-C) as a function of area per lipid molecule. The corresponding surface pressure is shown on the right ordinate.

In several investigations,[24,40-43] the surface pressure at which the isotherm of the mixed monolayer intersects that of the pure lipid is taken as the squeeze out pressure; however, from Figure 4.10 it is clear that the onset of the squeeze out process not necessarily agrees with this definition and Π alone provides at best an indication of its completion. Furthermore, it has been pointed out that due to the relatively short measuring times required for the construction of a Π-A isotherm under continuous compression, the extent of squeeze out may be controlled by kinetic factors.[44] Therefore, Π is not the most adequate variable for monitoring the process. The actual squeeze out onset pressure, Π_{out}, is more accurately defined as the surface pressure at which the copolymer starts to be pushed out of the mixed monolayer into the subphase, which implies that its surface concentration begins to decrease, as evidenced by a reduction in the intensity of IRRA bands coming from the copolymer blocks. According to this definition, the squeeze-out onset pressure was determined as Π_{out} = 38.2 mN/m (A = 83.0 Å²/lipid molecule) which is only slightly higher than the equilibrium pressure before compression Π_{in} = 38.1 mN/m. This small difference between both implies that the interaction between the PPO hydrophobic block and the fatty acid region of the monolayer is not particularly strong. Therefore, it appears to rule out a further conformational change of the PPO backbone once adsorbed, which would bring about a higher energetic barrier to squeeze-out and hence a higher squeeze-out pressure.

4.4 Conclusions

The incorporation process of novel water soluble amphiphilic triblock copolymers PGMA-*b*-PPO-*b*-PGMA into DPPC and DMPC monolayer films is studied using monolayer techniques in combination with IRRAS and BAM. In the case of $(PGMA_{14})_2$-PPO_{34} the maximum penetration surface pressure is ca. 39 mN/m, suggesting that the copolymer would be able to insert into intact biological membranes.

Comparative constant surface area experiments show that the copolymer surface concentration is higher when adsorbed to a DPPC-d_{62} monolayer than to a DMPC-d_{54} monolayer. Besides, for a given copolymer concentration in the bulk solution, the surface pressure reached after incorporation into DMPC-d_{54} is slightly higher (~0.5-1.5 mN/m) than for a DPPC-d_{62} monolayer. This difference tends to vanish with increasing copolymer concentration. Copolymer saturation concentrations after which no further increase in surface pressure is observed are 6.8 μM and 9.5 μM for mixed monolayers with DPPC-d_{62} and DMPC-d_{54} (Π_0~10.5 mN/m), respectively. The differences in the copolymer adsorption behavior are clearly a consequence of DMPC-d_{54} lacking an LE-LC phase transition, and being therefore unable to accommodate copolymer molecules by the excluded area mechanism as is the case for DPPC-d_{62}.

IRRAS experiments show that copolymer incorporation into a DPPC-d_{62} monolayer in a LE phase proceeds in a two-step mechanism:

(i) Initially only the more hydrophobic PPO middle block penetrates the lipid monolayer, while the hydrophilic PGMA blocks remain completely immersed in the subphase.

(ii) After the LE-LC phase transition of the lipid, the bulky PGMA hydrophilic blocks are dragged into the headgroup region of the lipid monolayer as the PPO hydrophobic block inserts further into the fatty acid region.

The adsorption kinetics is considerable faster to DMPC-d_{54} monolayers, which is attributed to a more fluid state of the monolayer, as verified from the frequencies of the lipid vibrational bands. Copolymer adsorption to a DPPC-d_{62} monolayer initially in LC condensed phase leads to a change in the monolayer packing by forcing the lipid alkyl chains into a more vertical orientation. Their tilt angle with respect to the surface normal reduces from initially (30 ± 3)° to (18 ± 3)°.

BAM imaging allows a direct observation of the changes in the morphology of the lipid monolayer as a result of adsorption of the copolymer and confirms that the lipid organization induced by the copolymer observed by IRRAS takes place indeed on the microscopic scale ruling out any macroscopic phase separation at the surface. It also shows that coalescence of DPPC-d_{62} LC domains takes place at relatively low surface pressures, $\Pi \geq 23$ mN/m, suggesting that $(PGMA_{14})_2$-PPO_{34} partitions not only into the fluid phase, but also into the LC domains. Compression experiments in combination with IRRAS measurements allow for the determination of the onset of the copolymer squeeze-out from a mixed monolayer. The squeeze-out onset pressure is slightly higher than the adsorption equilibrium pressure implying that the interaction between the PPO hydrophobic block and the fatty acid region of the monolayer is not particularly strong and tends to rule out a further conformational change of the PPO backbone once adsorbed.

4.5 References

[1] Blume, A. *Biochim. Biophys. Acta* **1979**, *557*, 32.

[2] Miller, A.; Möhwald, H. *J. Chem. Phys*. **1987**, *86*, 4258.

[3] Hénon, S.; Meunier, J. *Rev. Sci. Instrum*. **1991**, *62*, 936.

[4] Hönig, D.; Möbius, D. *Thin Solid Films* **1992**, *210/211*, 64.

[5] Hussain, H.; Kerth, A.; Blume, A., Kressler, J. *J. Phys. Chem. B*. **2004**, *108*, 9962.

[6] Mendelsohn, R.; Brauner, J. W.; Gericke, A. *Annu. Rev. Phys. Chem*. **1995**, *46*, 305

[7] Flach, C. R.; Gericke, A.; Mendelsohn, R. *J. Phys. Chem. B* **1997**, *101*, 58

[8] Kuzmin, V. L.; Mikhailov, A. V. *Opt. Spectrosc. [USSR]* **1981**, *51*, 383

[9] Kuzmin, V. L.; Romanov, V. P.; Michailov, A. V. *Opt. Spectrosc*. **1992**, *73*, 1.

[10] Gericke, A.; Michailov, A. V.; Hühnerfuss, H. *Vibr. Spectrosc*. **1993**, *4*, 335

[11] Flach, C. R.; Gericke, A.; Mendelsohn, R. *J. Phys. Chem. B* **1997**, *101*, 58

[12] Flach, C. R.; Xu, Z.; Bi, X.; Brauner, J. W.; Mendelsohn, R. *Appl. Spectrosc*. **2001**, *55*, 1060

[13] Flach, C. R.; Gericke, A.; Mendelsohn, R. *J. Phys. Chem. B* **1997**, *101*, 58

[14] Bertie, J. E.; Lan, Z. *Appl. Spectrosc*. **1996**, *50*, 1047

[15] Maget-Dana, R. *Biochim. Biophys. Acta* **1999**, *1462*, 109.

[16] Seelig, A.; Gerebtzoff, G. *Expert Opin. Drug Metabol. Toxicol*. **2006**, *2*, 733

[17] Discher, B.M.; Schief, W.R.; Vogel, V.; Hall, S.B. *Biophys. J*. **1999**, *77*, 2051.

[18] Pallas, N.R.; Pethica, B.A. *Langmuir* **1985**, *1*, 509.

[19] Hifeda, Y.F.; Rayfield, G.W. *Langmuir* **1992**, *8*, 197.

[20] Duncan, S.L.; Larson, R.G. *Biophys. J*. **2008**, *94*, 2965.

[21] Nielsen, L.K.; Bjornholm, T.; Mouritsen, O.G. *Langmuir* **2007**, *23*, 11684.

[22] Charron, J.R.; Tilton, R.D. *J. Phys. Chem*. **1996**, *100*, 3179.

[23] Wu, G.; Majewski, J.; Ege, C.; Kjaer, K.; Weygand, M.J.; Lee, K.Y. *Biophys. J*. **2005**, *89*, 3159.

[24] Maskarinec, S.A.; Lee, K.Y. *Langmuir* **2003**, *19*, 1809

[25] Charron, J.R.; Tilton, R.D. *Langmuir* **1997**, *13*, 5524.

[26] Bhakoo, M.; Birkbeck, T.H.; Freer, J.H. *Biochemistry* **1982**, *21*, 6879.

[27] Casal, H.L.; Mantsch, H.H. *Biochim. Biophys. Acta* **1984**, *779*, 381.

[28] Hübner, W.; Blume, A.; *Chem. Phys. Lipids* **1998**, *96*, 99.

[29] Tamm, L.K.; Tatulian, S.A. *Q. Rev. Biophys*. **1997**, *30*, 365.

[30] Lewis, R.N.; McElhaney, R.N. *Chem. Phys. Lipids* **1998**, *96*, 9.

[31] Maeda, Y.; Nakamura, T.; Ikeda, I. *Macromolecules* **2001**, *34*, 8246.

[32] Flach, C.R.; Gericke, A.; Keough, K.M.; Mendelsohn, R. *Biochim. Biophys. Acta* **1999**, *1416*, 11.

[33] Vaknin, D.; Kjaer, K.; Als-Nielsen, J.; Lösche, M. *Biophys. J.* **1991**, *59*, 1325

[34] Thirumoorthy, K.; Nandi, N. *Langmuir* **2007**, *23*, 6991.

[35] McConlogue, C.W.; Vanderlick, T.K. *Langmuir* **1997**, *13*, 7158.

[36] Naumann, C.; Dietrich, C.; Lu, J.R.; Thomas, R.K.; Rennie, A.R.; Penfold, J.; Bayerl, T.M. *Langmuir* **1994**, *10*, 1919.

[37] Flörsheimer, M.; Möhwald, H. *Chem. Phys. Lipids* **1989**, *49*, 231.

[38] Möhwald, H. *Thin Solid Film*s **1988**, *159*, 1.

[39] Kaushik, N.; Boland, C.; Rich, N.; Keough, K.M. *Biochim. Biophys. Acta* **1991**, *1068*, 157.

[40] Maskarinec, S.A.; Haning, J.; Lee, R.C.; Lee,K.Y. *Biophys. J*. **2002**, *82*, 1453.

[41] Frey, S.L.; Zhang, D.; Carignano, M.A.; Szleifer, I.; Lee, K.Y. *J. Chem. Phys*. **2007**, *127*, 114904.

[42] Chang, L.-C.; Lin C.-Y.; Kuo, M.-W.; Gau, C.-S. *J. Colloid Interface Sci*. **2005**, *285*, 640.

[43] Frey, S.L.; Lee, K.Y. *Langmuir* **2007**, *23*, 2631.

[44] Pastrana-Rios, B.; Taneva, S.; Keough, K.M.; Mautone, A.J.; Mendelsohn, R. *Biophys. J*. **1995**, *69*, 2531.

5 The Molecular Arrangement Induced by Adsorption of PGMA-*b*-PPO-*b*-PGMA at Phospholipid Monolayers

5.1 Introduction

As already mentioned, the ability exhibited by some water soluble amphiphilic polymers to interact with biological membranes plays a crucial role in their biomedical applications. Therefore, there is great interest in studying the nature of the various polymer-membrane interactions. In such investigations lipid monolayers are normally used as simplified models of the outer leaflet of cell membranes. However, most of the reports on the interaction between amphiphilic polymers and lipid monolayers focus on the kinetic aspects of the adsorption process as observed by surface pressure measurements,[1-4] or the visualization of the morphological changes by fluorescence microscopy techniques.[5,6] Only a few investigations deal with the arrangement on the molecular level of the resulting mixed monolayer, normally from neutron or x-ray reflectivity measurements.[7-9] At least in part because of this tendency, the detailed state of the mixed monolayers remains still an open question.

The present section focus on the unsolved issue of the equilibrium morphology on the molecular level of mixed monolayers formed after adsorption of the PGMA-*b*-PPO-*b*-PGMA triblock copolymer to phospholipid monolayers. The possible molecular arrangement is elucidated based on a comparative study of mixed monolayers formed with DPPC-d_{62} or DMPC-d_{54} after very long equilibration times, as investigated by infrared reflection absorption spectroscopy (IRRAS) coupled with Brewster Angle Microscopy (BAM). The simultaneous observation of the monolayer morphology by BAM during IRRA spectra acquisition allows ruling out of any macroscopic phase separation while investigating the molecular organization.

5.2 Experimental

5.2.1 Materials

The acyl chain perdeuterated phospholipids employed were already described in section 4.2.1.

5.2.2 Polymer Adsorption to Phospholipid Monolayers

Experiments were performed in the sample trough of the IRRAS setup described in section 4.2.4. First a fresh lipid solution in chloroform (0.8 mM, 10.3 μL) was spread onto the subphase forming a phospholipid monolayer with an initial surface pressure of 10.2 $mN \cdot m^{-1}$. After waiting for 15 min for complete solvent evaporation, an aqueous solution of $(PGMA_{14})_2$-PPO_{34} (6.0 mM, 20.9 μL) was injected below the phospholipid monolayer through a channel just above the bottom of the trough. The injected amount was enough for reaching a copolymer concentration of 8 μM in the bulk of the solution, which is at least six times lower than its CMC. The decrease in surface tension (γ) due to the injected copolymer was measured using a Wilhelmy film balance.

5.2.3 Brewster Angle Microscopy

The contrast in BAM images arises from differences in reflectivity of *p*-polarized light impinging under the Brewster angle onto the air-water interface. Changes in the reflectivity within a film are caused by variations in the refractive index, thickness or optical anisotropy of the film.[10] Such a sensitivity to film properties makes BAM a suitable technique for the visualization of monolayer domains without the necessity of adding any foreign probe. A BAM microscope (Nanofilm Technologie, Göttingen, Germany) mounted above the sample trough of the IRRAS setup allowed monitoring of changes in the morphology of a lipid monolayer caused by adsorption of the block copolymer. The air-monolayer interface was illuminated at an angle of incidence of ca. 53° by a *p*-polarized laser beam of wavelength 688 nm, the reflected light passed through an analyzer, and a lens system focused an image on a CCD camera. The analyzer was *p*-positioned after spreading the lipid monolayer (at Π_0=10.2 $mN \cdot m^{-1}$) for filtering out the residual *s*-polarized light before polymer injection, resulting in a black background, and was fixed at this position during the whole measurement. This system delivered images with a resolution of *ca.* 7 μm, which were further processed with the software Image-Pro Plus (Media Cybernetics, Bethesda, MD). The gain of the image acquisition system was maintained fixed during the experiments to ensure that grayscale values are linearly proportional to the reflectance of the interfacial structures to *p*-polarized light.[11] The grayscale of the pure lipid monolayer covered air-water interfaces (black background) corresponds to zero reflectivity.

5.3 Results and Discussion

5.3.1 Evolution of the Mesoscopic Morphology of Phospholipid Monolayers with Copolymer Adsorption

The difference of two methylene units between the acyl chains of DMPC-d_{54} and DPPC-d_{62} (y in Figure 4.4 equals 12 and 14, respectively) gives raise to substantial differences in their phase behavior. While DPPC-d_{62} monolayers at 20 °C undergo a first order phase transition between a liquid expanded (LE) fluid-like state and a more rigid liquid-condensed (LC) crystalline state at a transition pressure, $\Pi_{LE\text{-}LC}$, of *ca.* 10.4 mN·m^{-1}, DMPC-d_{54} monolayers do not exhibit such transition since at 20 °C they are already above the corresponding critical temperature, and stay in a liquid-expanded state up to surface pressures of around 40 mN·m^{-1}.[12] Consequently, some differences in the development and final state between the mixed monolayers of $(PGMA_{14})_2$-PPO_{34} with DPPC-d_{62} or DMPC-d_{54} are expected.

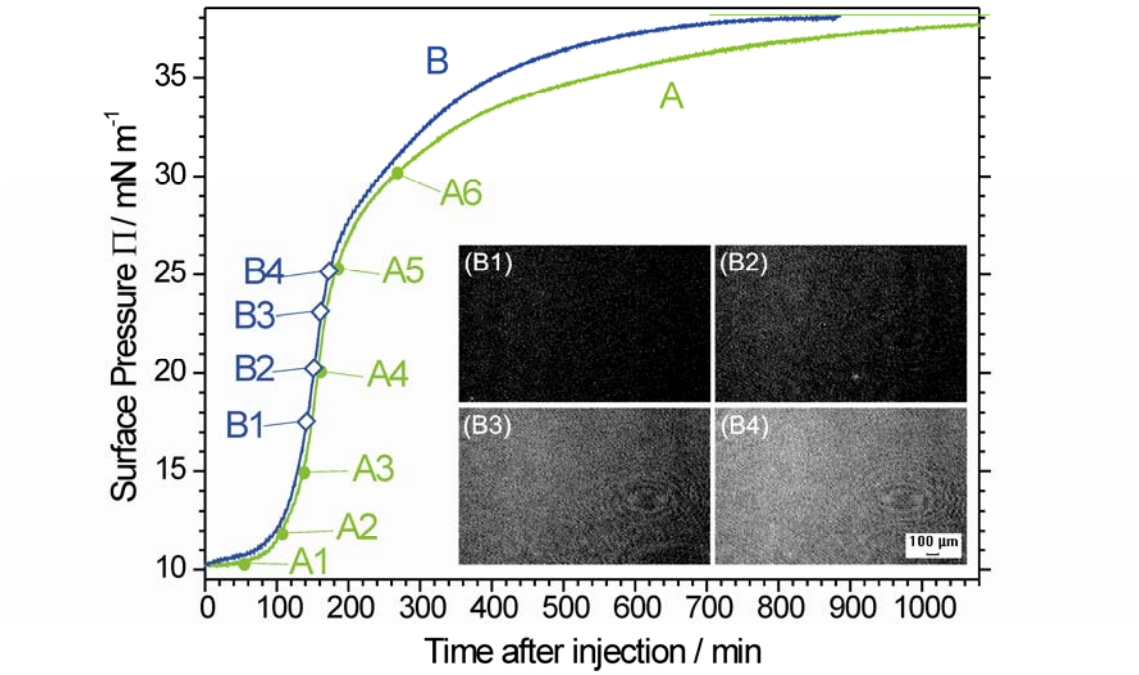

Figure 5.1: Increase in surface pressure due to the adsorption of $(PGMA_{14})_2$-PPO_{34} (8 µM) to DPPC-d_{62} (Curve A) and to DMPC-d_{54} (Curve B) monolayers at an initial surface pressure of $\Pi_0 = 10.2$ mN·m^{-1}. The inset shows a BAM sequence acquired during the adsorption to DMPC-d_{54}. Symbols on curve B (◊) indicate the corresponding acquisition time.

Curve A in Figure 5.1 illustrates the evolution of surface pressure during the adsorption of $(PGMA_{14})_2$-PPO_{34} to a DPPC-d_{62} monolayer at an initial surface pressure Π_0=10.2 mN·m^{-1}. Curve B corresponds to the analogous experiment with DMPC-d_{54}. The inset in Figure 5.1 shows a sequence of BAM images taken during the adsorption to the DMPC-d_{54} monolayer and the symbols on curve B mark the time at which each image was acquired. The sequence of images corresponding to curve A is shown separately in Figure 5.2.

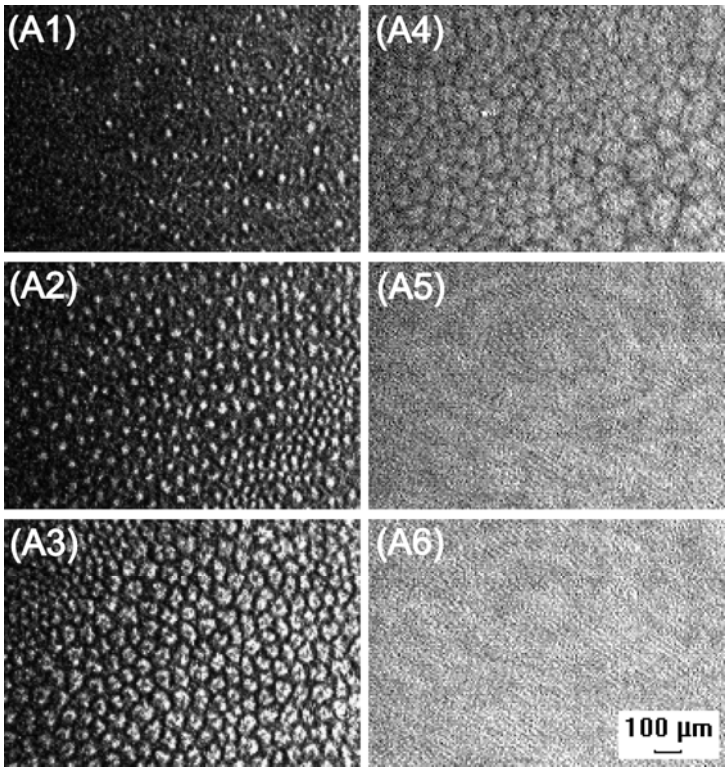

Figure 5.2: BAM sequence acquired during the adsorption of $(PGMA_{14})_2$-PPO_{34} (8 µM) to a DPPC-d_{62} monolayer initially at Π_0 = 10.2 mN·m^{-1}. The corresponding acquisition times are indicated by symbols (•) on curve A of Figure 5.1.

The DMPC-d_{54} monolayer maintains its initial homogeneity throughout the adsorption process, which is accompanied by variations in brightness of the images (Figure 5.1, B1-B4). An analysis of the grayscale values of the images allows a more quantitative assessment of the reflected light intensity, as presented in Figure 5.3. By comparing the development of the surface pressure (Figure 5.3, Curve A) with that of the BAM reflected intensity (Curve B) it becomes clear that the increase of the reflected intensity is caused by the increasing amount of $(PGMA_{14})_2$-PPO_{34} being adsorbed at the interface, although the exact relationship between the two curves is quite complex due to the dependence of the reflectivity on film optical parameters and thickness.

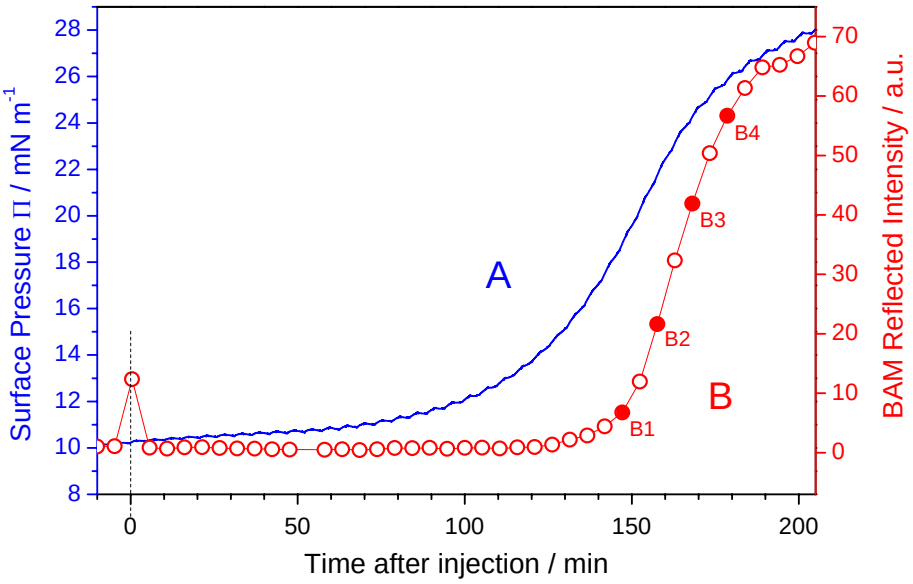

Figure 5.3: Development of the surface pressure (Curve A) and BAM reflected intensity (Curve B) during the adsorption of $(PGMA_{14})_2$-PPO_{34} (8 μM) to a DMPC-d_{54} monolayer initially at Π_0 = 10.2 mN·m^{-1}. Full symbols on curve B correspond to the reflected intensity from images B1 to B4 shown in Figure 5.1.

On the other hand, adsorption of $(PGMA_{14})_2$-PPO_{34} to DPPC-d_{62} monolayers at Π_0=10.2 mN·m^{-1} leads initially to the formation of liquid-condensed lipid domains of microscopic dimensions. These can be observed in BAM images as bright patches surrounded by a dark fluid phase (Figure 5.2, A1). Such domains are typically observed for DPPC-d_{62} monolayers at surface pressures above its liquid expanded to liquid condensed transition pressure of approximately 10.4 mN·m^{-1}. It has been found that although $(PGMA_{14})_2$-PPO_{34} adsorbs preferentially to lipid regions in the fluid phase, it also partitions into LC domains.[12] Accordingly, as adsorption proceeds the domains grow (Figure 5.2, A2-A3) incorporating increasing quantities of adsorbed copolymer. An estimate of the amount of copolymer adsorbed can be obtained from the lipid surface pressure/area isotherm (Π-A) assuming that the effect of copolymer penetration is equivalent, to some extent, to a mechanical compression of the lipid film between the initial surface pressure (Π_0=10.2 mN·m^{-1}; A_0=71.3 Å² per lipid molecule) and the equilibrium surface pressure (Π_{eq}=37.8 mN·m^{-1}; A_{eq}=45.2 Å² per lipid molecule). With a copolymer molecular area of 55.3 Å² at Π_{eq}, obtained from copolymer compression isotherms (see Appendix 8.4 for details), the number of copolymer chains adsorbed per 100 DPPC-d_{62} lipid molecules amounts to approximately 47. Subsequently, the domains fuse together (Figure 5.2, A4-A5), and at longer equilibration times an optically homogenous mixed monolayer is obtained. (Figure 5.2, A6).

5.3.2 Changes in the Phospholipid Molecular Organization with Copolymer Adsorption

Figure 5.4a presents an overview of the IRRA spectra collected during the adsorption of $(PGMA_{14})_2$-PPO_{34} to a DMPC-d_{54} monolayer at Π_0=10.2 mN·m^{-1}. The most characteristic feature is the band centered at around 3580 cm^{-1} corresponding to the stretching vibration of the O-H bonds from water, ν(O-H). Its gradual decrease in intensity after copolymer injection correlates with the progress of adsorption. The ν(O-H) band is so strong and broad that it completely hides the comparatively weak band coming from the stretching vibration of the hydroxyl groups in the diol function of the PGMA blocks, which is expected to be found in this region.

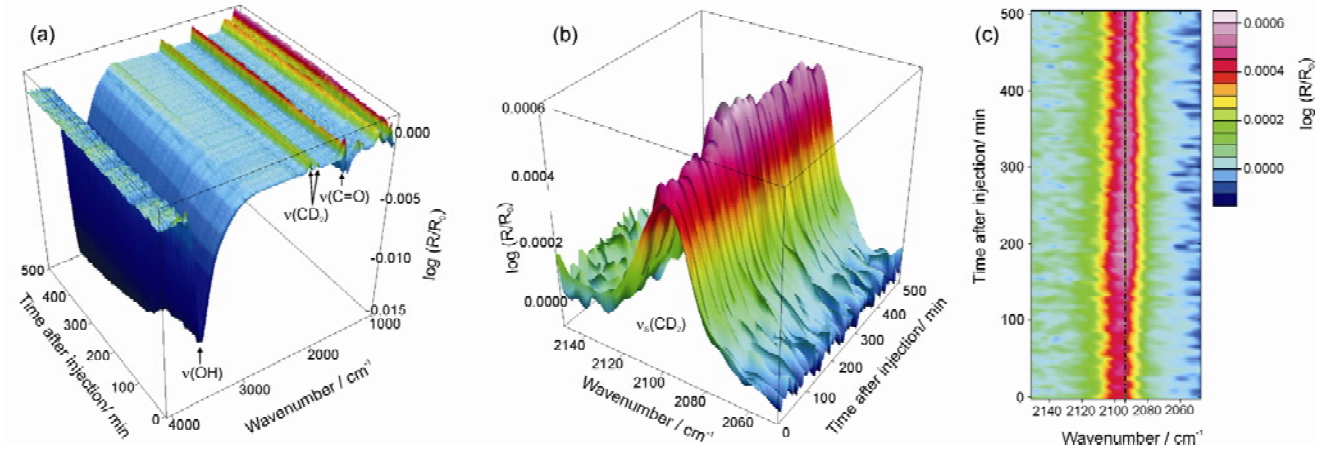

Figure 5.4: Development of inverted IRRA spectra collected during the adsorption of $(PGMA_{14})_2$-PPO_{34} to a DMPC-d_{54} monolayer (Π_0=10.2 mN·m^{-1}). (a) Overview of the region 4000-1000 cm^{-1}. The positions of the most characteristic vibrational bands are marked with arrows. (b) Development of the perdeuterated methylene symmetric $\nu_s(CD_2)$ stretching band coming from the lipid perdeuterated acyl chains. The corresponding contour plot is shown in (c), the dashed line at 2093 cm^{-1} indicate the average equilibrium position of the $\nu_s(CD_2)$ band.

Particularly relevant for this study is the perdeuterated methylene symmetric $\nu_s(CD_2)$ stretching band, which is sensitive to the conformational order of the lipid perdeuterated acyl chains and responds to changes in their *trans*/*gauche* ratio.[13] The development of the $\nu_s(CD_2)$ band is visualized in detail in Figure 5.4b and the corresponding contour plot Figure 5.4c. It is clearly seen that copolymer adsorption progressively shifts the frequency of the $\nu_s(CD_2)$ band to lower wavenumbers, which is an indication of a higher conformational order of the acyl chains.

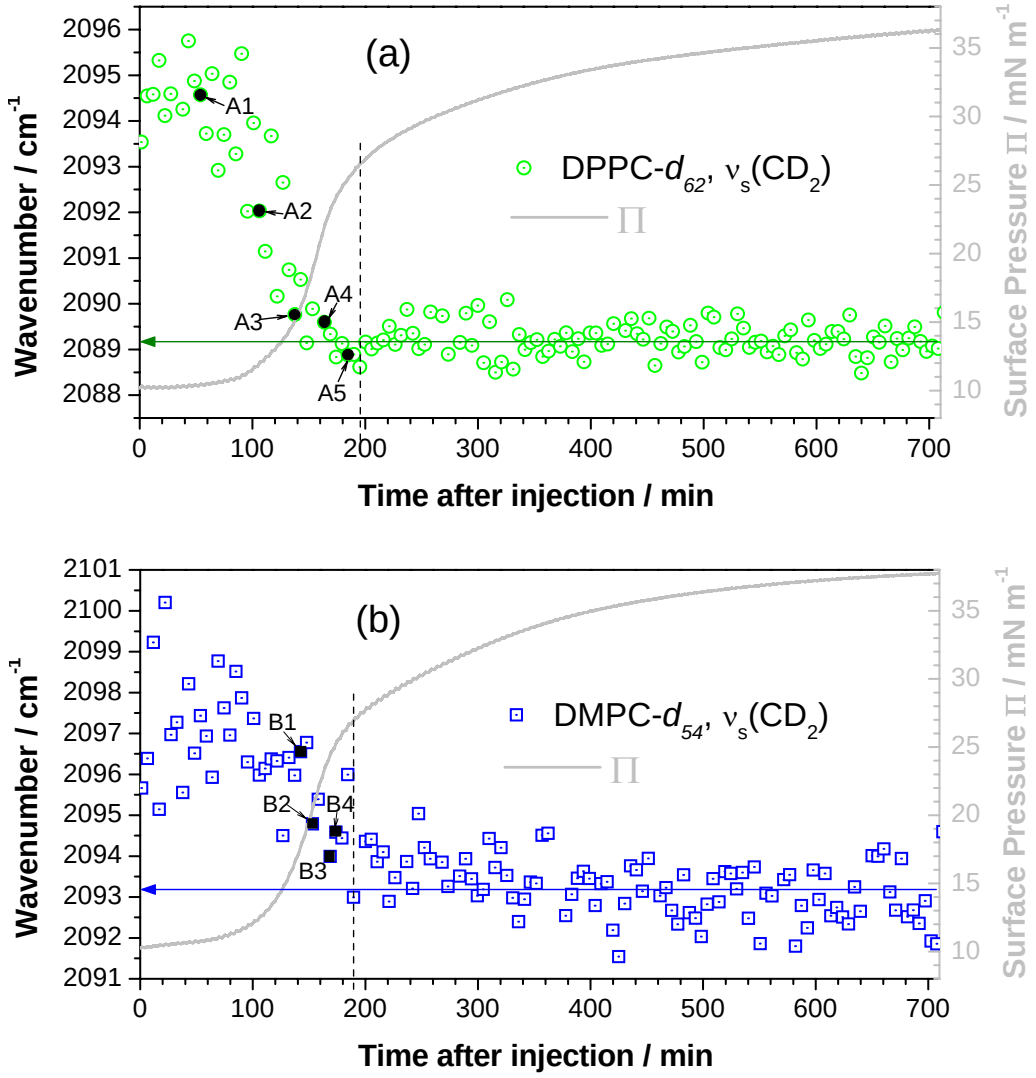

Figure 5.5: Changes in the frequency of the band maximum for the $\nu_s(CD_2)$ vibrational mode from the lipid perdeuterated acyl chains due to $(PGMA_{14})_2$-PPO_{34} adsorption to (a) DPPC-d_{62} monolayer and (b) DMPC-d_{54} monolayer. Dashed lines at 2089.2 cm^{-1} in (a) and 2093.2 cm^{-1} in (b) indicate the corresponding average frequency at equilibrium. Full symbols A1-A5 and B1-B4 correspond to the $\nu_s(CD_2)$ frequencies for the images shown in Figure 5.2 and Figure 5.1, respectively.

For a more quantitative analysis, the position of the maximum for the $\nu_s(CD_2)$ vibrational band is determined for each IRRA spectrum by the standard method of the OPUS software package (Bruker). Its development is presented in Figure 5.5. For adsorption of $(PGMA_{14})_2$-PPO_{34} to DMPC-d_{54} (Figure 5.5b) the $\nu_s(CD_2)$ band shifts from approximately 2099 cm^{-1} before adsorption takes place down to 2093 cm^{-1} after most of the copolymer has adsorbed (t >190 min).

For comparison, an analogous experiment with DPPC-d_{62} was also carried out (Figure 5.5a). In that case the $\nu_s(CD_2)$ band shifts from approximately 2096 cm^{-1} to 2089 cm^{-1}. The latter value is typical for perdeuterated acyl chains with substantial conformational order (*i.e.*, a larger population of *trans* conformers).[14] The frequencies of the maxima after most of the adsorption has taken place (t >195 min) fluctuate around the equilibrium average value only

slightly ($\tilde{\nu}_{eq}$ =2089.2 ± 0.3 cm^{-1}) in comparison to the higher scattering of values observed with a DMPC-d_{54} monolayer ($\tilde{\nu}_{eq}$ =2093.2 ± 0.8 cm^{-1}). Besides, DPPC-d_{62} shows a larger frequency shift. These observations are in agreement with higher monolayer fluidity of DMPC-d_{54} at 20 °C, due to the fact that its acyl chains are two perdeuterated methylene units shorter than those of DPPC-d_{62}. In spite of these differences the basic features of the adsorption processes are similar for both lipids. In particular, once the $\nu_s(CD_2)$ band is shifted to lower frequencies it remains at this position even after equilibration for long times.

5.3.3 General Molecular Level Organization in Lipid-Amphiphilic Block Copolymer Mixed Monolayers

According to IRRAS results with DPPC-d_{62} monolayers, the substantial conformational order of the phospholipid acyl chains reached during the lipid condensation into LC domains, brought about by the adsorption of $(PGMA_{14})_2$-PPO_{34}, is not disturbed during domain growth and subsequent coalescence, in spite of increasing amounts of copolymer being incorporated. This conformational order is preserved even after, according to BAM images, the lipid domains have completely disappeared and a homogeneous mixed monolayer has been obtained, at least on the microscopic scale. Two possible explanations for this phenomenon for mixed monolayers of phospholipid and amphiphilic block copolymers in general are discussed below.

5.3.3.1 Homogeneous Mixed Monolayer

It could be that after coalescence of the LC domains, the block copolymer and lipid molecules are homogeneously distributed throughout the monolayer, which would imply a high affinity between the lipid acyl chains and the copolymer hydrophobic PPO blocks, which protrude from the interface, while the hydrophilic blocks remain immersed in the subphase. A similar molecular arrangement with polymer chains intercalated between lipid molecules has been previously postulated for mixed monolayers of phosphatidylcholine lipids and PEO-*b*-PPO-*b*-PEO block copolymers (Poloxamers).[15]

However, it has been pointed out that the miscibility between PPO blocks and phosphatidylcholine lipids is very low,[16] and that they tend to phase separate.[17] Furthermore, this explanation would require that the chemical environment created around the lipid acyl chains by PPO blocks be equivalent to the solid-hydrocarbon like environment that is found in the hydrophobic region of lipid LC domains. This is clearly not the case due to the higher polarity of the ether groups present in PPO as compared against lipid alkyl chains. Additionally, the progressive isolation of the perdeuterated lipid acyl chains from each other due to the intercalated PPO blocks would prevent the interchain vibrational coupling of their perdeuterated methylene stretching vibrations. This isotopic dilution effect would shift the frequency of the $\nu_s(CD_2)$ bands toward higher frequencies (typically up to +0.4 cm^{-1}).[18] Nevertheless, such a positive frequency shift was not observed.

5.3.3.2 Lipids' Mesoscopic Clustering

A more likely explanation is that during the growth and coalescence of the LC domains, the lipid molecules aggregate into clusters of mesoscopic to nanoscopic dimensions which are surrounded by a network of block copolymer chains. The lipid acyl chains inside such clusters should exhibit a considerable conformational order similar to that of the original LC domains.

The viability of such an organization into lipid nanoscopic clusters in mixed phospholipid monolayers has been recently confirmed experimentally by AFM on monolayers consisting of a 1:1 mixture of the lipids DMPC and DSPC, both being phosphatidylcholines and differing only in the length of their acyl chains (*y* in Figure 4.4 equals 12 and 16, respectively). Although the difference of four methylene units is equivalent to a length difference between their acyl chains of just 0.5 nm, it is enough for driving an organization into clusters below a size of 25 nm.[19] Similarly, infrared spectroscopy measurements with binary mixtures of phosphatidylcholine lipid isotopes (proteated and deuterated) with differences in the length of their acyl chains of 0, 2, 4 or 6 methylene units have evidenced aggregation into clusters in the size range of 1-100 molecules for differences of two and four methylene units, implying the formation of lipid clusters whose dimensions are smaller than 10 nm; whereas a difference of six units leads to nearly complete phase separation.[20]

The conditions that would enable the proposed formation of clusters with crystalline-like order in two dimensions of a substance of small molecular size surrounded by a percolating network of a second component having a considerably larger size has been analyzed theoretically and modeled using Monte Carlo simulations in a recent publication.[21] The necessary general conditions enabling this type of organization in a phospholipid-amphiphilic block copolymer system are:

(i) A size mismatch between the hydrophobic segment of the lipid and the hydrophobic block of the copolymer.

(ii) A long-range soft repulsive interaction between the hydrophilic blocks of the copolymer.

Although a size mismatch alone would lead to macroscopic phase separation, and long-range repulsive interactions without size mismatch would promote complete mixing for minimizing the repulsion between the copolymer hydrophilic blocks, the compromise between these opposite tendencies would lead to the formation of stable clusters ("lipid corralling").[21]

Experimental studies dealing with the molecular arrangement in mixed monolayers of lipids and polymers are scarce. There have been some recent reports on Poloxamer 188 (PEO_{76}-PPO_{29}-PEO_{76}) adsorption to DPPC monolayers which seem to support the formation of lipid clusters as the preferred structure.[22,23] However, they are not conclusive, in part because the investigation of the macroscopic morphology and the molecular order are carried out in an isolated way. Consequently, a macroscopic phase separation while trying to measure the molecular ordering cannot be ruled out and leads to misleading conclusions.

5.3.4 Molecular Level Organization in Mixed Monolayers of DPPC-d_{62} and $(PGMA_{14})_2$-PPO_{34}

In the specific case of mixed monolayers of DPPC-d_{62} and $(PGMA_{14})_2$-PPO_{34}, the length of the extended lipid alkyl tail in an all-*trans* conformation is approximately 1.9 nm, while for the PPO block the contour length in a fully extended conformation assuming bond angles of 110° together with the characteristic bond length for carbon-carbon bonds (1.54 Å) and for carbon-oxygen bonds (1.43 Å) is 12.2 nm. Even considering that due to the location of both PGMA outer blocks in the subphase a PPO block can protrude into the hydrophobic region of the lipid monolayer only in a folded conformation, there is still a considerable size mismatch with the lipid alkyl tails.

Regarding the second condition (ii), *i.e.* the existence of a long-range soft repulsive interaction between the hydrophilic blocks of the copolymer, it is widely accepted that non-ionic hydrophilic macromolecules in water are subject to a repulsive force when they approach each other.[24] In fact, it is the reason for using grafted non-ionic hydrophilic polymers for the steric stabilization of colloidal particles.[25] However, the origin of such repulsion is still a topic of discussion. It was initially assumed to arise from the work required to disrupt the structured layer of water molecules surrounding the macromolecules before they could come into contact; therefore, it was referred to as "hydration force". More recently, it has been proposed to be an entropic repulsion arising from the confinement of thermally mobile groups when two macromolecules approach and begin to overlap.[26] In any case, the PGMA blocks of $(PGMA_{14})_2$-PPO_{34} being highly hydrated are also subjected to such a repulsive force, whose effective range is of the order of the block size. The PGMA blocks are in a quite extended conformation and have a weight-average contour length of approximately 4.7 nm,[27] which gives the range of the corresponding repulsive force.

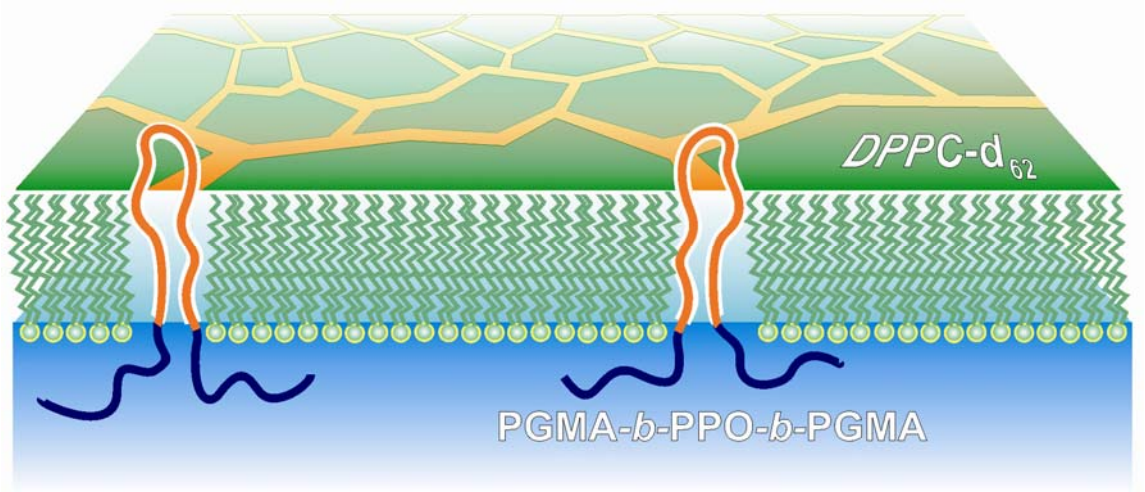

Figure 5.6: Schematic illustration of the morphology of the mixed monolayer of $(PGMA_{14})_2$-PPO_{34} and DPPC-d_{62} at the air-water interface. Lipid clusters with crystalline-like order are colored in green. The surrounding network of block copolymer chains is colored orange.

From these considerations it is evident that the system under investigation fulfills indeed both necessary conditions for the formation of clusters of lipid molecules with crystalline-like order surrounded by a percolating network of the block copolymer. A schematic representation of the plausible morphology of the mixed monolayer is presented in Figure 5.6.

It is interesting to note the decisive influence of the length of PPO and PGMA blocks, respectively, on the stability of the clustered morphology in the mixed monolayers: shorter PGMA blocks or a PPO block much longer than the lipid alkyl chains would promote macroscopic phase separation; conversely, longer PGMA blocks or a PPO block with a length closer to that of the lipid alkyl chains would increase the tendency to a more homogeneous distribution of the block copolymer in the monolayer.

5.4 Conclusions

The investigation of the molecular level organization of mixed monolayers resulting from the adsorption process of the triblock copolymer $(PGMA_{14})_2$-PPO_{34} to DMPC-d_{54} and DPPC-d_{62} monolayers at intermediate initial surface pressures has shown that neither a perfectly mixed monolayer of polymer chains intercalated between lipid molecules, nor a macroscopically phase separated interface is obtained after long equilibration times. Accordingly to IRRAS and BAM experimental results, it is most likely that the final molecular organization of the mixed monolayer is in clusters of lipid molecules, exhibiting internally a high conformational order and mesoscopic to nanoscopic dimensions, surrounded by a network of block copolymer chains.

5.5 References

[1] L.-C. Chang, Y.-Y. Chang, C.-S. Gau, *J. Colloid Interface Sci.*, **2008,** *322*, 263.

[2] P. Mudgil, G. R. Dennis, T. J. Millar, *Langmuir*, **2006**, *22*, 7672.

[3] V. B. Fainerman, D. Vollhardt, *Langmuir*, **1999**, *15*, 1784.

[4] S. Sundaram, K. J. Stebe, *Langmuir*, **1997**, *13*, 1729.

[5] L.-C. Chang, C.-Y. Lin, M.-W. Kuo, C.-S. Gau, *J. Colloid Interface Sci*., **2005**, *285*, 640.

[6] S.L. Frey, K.Y. Lee, *Langmuir,* **2007**, *23*, 2631.

[7] C. Naumann, C. Dietrich, J.R. Lu, R.K. Thomas, A.R. Rennie, J. Penfold, T.M. Bayerl, *Langmuir,* **1994**, *10*, 1919.

[8] G. Wu, J. Majewski, C. Ege, K. Kjaer, M. J. Weygand, K. Y. C. Lee, *Biophys. J*., **2005**, *89*, 3159.

[9] S.L F. Neville, Y. Ishitsuka, C. S. Hodges, O. Konovalov, A. J. Waring, R. Lehrer, K. Y. C. Lee, D. Gidalevitz, *Soft Matter,* **2008**, *4*, 1665.

[10] S. Hénon, J. Meunier, *Rev. Sci. Instrum*., **1991**, *62*, 936.

[11] B.M. Discher, W.R. Schief, V. Vogel, S. B. Hall, *Biophys. J*., **1999**, *77*, 2051.

[12] E. Amado, A. Kerth, A. Blume, J. Kressler, *Langmuir,* **2008**, *24*,10041.

[13] H. L. Casal, H.H. Mantsch, *Biochim. Biophys. Acta,* **1984**, *779*, 381.

[14] L.K. Tamm, S. A. Tatulian, *Q. Rev. Biophys*., **1997**, *30*, 365.

[15] C. Weingarten, N. S. Santos Madalhaes, A. Baszkin, S. Benita, M.Seiller, *Int. J. Pharm.*, **1991**, *75*, 171.

[16] K. Bryskhe, K. Schillén, J.-E. Löfroth, U. Olsson, *Phys. Chem. Chem. Phys.*, **2001**, *3*, 1303.

[17] J. D. Castile, K. M. G. Taylor, G. Buckton, *Int. J. Pharm.*, **2001**, *221*, 197.

[18] V. R. Kodati, R. El-Jastimi, M. Lafleur, *J. Phys. Chem.*, **1994**, *98*, 12191.

[19] L. K. Nielsen, T. Bjornholm, O. G. Mouritsen, *Langmuir,* **2007**, *23*, 11684.

[20] R. Mendelsohn, G. L. Liang, H. L. Strauss, R. G. Snyder, *Biophys. J*., **1995**, *69*, 1987.

[21] D. Zhang, M. A. Carignano, I. Szleifer, *Phys. Rev. Lett.*, **2006**, *96*, 028701.

[22] S. L. Frey, D. Zhang, M.A. Carignano, I. Szleifer, K. Y. C. Lee, *J. Chem. Phys*. **2007**, *127*, 114904.

[23] G. Wu, J. Majewski, C. Ege, K. Kjaer, M. J. Weygand, K. Y. C. Lee, *Phys. Rev. Lett.*, **2004**, *93*, 028101.

[24] P. M. Claesson, J. C. Eriksson, C. Herder, B. A. Bergenstahl, E. Pezron, I. Pezron, P.Stenius, *Faraday Discuss. Chem. Soc.,* **1990**, *90*, 129.

[25] V. O. Aseyev, H. Tenhu, F. M. Winnik, *Adv. Polym. Sci.,* **2006**, *196*, 1.

[26] J. Israelachvili, H. Wennerström, *Nature,* **1996**, *379*, 219.

[27] E. Amado, C. Augsten, K. Maeder, A. Blume, J. Kressler, *Macromolecules,* **2006**, *39*, 9486.

6 Summary

An in-depth understanding of the interaction mechanism between nonionic amphiphilic block copolymers and biological membranes is a key requirement in order to improve their current biomedical uses, and also to explore future applications. The present lack of comprehension in this topic is partially related to research activities being concentrated almost exclusively on a single family of commercially available block copolymers, namely on Poloxamers. Therefore, a first step for a better understanding of the interactions with lipids is the synthesis of tailor-made and thoroughly characterized model amphiphilic block copolymers. Besides, the incorporation of hydrophilic blocks having novel chemical functionalities and molecular architecture compared to traditional poly(ethylene oxide)-based blocks opens new applications horizons.

The aim of the present work was to synthesize a series of novel water soluble amphiphilic triblock copolymers of ABA architecture comprising a PPO middle block and two poly(2,3-dihydroxypropyl methacrylate) outer blocks of varying length. In a second stage of the investigation their micellization in aqueous solutions was studied, as well as their adsorption behavior at the air-water interface. Finally, their adsorption kinetics and concomitant interactions with phospholipid model membranes were investigated in order to gain a better insight into the PGMA-*b*-PPO-*b*-PGMA-membrane interactions on a molecular level. The main results obtained are summarized in the next paragraphs.

Synthesis by Atom Transfer Radical Polymerization (ATRP)

Novel water soluble PGMA-*b*-PPO-*b*-PGMA triblock copolymers were successfully synthesized via ATRP technique. The blocks comprised a thermoresponsive poly(propylene oxide) (PPO) middle block with a molar mass of around 2000 $g \cdot mol^{-1}$ and two hydroxy-functional poly(2,3-dihydroxypropyl methacrylate) (PGMA) outer blocks with lengths varying from 14 to 221 monomeric units per block. Molar mass values were obtained from ^{1}H-NMR measurments.

Gel permeation chromatography analysis confirmed unimodal molar mass distributions with polydispersity indexes ranging between 1.29 and 1.40 for different lengths of the PGMA block.

Micellization in Aqueous Solutions

The association behavior of PGMA-*b*-PPO-*b*-PGMA in aqueous solutions was studied by dynamic light scattering. Not only the size of the micelles formed, but also its temperature dependence was followed by DLS measurements between 4-40°C. Depending on the length of the PGMA blocks, micelles showed an average hydrodynamic diameter in the range from 20 to 30 nm. Triblock copolymers having PGMA blocks with a degree of polymerization around half of that of the PPO block formed micelles with a well defined and practically constant size with apparent hydrodynamic radii R_h~10-15 nm in the temperature range of 15-40°C; and exhibited a critical micellization temperature at about 8°C (*C*~1 mM), above which micelles could be formed. Copolymers having PGMA blocks of length comparable to that of the PPO block exhibited a critical micellization temperature at about 19°C. Also aggregates with sizes in the range of R_h~175-215 nm were formed at temperatures below CMT. Triblock copolymers having much longer PGMA blocks were present mostly as unimers.

Critical micellization concentrations (CMC) were determined using surface tension measurements, fluorescent probe technique with pyrene as probe molecule and isothermal titration calorimetry (ITC). CMCs were found to be in the range from 8×10^{-6} to 2×10^{-4}M depending on the length of the PGMA block and on the method used. A relatively good agreement was found between the CMC values obtained using the different methods.

Adsorption Behavior at the Air-Water Interface

The features of PGMA-*b*-PPO-*b*-PGMA adsorption at the air-water interface and its spatial arrangement were studied by tensiometry and monolayer techniques. Surface layers were prepared by adsorption from the bulk as well as by spreading at the air-water interface from a polymer solution in a volatile solvent.

For $(PGMA_{14})_2$-PPO_{34}, time-dependent measurements exhibit a bimodal adsorption kinetics related to the appearance of a high energy barrier against adsorption from the solution bulk. Monolayers deposited by spreading are found to be stable enough to withstand compression up to high surface pressures, and to form pseudo-Langmuir films even though $(PGMA_{14})_2$-PPO_{34} is highly water-soluble at room temperature.

The following conformational transitions, identified from the changes in dilatational surface elasticity in combination with the compression isotherm, take place within the surface layer with increasing surface pressure for both adsorbed and spread layers:

(i) Transition from a dilute, two-dimensional gas-like regime, to a semidilute regime occurs at a molecular area of ~ 4424 Å²/molecule (Π = 0.03 mN/m). $(PGMA_{14})_2$-PPO_{34} chains maintain a flat conformation with most segments in contact with the interface up to Π ~ 2 mN/m.

(ii) Above Π = 2.1 mN/m (1291 Å²/molecule) PGMA segments begin to change from a flat conformation to loops and tails protruding into the subphase, and form an increasingly condensed swollen layer with increasing pressures.

(iii) The onset of the conformational change for PO segments takes place at a molecular area of ~ 625 Å²/molecule (Π = 15.5 mN/m).

(iv) In the range Π ~ 21.4 to 23.8 mN/m the PPO blocks adopt a three-dimensional conformation, and the layer thickness increases accordingly. This process continues up to about Π ~ 34.5 mN/m, corresponding to an average area per PO monomeric unit of approximately 4 Å².

A theoretical multiple conformation model was applied to describe the adsorption of $(PGMA_{14})_2$-PPO_{34} at the air-water interface. A ratio of approximately eight between the average molecular areas at low coverage and at full coverage confirms that $(PGMA_{14})_2$-PPO_{34} molecules are highly flexible; and that they are able to adopt very different conformations during the transition of the adsorbed polymer film from a highly diluted to a nearly saturated state.

Interactions with Phospholipid Model Membranes

The incorporation process of PGMA-*b*-PPO-*b*-PGMA into DPPC and DMPC monolayers located at the air-water interface was studied using monolayer techniques in combination with infrared reflection absorption spectroscopy (IRRAS) and Brewster Angle Microscopy (BAM). In the case of $(PGMA_{14})_2$-PPO_{34} the maximum penetration surface pressure of ~39 mN/m, suggests that the copolymer is able to insert into lipid monolayers even above the so-called monolayer-bilayer equivalent pressure of 30-35 mN/m, and thus it would be able to insert into intact biological membranes too.

Comparative adsorption experiments to perdeuterated lipid monolayers show that the copolymer surface concentration is higher when adsorbed to a DPPC-d_{62} monolayer than to a DMPC-d_{54} monolayer. This and other differences in the copolymer adsorption behavior are attributed to DMPC-d_{54} lacking a liquid expanded (LE) to liquid condensed (LC) first order transition of the monolayer, and being therefore unable to accommodate copolymer molecules by the excluded area mechanism present in the case of DPPC-d_{62}. Adsorption kinetics is considerable faster to DMPC-d_{54} monolayers, which is attributed to a more fluid state of the monolayer.

IRRAS experiments show that copolymer incorporation into a DPPC-d_{62} monolayer in a LE phase proceeds in a two-step mechanism:

(i) Initially only the more hydrophobic PPO middle block penetrates the lipid monolayer, while the hydrophilic PGMA blocks remain completely immersed in the subphase.

(ii) After the LE-LC phase transition of the lipid, the bulky PGMA hydrophilic blocks are dragged into the headgroup region of the lipid monolayer as the PPO hydrophobic block inserts further into the fatty acid region.

Copolymer adsorption to a DPPC-d_{62} monolayer initially in LC condensed phase leads to a change in the monolayer packing by forcing the lipid alkyl chains into a more vertical orientation. Their tilt angle with respect to the surface normal reduces from initially (30 ± 3)° to (18 ± 3)°.

Molecular level organization of mixed monolayers

The equilibrium morphology on the molecular level of mixed monolayers formed after adsorption of PGMA-*b*-PPO-*b*-PGMA to phospholipid monolayers was elucidated based on a comparative study of mixed monolayers formed with DPPC-d_{62} or DMPC-d_{54} after very long equilibration times, investigated by IRRAS coupled with BAM. The simultaneous observation of the monolayer morphology by BAM during IRRA spectra acquisition ruled out any macroscopic phase separation while investigating the molecular organization.

In the case of $(PGMA_{14})_2$-PPO_{34} it was found that neither a perfectly mixed monolayer of polymer chains intercalated between lipid molecules, nor a macroscopically phase separated interface is obtained after long equilibration times. The most likely molecular organization of the mixed monolayer is in clusters of lipid molecules surrounded by a network of block copolymer chains (“lipid corralling”). Such lipid clusters exhibit a high conformational order and mesoscopic to nanoscopic dimensions.

Recent improvements in the techniques for transferring monolayers from the air-water interface to solid supports, aimed to ensure the preservation of the original structure of the monolayer, would possibly enable a detailed visualization of the clustered structure in the range of several nanometers by scanning probe methods in future investigations. Since lipid monolayers are a simplified model of the outer leaflet of a cell membrane, the results from this study are particularly significant for a better understanding of the interactions between amphiphilic block copolymers and the lipid bilayer of cell membranes, which is vital for their application as drug delivery systems for poorly soluble drugs or as coadjuvants in pharmaceutical formulations.

7 Zusammenfassung

Ein eingehendes Verständnis des Mechanismus' der Wechselwirkungen zwischen nichtionischen amphiphilen Blockcopolymeren und biologischen Membranen ist eine wesentliche Voraussetzung, um sowohl ihre aktuellen biomedizinischen Anwendungen zu verbessern als auch zukünftige Anwendungen zu erforschen. Ein derzeitiger Mangel an Verständnis in diesem Thema ist zum Teil auf eine übermäßige Fokussierung von Forschungsaktivitäten auf eine einzige Familie von kommerziell erhältlichen Blockcopolymeren, nämlich Poloxamere, zurückzuführen. Daher ist die Synthese von maßgeschneiderten und umfassend charakterisierten Modellen amphiphiler Blockcopolymere ein nötiger Schritt, um ein besseres Verständnis der Wechselwirkungen mit Lipiden zu gewinnen. Außerdem eröffnet der Einbau von hydrophilen Blöcken mit neuen chemischen Funktionalitäten und molekularer Architektur im Vergleich zu den traditionellen Poly(ethylenoxid)-Blöcken neue Horizonte für Anwendungen.

Das Ziel der vorliegenden Arbeit war es, eine Reihe von neuen wasserlöslichen amphiphilen Triblockcopolymeren des Architekturtyps ABA, bestehend aus einem PPO-Block in der Mitte des Polymers und zwei Poly(2,3-dihydroxymethacrylat)-Bausteinen als äußere Blöcke unterschiedlicher Länge, zu synthetisieren. Anschliessend, wurden ihre Mizellbildung in wässrigen Lösungen sowie das Adsorptionsverhalten an der Luft-Wasser-Grenzfläche untersucht. Schließlich wurden ihre Adsorptionskinetik und die gleichzeitige Interaktion mit Phospholipid-Modell Membranen analysiert, um einen besseren Einblick in die PGMA-*b*-PPO-*b*-PGMA-Membran-Wechselwirkungen auf der molekularen Ebene zu gewinnen. Die wichtigsten Ergebnisse werden in den nächsten Abschnitten zusammengefasst.

Synthese mittels radikalischer Polimerisation mit Atomtransfer (ATRP)

Neuartige wasserlösliche PGMA-*b*-PPO-*b*-PGMA Triblockcopolymere wurden mittels ATRP Technik synthetisiert. Die Blockcopolymere enthalten einen temperatursensitiven mittleren Block aus Poly(propylenoxid) (PPO) mit einer Molmasse von ca. 2000 $g \cdot mol^{-1}$ und zwei äußeren Blöcken aus Poly(2,3-dihydroxymethacrylat) (PGMA) mit einer Länge von 14 bis 221 Monomereinheiten pro Block. Die Molmassen wurden mittels ^{1}H-NMR-Messungen erhalten. Gelpermeationschromatographische Untersuchungen bestätigten unimodale Molmassenverteilungen mit einem Polydispersitätsindex zwischen 1,29 und 1,40 für unterschiedliche Längen der PGMA Blöcke.

Mizellbildung in wässrigen Lösungen

Das Aggregationsverhalten PGMA-*b*-PPO-*b*-PGMA in wässrigen Lösungen wurde mit dynamischer Lichtstreuung untersucht. Nicht nur die Größe der gebildeten Mizellen, sondern auch die Temperaturabhängigkeit wurde durch DLS-Messungen zwischen 4–40°C verfolgt. Je nach Länge der PGMA-Blöcke wiesen die Mizellen einen durchschnittlichen hydrodynamischen Durchmesser im Bereich von 20 bis 30 nm auf. Triblockcopolymere mit PGMA-Blöcken, deren Polymerisationsgrad etwa der Hälfte des Polymerisationsgrades des PPO-Blockes entspricht, bildeten Mizellen mit einer wohl definierten und nahezu konstanten Größe und einem hydrodynamischen Radius R_h von 10–15 nm im Temperaturbereich von 15–40°C. Sie wiesen eine kritische Mizellbildungstemperatur bei etwa 8°C (C~1 mM) auf. Copolymere mit PGMA-Blöcken einer vergleichbaren Länge zum PPO-Block zeigten eine kritische Mizellbildungstemperatur bei etwa 19°C. Triblockcopolymere mit viel längeren PGMA- Blöcken lagen meist als Unimere vor.

Die kritischen Mizellbildungskonzentrationen (CMC) wurden durch Messungen der Oberflächenspannung, Fluoreszenz (mit Pyren als Sondenmolekül) und Isothermer Titrationskalorimetrie (ITC) ermittelt. Die CMCs liegen im Bereich von 8×10^{-6} bis 2×10^{-4} M, abhängig von der Länge des PGMA-Blocks.

Adsorptionsverhalten an der Luft-Wasser-Grenzfläche

Die Merkmale der PGMA-*b*-PPO-*b*-PGMA-Adsorption an der Luft-Wasser-Grenzfläche und ihrer räumlichen Anordnung wurden mittels Tensiometrie untersucht. Für $(PGMA_{14})_2$-PPO_{34} zeigen zeitabhängige Messungen eine bimodale Adsorptionskinetik, die im Zusammenhang mit einer hohen energetischen Barriere gegenüber der Adsorption steht. Monoschichten, die durch Spreiten präpariert wurden, erweisen sich als stabil genug, um Pseudo-Langmuirfilme zu bilden, obwohl $(PGMA_{14})_2$-PPO_{34} bei Raumtemperatur hoch wasserlöslich ist.

Die folgenden Konformationsübergänge wurden mit zunehmendem Oberflächendruck im Bereich der Oberflächenschicht, sowohl für adsorbierte als auch für gespreitete Schichten, identifiziert:

(i) Übergang von einem verdünnten, zweidimensionalen gasähnlichen Regime zu einem halbverdünnten Regime, der bei einem Oberflächendruck Π = 0,03 mN/m stattfindet. $(PGMA_{14})_2$-PPO_{34}-Ketten liegen bis zu einem Oberflächendruck Π = 2,1 mN/m in einer flachen Konformation auf der Wasseroberfläche vor.

(ii) Oberhalb Π = 2,1 mN/m wandeln sich die PGMA-Segmente von einer flachen Konformation in Schleifen- und Schwanz-Konformationen um, die in die Subphase ragen. Dort bilden sie mit zunehmendem Druck eine immer weiter anschwellende kondensierte Schicht.

(iii) Der Beginn der Konformationsänderung für POP-Segmente erfolgt bei Π = 15,5 mN/m.

(iv) Im Bereich Π ~ 21,4–23,8 mN/m nehmen die PPO Blöcke eine dreidimensionale Konformation an. Die Schichtdicke erhöht sich entsprechend.

Ein theoretisches, multiples Konformations-Modell wurde angewandt, um die Adsorption von $(PGMA_{14})_2$-PPO_{34} an der Luft-Wasser-Grenzfläche zu beschreiben. Es wurde bestätigt, dass die $(PGMA_{14})_2$-PPO_{34}-Moleküle sehr flexibel sind und dass sie in der Lage sind, unterschiedliche Konformationen anzunehmen.

Wechselwirkungen mit Phospholipidmodellmembranen

Der Adsorptionsprozess von PGMA-*b*-PPO-*b*-PGMA an DPPC- und DMPC-Monoschichten an der Luft-Wasser-Grenzfläche wurde mittels Infrarot-Reflexions-Absorptions-Spektroskopie (IRRAS) und Brewster-Winkel-Mikroskopie (BAM) untersucht. Im Falle von $(PGMA_{14})_2$-PPO_{34} deutet der maximale Penetrationsoberflächendruck von ca. 39 mN/m darauf hin, dass das Copolymer in der Lage ist, sich in intakte biologische Membranen einzubauen.

IRRAS-Experimente zeigten, dass der Einbau des Copolymers in eine DPPC-d_6 Monoschicht in einem flüssig-expandierten (LE) Zustand nach einem zweistufigen Mechanismus abläuft:

(i) Zunächst dringt nur der hydrophobere mittlere PPO-Block in die Lipidmonoschicht ein, während die hydrophilen PGMA-Blöcke vollständig in der Subphase bleiben.

(ii) Nach dem LE-LC-Phasenübergang des Lipids werden die sperrigen hydrophilen PGMA-Blöcke in den Bereich der Kopfgruppe der Lipidmonoschicht gezogen, während der PPO-Block sich weiter in den Bereich der Alkylgruppen der Fettsäuren einbaut.

Organisation gemischter Monoschichten auf Molekularer Ebene

Die Gleichgewichtsmorphologie auf molekularer Ebene von gemischten Monoschichten, die nach der Adsorption von PGMA-*b*-PPO-*b*-PGMA an Phospholipidmonoschichten gebildet werden, wurde mittels IRRAS, gekoppelt mit BAM, untersucht.

Im Falle von $(PGMA_{14})_2$-PPO_{34} wurde festgestellt, dass weder eine perfekt gemischte Monoschicht von Polymerketten und Lipid-Molekülen, noch zwei makroskopisch getrennte Phasen erreicht werden. Die wahrscheinlichste molekulare Organisation der gemischten Monoschicht ist die in Clustern von Lipid-Molekülen, die von einem Netz von Blockcopolymerketten umgeben werden. Diese Lipid-Cluster weisen eine hohe Konformationsordnung und mesoskopische bis nanoskopische Dimensionen auf.

8 Appendix

8.1 Synthesis of Rhodamine Conjugated PGMA-*b*-PPO-*b*-PGMA Copolymers

Rhodamine conjugates of PGMA-*b*-PPO-*b*-PGMA were synthesized by reacting some primary hydroxyl groups of the PGMA blocks with the fluorescence label tetramethylrhodamine-5-carbonyl azide (TMR) (Invitrogen T6219) in a molar ratio 1:1 according to the reaction scheme shown in Figure 8.1.

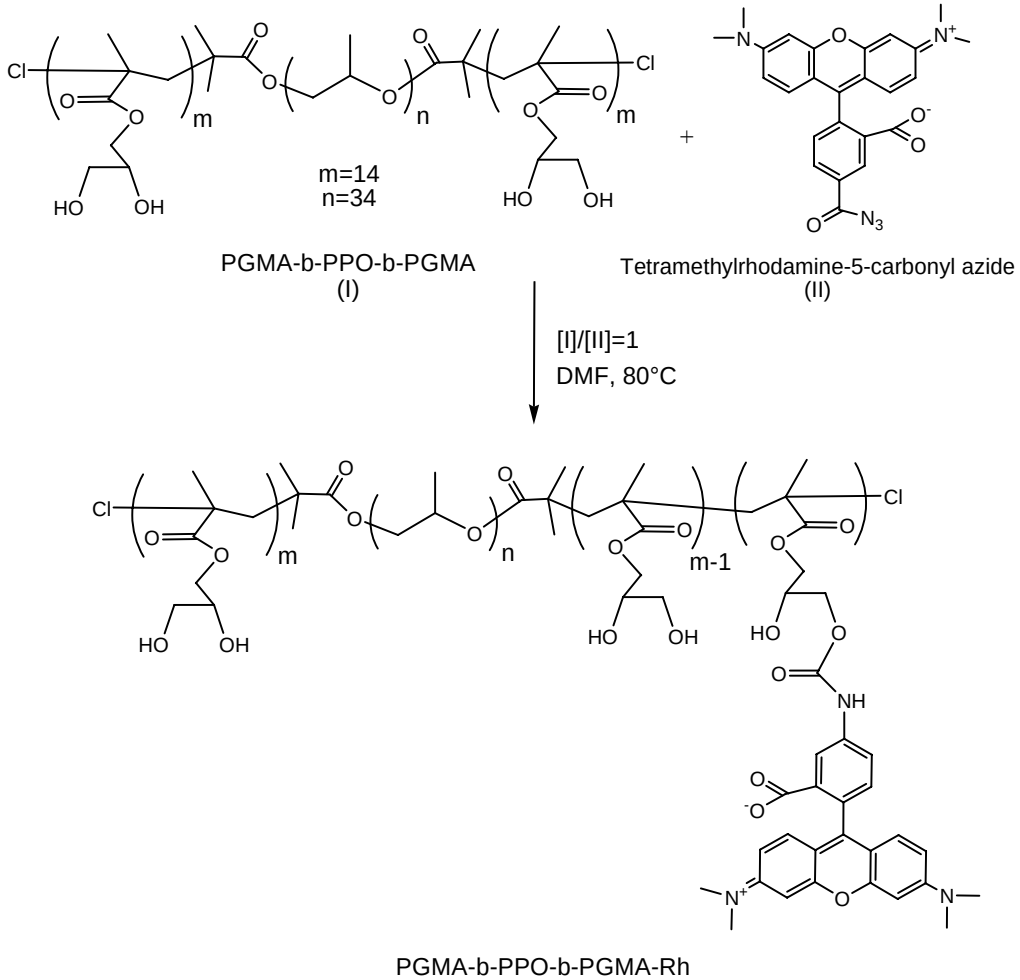

Figure 8.1: Reaction scheme for the synthesis of conjugates of PGMA-*b*-PPO-*b*-PGMA and the fluorescence label tetramethylrhodamine.

In a typical procedure, a solution of PGMA-*b*-PPO-*b*-PGMA triblock copolymer in anhydrous Dimethylformamide (DMF) was left to dry over 3A molecular sieve overnight. A TMR solution in DMF was added dropwise under argon within 5 h at 80°C. The reaction was continued for 24 h more. After completion of the reaction the solution was dialyzed against DMF through a membrane with molar mass cut off of 3500 $g \cdot mol^{-1}$ for removing un-conjugated tetramethylrhodamine. Both the dialysis bag and the DMF were changed daily for 4 days. Then the conjugated polymer solution was dialyzed against pure water for 3 days for removing the organic solvent. Again, both the dialysis bag and the water were changed daily until no trace of TMR in the external solvent could be detected by fluorescence spectroscopy. Finally, the aqueous solution was freeze-dried for obtaining the conjugated polymer PGMA-*b*-PPO-*b*-PGMA-TMR as a slightly pink powder, readily soluble in water.

8.1.1 PGMA-*b*-PPO-*b*-PGMA-TMR Fluorescence Spectra

Figure 8.2 shows a typical example of the fluorescence excitation and emission spectra obtained for the conjugated polymers PGMA-*b*-PPO-*b*-PGMA-TMR in water at 25°C.

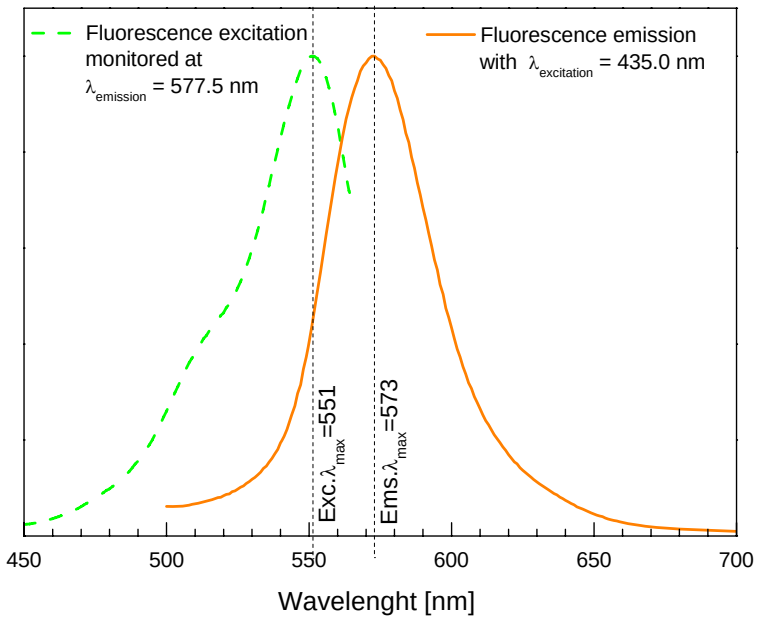

Figure 8.2: Fluorescence spectra for the conjugated polymer $(PGMA_{15})_2$-PPO_{34}-TMR in water at 25°C.

The fluorescence emission spectrum of $(PGMA_{15})_2$-PPO_{34}-TMR for an excitation wavelength $\lambda_{excitation}$ = 435.0 nm shows a maximum at λ = 573.0 nm, just slightly shifted if compared to the emission maximum of pure TMR (λ= 577.0 nm). This indicates that the conjugation did not influence considerably the fluorescence of the original TMR. The fluorescence excitation spectra were taken at an emission wavelength equal to the corresponding emission maximum.

8.2 Asymmetrical Flow Field-Flow Fractionation and Multiangle Light Scattering Measurements

Asymmetrical Flow Field-Flow Fractionation (AF4) coupled online with Multiangle Light Scattering (MALS) detection in water, was used for determining molar masses. A deeper introduction to field flow fractionation and particularly to AF4 and its underlying principles can be found elsewhere.[1,2] Briefly, the sample species are fractionated within a narrow ribbon-like channel after being injected into the channel near the inlet. From the inlet, a carrier liquid is pumped through the channel, transporting the sample towards the outlet. Due to the wall friction a parabolic laminar flow profile is established. Simultaneously, a part of the carrier liquid leaves the channel via an ultrafiltration membrane covering the bottom of the channel. This cross-flow perpendicular to the laminar flow exerts a separation field on the sample. The cross-flow forces the sample components to accumulate near to the membrane establishing a concentration gradient. Accordingly, a diffusion flux back into the interior of the channel is induced. Depending on the sample size, equilibrium between the two opposite processes is achieved. Those species with larger hydrodynamic diameters and smaller diffusion coefficients accumulate near to the membrane of the channel being positioned in a slower flow laminae of the parabolic laminar flow and are gradually separated from smaller species positioned further from the wall in faster laminae, which elute therefore prior to the larger species.[3] By on-line coupling of a MALS detector absolute molar masses and gyration radii can be determined from each fraction eluting from the channel.[4] The plotting of intensity of the detector signal *versus* elution time or elution volume is referred to as a fractogram.

Although field-flow fractionation (FFF) techniques are elution techniques with inherent differential flow displacement phenomena just like GPC and other chromatographic methods, in comparison to them FFF techniques have the advantage that the separation of components is achieved exclusively through the interaction of the sample with an external, perpendicular physical field, rather than by the interaction with a stationary phase, which results in nondestructive fractionation of the samples.[5] Besides, FFF is suitable for the characterization of complex samples such as mixtures with broad molar masses or particle size ranges.

8.2.1 AF4 Equipment

The AF4 experiments were carried out in a set up consisting of a separation channel coupled to an Eclipse F (organic version) separation system and a MALS detector Dawn EOS, all from Wyatt Technology Europe. Additionally, an in-line degasser and pump from the Series 1100 from Agilent Technologies and a Refractive Index (RI) detector RI-101 from Shodex were used. The channel thickness was 350 μm, the regenerated cellulose membranes used (from Microdyn-Nadir) had a cutoff of 10 kDa. All measurements were performed in double-distilled water with 0.02% NaN_3, prefiltered through a 100 nm filter (VVLP-Filter from Millipore). For separation, after several pre-measurements a linear cross-flow rate gradient between 3 mL/min and 0 mL/min within 20 min was found to be optimal. Detector

flow rates were constant at 1 mL/min. For each AF4 experiment, 100 μL samples were injected into the channel at a 0.2 mL/min rate. The refractive index increment, d*n*/d*c* was measured separately for each sample. Sample concentrations were determined from the RI signal. All measurements were performed at ambient temperature. To evaluate the MALS signals in order to obtain the values for molar mass, the Zimm plot method was used. The details of the method are described elsewhere.[6]

8.2.2 AF4 Results

Within the MALS unit, scattered light was detected by an array of 18 photodiodes arranged at various angles relative to the incoming laser beam ($\lambda = 690$ nm). Absolute molar masses (M_w) were determined from the measured scattering intensity by a extrapolation procedure according to the Zimm method included within the Astra 4.9 software (Wyatt Technology Corp.). The fractionations obtained through AF4 for the different samples are shown in Figure 8.3. In such fractograms, fractions of lower molar masses elute earlier than fractions with higher ones, according to the FFF theory.[1] The average molar masses and micellar aggregation numbers obtained are presented in Table 8.1

Table 8.1: Weight Average Molar Masses (M_w), Refractive Index Increment (d*n*/d*C*) and Aggregation numbers of Micelles (N_{agg}) for the PGMA-*b*-PPO-*b*-PGMA Triblock Copolymers in Water from MALS.

Sample	d*n*/d*C*	M_w [g·mol^{-1}]	Micelles	
			M_w [g·mol^{-1}]	N_{agg}
$(PGMA_{221})_2$-PPO_{34}	0.136	88 400	-	-
$(PGMA_{36})_2$-PPO_{34}	0.130	28 000	880 000	32
$(PGMA_{15})_2$-PPO_{34}	0.130	24 600	981 200	40
$(PGMA_{14})_2$-PPO_{34}	0.130	21 400	670 000	31

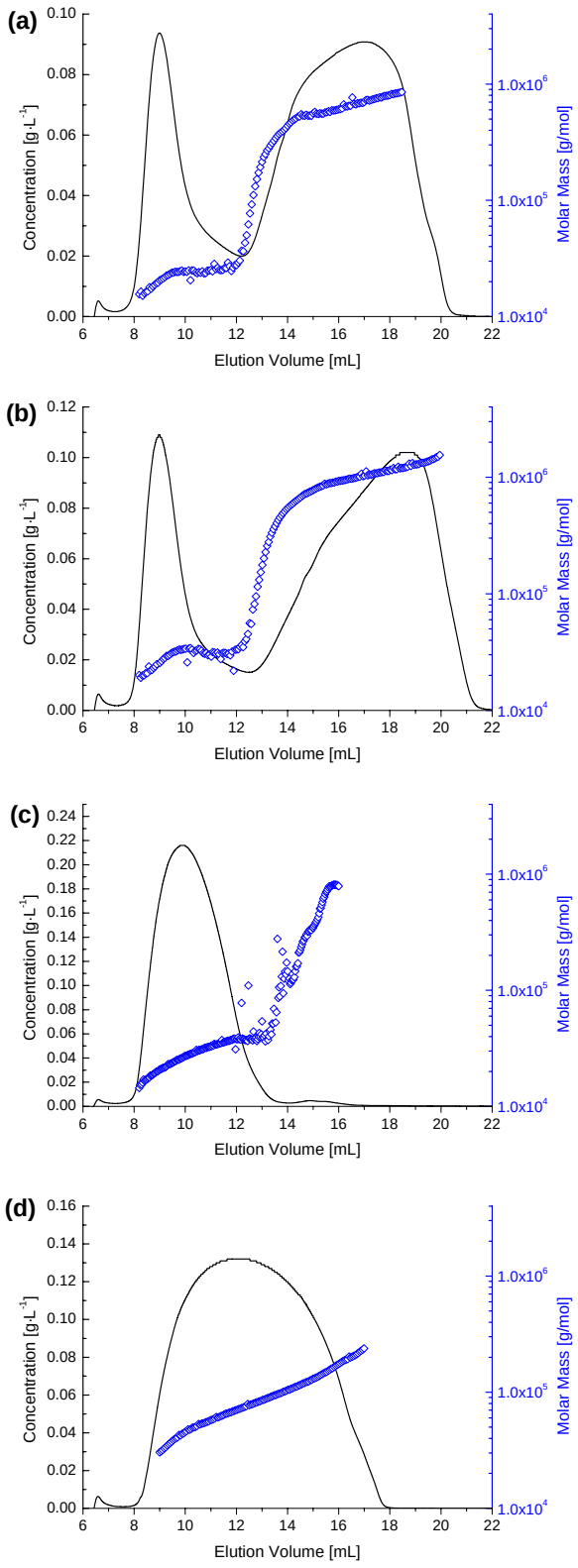

Figure 8.3: AF4 Analysis of the triblock copolymers in water at room temperature. Solid lines correspond to the concentration derived from RI signal. Symbols (◊) represent the calculated molar masses (M_w) from MALS. (a) $(PGMA_{14})_2$-PPO_{34} (b) $(PGMA_{15})_2$-PPO_{34} (c) $(PGMA_{36})_2$-PPO_{34} (d) $(PGMA_{221})_2$-PPO_{34} . Concentration 1 % w/w. Detector flow rate 1 mL/min. Cross-flow rates 3 to 0 mL/min..

Both $(PGMA_{14})_2$-PPO_{34} and $(PGMA_{15})_2$-PPO_{34} triblock copolymer exhibited a clearly bimodal distribution, with M_w for the smaller species separated (peak at earlier elution times) being around 21 and 25 kg·mol^{-1}, respectively. For the larger species (peak at later elution times) M_w was 670 and 981 kg·mol^{-1}, respectively. The low molar mass species should correspond to single dissolved chains (unimers) of the triblocks, meanwhile the high molar mass species can be attributed to micelles or other supramolecular aggregates. A similar elution behavior of micelles and its macromolecular monomers in Flow Field-Flow Fractionation has already been described for other copolymers.[7] From the molar mass ratio of micelles to unimers aggregation numbers for the micelles (N_{agg}) of 31 and 40, respectively, were obtained. The fractogram for $(PGMA_{36})_2$-PPO_{34} also exhibits a bimodal distribution, but in comparison to the shorter triblocks the fraction of micelles present is considerably lower. The micelles peak shows a shoulder indicating the presence of even larger associated species (apparent M_w being around 380 kg·mol^{-1} for the main peak and 880 kg·mol^{-1}for the shoulder). On the other hand, the distribution of unimers is broader than in the case of the shorter triblocks. In the fractogram of $(PGMA_{221})_2$-PPO_{34} only a single extremely broad peak with an apparent M_w of 88 kg·mol^{-1} is observed. This peak covered a wide range from approximately 30 to 230 kg·mol^{-1} being far broader than the peaks obtained for the previous samples. Although the peak might correspond not only to unimers the presence of well defined micelles was not evidenced.

Finally, it must be pointed out that after comparing the AF4/MALS data with the results coming from ^{1}H-NMR and DLS some inconsistencies were found indicating that the M_w values coming from AF4/MALS measurements are strongly affected by the perturbation of the unimer-micelle equilibrium during dilution inside the separation channel. Unfortunately the exact way in which the dilution process affects the measurement cannot be predicted.

8.3 Mass Weighted Distributions of Apparent Hydrodynamic Radii (R_h) from DLS Measurements

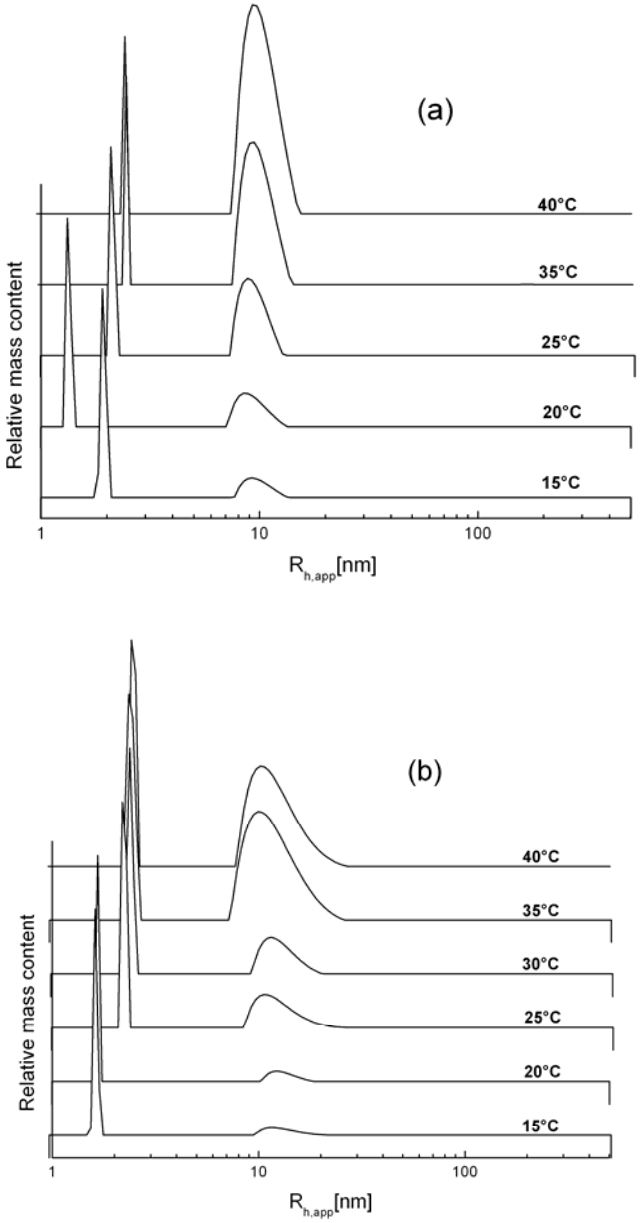

Figure 8.4: Mass weighted distributions of apparent hydrodynamic radii (R_h) in the temperature range 15-40°C for (a) $(PGMA_{14})_2$-PPO_{34} and (b) $(PGMA_{15})_2$-PPO_{34} triblock copolymer at concentrations of 1.4 mM and 6.9mM, respectively .

8.4 $(PGMA_{14})_2$-PPO_{34} Molecular Area

Variable area experiments, namely surface pressure (Π)/area (A) isotherms for monolayer films of the lipid DPPC-d_{62} and the block copolymer $(PGMA_{14})_2$-PPO_{34} at the air-water interface, see Fig.8.5, were carried out in a rectangular Teflon trough (Riegler & Kirstein, Berlin, Germany) with dimensions 300 mm × 60 mm equipped with a Wilhelmy film balance for monitoring the surface pressure Π. The available area was varied during the experiment by changing the distance between two mobile Teflon barriers positioned symmetrically to the trough center at a compression rate of 1 $Å^2$ or 2.6 $Å^2$ per molecule per min for lipid and copolymer, respectively. The temperature of the trough was maintained constant at 20°C.

Since the copolymer isotherm approximates the reduction in the surface occupied by a copolymer molecule with increasing surface pressure as adsorption proceeds, the copolymer molecular area at the equilibrium surface pressure (Π_{eq}=37.8 $mN \cdot m^{-1}$) was taken as a first approximation from the copolymer compression isotherm at the same Π value.

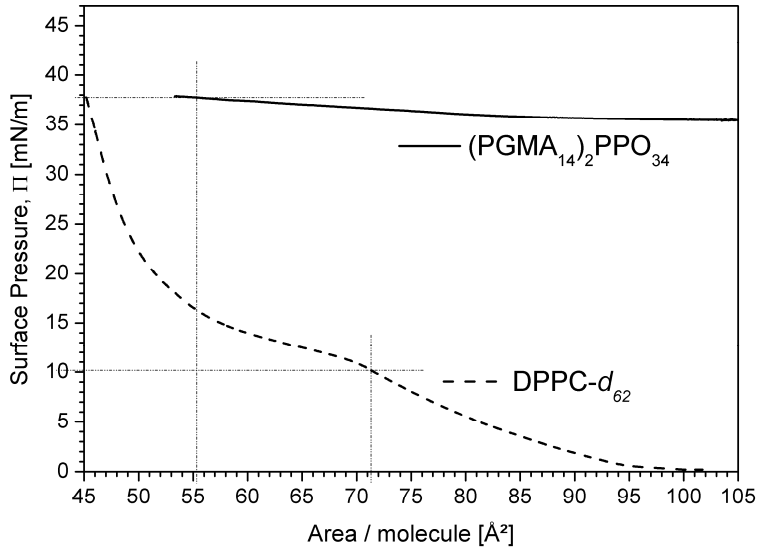

Figure 8.5: Surface pressure (Π) / area (A) isotherms of 1,2-dipalmitoyl-d_{62}-sn-glycero-3-phosphocholine (DPPC-d_{62}) and $(PGMA_{14})_2$-PPO_{34} monolayer films at the air-water interface at 20°C.

8.5 References

[1] Giddings, J. C. *Science* **1993**, *260*, 1456-1465.

[2] Wahlund, K.-G.; Giddings, *J. C. Anal. Chem*. **1987**, *59*, 1332-1339.

[3] Fraunhofer, W.; Winter, G. *Eur. J. Pharm. Biopharm.* **2004**, *58*, 369-383.

[4] Thielking, H.; Kulicke, W.-M. *Anal. Chem.* **1996**, *68*, 1169-1173.

[5] Fraunhofer, W.; Winter, G.; Coester, C. *Anal. Chem.* **2004**, *76*, 1909-1920.

[6] Wyatt, P. J. *Anal. Chim. Acta* **1993**, *272*, 1-40.

[7] Awan, M. A.; Dimonie, V. L.; Ou-Yang, D.; El-Aasser, M. S. *Langmuir* **1997**, *13*, 140-146.

9 Acknowledgments

I would like to express my deepest gratitude towards those who, in one or another way, made this work possible:

In the first place Prof. Dr. J. Kreßler and Prof. Dr. A. Blume, for their strong support and permanent scientific guidance during these years; for letting me to explore my not always Orthodox points of view; and above all, for looking after me not only as a docent should, but also as a father would. I am honored to be allowed to call them "Doktorvater".

Dr. Andreas Kerth for introducing me in an almost mystical way to the essential working methods with surface monolayers, and to many physico-chemical methods including IRRAS. Also for the evaluation of the angular dependent IRRAS measurements.

Dr. S. Kaiser for his support and guidance during the polymer synthesis.

Dr. K. Busse for the performance of X-ray scattering measurements.

Dr. Annette Meister for their valuable advices and hints.

Prof. Dr. Karsten Mäder and Dr. Christian Augsten at the Institute of Pharmaceutics and Biopharmaceutics - MLU for performing the AF4 measurements.

Prof. P. Pohl at the Institute for Biophysics - Johannes Kepler Universität Linz, for introducing me to the technique of black lipid membranes.

Prof. Dr. Hans-Joachim Galla at the Institut für Biochemie - WWU Münster, for introducing me to the technique of fluorescence microscopy on monolayers.

Ingrid Schaller and Bettina Fölting for their technical assistance with transmission IR, ITC and DSC measurements.

Andreas Lonitz for keeping my PC flying.

My colleagues at the institute of Physical Chemistry for many fruitful academic and non-academic discussions, for teaching me German, for making me to feel welcome in spite of my foreign manners, for showing me the beauty of German natural landscapes… in summary, for showing me the nicest face of Germany. In particular, I would like to thank Martin Schiewek, Christian Schwieger, and Andreas Kerth for their friendship.

My family, source, sense, and end of my life.

10 Publications

1. Synthesis and hydrolysis of α,ω-perfluoroalkyl-functionalized derivatives of poly(ethylene oxide).
E. Amado, J. Kressler, *Macromolecular Chemistry and Physics* **2005**, *206*, 850-859.

2. Amphiphilic Water Soluble Triblock Copolymers Based on Poly(2,3-dihydroxypropyl methacrylate) and Poly(propylene oxide): Synthesis by Atom Transfer Radical Polymerization and Micellization in Aqueous Solutions.
E. Amado, C. Augsten, K. Maeder, A. Blume and J. Kressler, *Macromolecules* **2006**, *39*, 9486-9496.

3. Synthesis and characterization of random copolymers of (2,2-dimethyl-1,3-dioxolan-4-yl)methyl methacrylate and 2,3-dihydroxypropyl methacrylate.
S. O. Kyerematen, E. Amado, J. Kressler, *European Polymer Journal* **2007**, *43*, 3380-3391.

4. Infrared Reflection Absorption Spectroscopy Coupled with Brewster Angle Microscopy for Studying Interactions of Amphiphilic Triblock Copolymers with Phospholipid Monolayers.
E. Amado, A. Kerth, A. Blume, J. Kressler, *Langmuir* **2008**, *24*, 10041-10053.

5. Synthesis of ABC and CABAC triphilic block copolymers by ATRP combined with 'click' chemistry.
S. O. Kyerematen, E. Amado, A. Blume, J. Kressler, *Macromolecular Rapid Communications* **2008**, *29*, 1140-1146.

6. Novel non-ionic block copolymers tailored for interactions with phospholipids.
E. Amado, A. Blume, J. Kressler, *Reactive & Functional Polymers* **2009**, *69*, 450-456.

7. Phospholipid crystalline clusters induced by adsorption of novel amphiphilic triblock copolymers to monolayers.
E. Amado, A. Kerth, A. Blume, J. Kressler, *Soft Matter* **2009**, *5*, 669-675.

8. Adsorbed and Spread Films of Amphiphilic Triblock Copolymers Based on Poly-(2,3-dihydroxypropyl methacrylate) and Poly(propylene oxide) at the Air-Water Interface.
E. Amado, A. Blume, J. Kressler, *Langmuir* **2010**, DOI: 10.1021/la903748z

9. *In vivo* Studies on Intraperitoneally Administrated Poly(vinyl alcohol).
Y. Jiang, A. Schädlich, E. Amado, C. Weis, E. Odermatt, K. Mäder, J. Kressler,
Journal of Biomedical Materials Research Part B: Applied Biomaterials **2010**, DOI: 10.1002/jbm.b.31585

Meeting Abstracts

- Synthesis and characterization of perfluoroalkyl end functionalized derivatives of poly(ethylene oxide). E. Amado, J. Kressler. *Polymer Preprints* **2005**, *46(2)*, 643-644. Abstracts of Papers, 230th ACS National Meeting, Washington, DC, United States, Aug. 28-Sept. 1, 2005, POLY-572.
- Amphiphilic water soluble triblock copolymers based on poly(2,3-dihydroxypropyl methacrylate) and poly(propylene oxide): Synthesis, micellization and interaction with model lipid layers. E. Amado, A. Blume, J. Kressler, *Polymer Preprints* **2006**, *47(2)*, 5-6. Abstracts of Papers, 232nd ACS National Meeting, San Francisco, CA, United States, Sept. 10-14, 2006, POLY-412.
- Adsorption kinetics of amphiphilic water soluble triblock copolymers based on poly(2,3-dihydroxypropyl methacrylate) and poly(propylene oxide) at the air-water interface. E. Amado, J. Kressler, A. Blume, A. Kerth, *PMSE Preprints* **2008**, *98*, 36-37. Abstracts of Papers, 235th ACS National Meeting, New Orleans, LA, United States, April 6-10, 2008, PMSE-024.
- Structure formation of triphilic block copolymers and their interactions with phospholipids. S. O. Kyerematen, E. Amado, J. Kressler, submitted to: *Polymer Preprints*. Abstracts of Papers, 239th ACS National Meeting, San Francisco, CA, United States, March. 21-25, 2010.

11 Curriculum Vitae

Personal Details:

Name:	Elkin Mauricio Amado Zúñiga
Date of Birth:	April 18th 1974
Place of Birth:	Bogotá, Colombia
Nationality:	Colombian
Marital Status:	Married

Educational Details:

08/2004 - 10/2009	Ph.D. student at the Institute of Chemistry Martin-Luther-Universität Halle-Wittenberg, Halle (Saale), in the groups of Prof. Dr. A. Blume (Physical Chemistry) and Prof. Dr. Jörg Kreßler (Physical Chemistry of Polymers).
10/2002 - 07/2004	***Master of Science (M. Sc.) in Applied Polymer Science*** Martin-Luther-Universität Halle-Wittenberg Thesis: "*Synthesis, characterization and hydrolysis of α,ω-perfluoroalkyl-functionalized derivatives of poly(ethylene oxide)".* Final grade: 1.2 - "excellent".
01/1991 - 12/1997	***Chemical Engineering*** Universidad Nacional de Colombia, Bogotá , Colombia. Thesis: *"Modeling of the regeneration process of a catalyst particle in a Fluid Catalytic Cracking Unit".* Title: ***Diploma Chemical Engineer.*** Graduation rank: 1st place.
01/1985 - 12/1990	***High School*** Colegio Hermanos Corazonistas, Bogotá, Colombia. Leaving Cerificate: "Very superior".

Awards:

Honored with the DAAD (*Deutscher Akademischer Austauschdienst*)-Prize 2004, for outstanding achievements among foreign students at the Martin-Luther-Universität Halle-Wittenberg.

Eidesstattliche Erklärung

Hiermit erkläre in an Eides statt, dass ich die vorliegende Arbeit selbständig und ohne Fremde Hilfe verfasst habe. Ich habe keine anderen Quellen und Hilfsmittel als die angegebenen verwendet und anderen Werken wörtlich oder inhaltlich entnommene Stellen als solche gekennzeichnet. Diese Arbeit habe ich an keiner anderen Hochschule vorgelegt und mich zu keinem früheren Zeitpunkt um den Doktorgrad beworben.

Elkin M. Amado Z.

Halle (Saale), 14.01.2010